Selection and Characterization of the Foundation Materials for the Third-Generation FHWA Pavement Test Facility

December 2024

Publication No. FHWA-HRT-25-023

U.S. Department of Transportation
Federal Highway Administration

Research, Development, and Technology
Turner-Fairbank Highway Research Center
6300 Georgetown Pike McLean, VA 22101-2296

Turner-Fairbank
Highway Research Center

FOREWORD

Since 1986, the Federal Highway Administration (FHWA) has conducted accelerated pavement testing and experimentation at the Turner-Fairbank Highway Research Center's Pavement Testing Facility (PTF). In 2023, FHWA constructed a new, improved, third-generation PTF, with 11 test lanes and 44 test sites. The new facility expands the scope of the research that will be conducted to include holistic pavement design and performance. This new pavement field enables researchers to consider the impact of various pavement foundation designs on the performance of the pavement. Inclusion of pavement foundation considerations is fundamental to the PTF's research objectives related to innovative pavement design concepts, evaluation of design methodologies, sustainability, and resilience.

This report documents the selection process for the new PTF pavement foundation materials and the laboratory characterization necessary to achieve many of the research objectives. The report is intended to serve as a reference document for the planned research at the new PTF. The results of this work will assist State and local transportation agencies, design consultants, contractors, and researchers in evaluating appropriate geomaterials, including stabilization techniques, for more durable pavement systems.

Jean Nehme, Ph.D., P.E.
Director, Office of Infrastructure
Research and Development

Notice

This document is disseminated under the sponsorship of the U.S. Department of Transportation (USDOT) in the interest of information exchange. The U.S. Government assumes no liability for the use of the information contained in this document.

Non-Binding Contents

Except for the statutes and regulations cited, the contents of this document do not have the force and effect of law and are not meant to bind the States or the public in any way. This document is intended only to provide information regarding existing requirements under the law or agency policies.

Quality Assurance Statement

The Federal Highway Administration (FHWA) provides high-quality information to serve Government, industry, and the public in a manner that promotes public understanding. Standards and policies are used to ensure and maximize the quality, objectivity, utility, and integrity of its information. FHWA periodically reviews quality issues and adjusts its programs and processes to ensure continuous quality improvement.

Disclaimer for Product Names and Manufacturers

The U.S. Government does not endorse products or manufacturers. Trademarks or manufacturers' names appear in this document only because they are considered essential to the objective of the document. They are included for informational purposes only and are not intended to reflect a preference, approval, or endorsement of any one product or entity.

Recommended citation: Federal Highway Administration, *Selection and Characterization of the Foundation Materials for the Third-Generation FHWA Pavement Test Facility* (Washington, DC: 2024) https://doi.org/10.21949/1521622

TECHNICAL REPORT DOCUMENTATION PAGE

1. Report No. FHWA-HRT-25-023	2. Government Accession No.	3. Recipient's Catalog No.
4. Title and Subtitle Selection and Characterization of the Foundation Materials for the Third-Generation FHWA Pavement Test Facility		5. Report Date December 2024
		6. Performing Organization Code:
7. Author(s) Michael T. Adams (ORCID: 0000-0003-2358-4128), Jennifer E. Nicks (ORCID: 0000-0001-7230-3578), Isaac E. Zuniga (ORCID: 0000-0003-4591-2057), Ismaail I. Ghaaowd (ORCID: 0000-0003-2600-0167), and Nicholas A. Culbreth (ORCID: 0000-0003-0434-230X)		8. Performing Organization Report No.
9. Performing Organization Name and Address Office of Infrastructure Research and Development Federal Highway Administration 6300 Georgetown Pike McLean, VA 22101		10. Work Unit No.
		11. Contract or Grant No. 693JJ323F00187N/693JJ319D000056
12. Sponsoring Agency Name and Address Office of Infrastructure Research and Development Federal Highway Administration 6300 Georgetown Pike McLean, VA 22101-2296		13. Type of Report and Period Covered Final Report; June 2021–June 2024
		14. Sponsoring Agency Code HRDI-10 and HRDI-40
15. Supplementary Notes The contracting officer's representative was Jennifer E. Nicks (HRDI-40; ORCID: 0000-0001-7230-3578).		

16. Abstract

The reconstruction of the Federal Highway Administration's (FHWA) third-generation Pavement Testing Facility (PTF-3) provided a unique opportunity to incorporate the geotechnical aspects of pavements within the agency's accelerated pavement testing program. These geotechnical aspects included various unbound and asphalt-treated base materials to estimate pavement drainage and resilience through time-to-drain experiments; stabilized, cement-treated bases to evaluate a different type of pavement foundation structure through inverted pavement experiments; and No. 10 screenings (i.e., stone dust) to assess the suitability of quarry byproducts as a durable and sustainable subbase material and as a constituent in a cement-treated base. FHWA's Geotechnical Laboratory conducted an extensive testing program to characterize all the pavement foundation materials. The materials included the homogeneous subgrade across the pavement field, from sieve, density, and specific gravity to permeability and resilient modulus, among other physical, hydraulic, mechanical, and durability properties. This report documents the selection and laboratory characterization of the geotechnical materials as part of the PTF-3 research program and objectives, including the challenges and thought processes leading to the selection and testing of the pavement subsurface layers (i.e., base, subbase, and subgrade) placed during its reconstruction. Key findings relate to the variability of geotechnical materials; the sensitivity of gradation, particularly the gravel-to-sand ratio, on permeability and effective porosity; the use of quarry byproducts in pavements; and the geotechnical inputs for pavement design. This initial baseline characterization study should allow for the future assessment and potential improvements of various flexible pavement designs.

17. Key Words Pavement test facility, accelerated pavement testing, unbound aggregate, cement-treated base, asphalt-treated permeable base, inverted pavement, quarry byproduct, permeability, resilient modulus, MEPDG, PMED	18. Distribution Statement No restrictions. This document is available to the public through the National Technical Information Service, Springfield, VA 22161. https://www.ntis.gov

19. Security Classif. (of this report) Unclassified	20. Security Classif. (of this page) Unclassified	21. No. of Pages 110	22. Price N/A

Form DOT F 1700.7 (8-72) Reproduction of completed page authorized.

SI* (MODERN METRIC) CONVERSION FACTORS

APPROXIMATE CONVERSIONS TO SI UNITS

Symbol	When You Know	Multiply By	To Find	Symbol
		LENGTH		
in	inches	25.4	millimeters	mm
ft	feet	0.305	meters	m
yd	yards	0.914	meters	m
mi	miles	1.61	kilometers	km
		AREA		
in^2	square inches	645.2	square millimeters	mm^2
ft^2	square feet	0.093	square meters	m^2
yd^2	square yard	0.836	square meters	m^2
ac	acres	0.405	hectares	ha
mi^2	square miles	2.59	square kilometers	km^2
		VOLUME		
fl oz	fluid ounces	29.57	milliliters	mL
gal	gallons	3.785	liters	L
ft^3	cubic feet	0.028	cubic meters	m^3
yd^3	cubic yards	0.765	cubic meters	m^3
	NOTE: volumes greater than 1,000 L shall be shown in m^3			
		MASS		
oz	ounces	28.35	grams	g
lb	pounds	0.454	kilograms	kg
T	short tons (2,000 lb)	0.907	megagrams (or "metric ton")	Mg (or "t")
		TEMPERATURE (exact degrees)		
°F	Fahrenheit	5 (F-32)/9 or (F-32)/1.8	Celsius	°C
		ILLUMINATION		
fc	foot-candles	10.76	lux	lx
fl	foot-Lamberts	3.426	$candela/m^2$	cd/m^2
		FORCE and PRESSURE or STRESS		
lbf	poundforce	4.45	newtons	N
lbf/in^2	poundforce per square inch	6.89	kilopascals	kPa

APPROXIMATE CONVERSIONS FROM SI UNITS

Symbol	When You Know	Multiply By	To Find	Symbol
		LENGTH		
mm	millimeters	0.039	inches	in
m	meters	3.28	feet	ft
m	meters	1.09	yards	yd
km	kilometers	0.621	miles	mi
		AREA		
mm^2	square millimeters	0.0016	square inches	in^2
m^2	square meters	10.764	square feet	ft^2
m^2	square meters	1.195	square yards	yd^2
ha	hectares	2.47	acres	ac
km^2	square kilometers	0.386	square miles	mi^2
		VOLUME		
mL	milliliters	0.034	fluid ounces	fl oz
L	liters	0.264	gallons	gal
m^3	cubic meters	35.314	cubic feet	ft^3
m^3	cubic meters	1.307	cubic yards	yd^3
		MASS		
g	grams	0.035	ounces	oz
kg	kilograms	2.202	pounds	lb
Mg (or "t")	megagrams (or "metric ton")	1.103	short tons (2,000 lb)	T
		TEMPERATURE (exact degrees)		
°C	Celsius	1.8C+32	Fahrenheit	°F
		ILLUMINATION		
lx	lux	0.0929	foot-candles	fc
cd/m^2	candela/m2	0.2919	foot-Lamberts	fl
		FORCE and PRESSURE or STRESS		
N	newtons	2.225	poundforce	lbf
kPa	kilopascals	0.145	poundforce per square inch	lbf/in^2

*SI is the symbol for International System of Units. Appropriate rounding should be made to comply with Section 4 of ASTM E380. (Revised March 2003)

TABLE OF CONTENTS

LIST OF FIGURES

LIST OF TABLES

LIST OF ABBREVIATIONS AND VARIABLES

Abbreviations

21A	Virginia Department of Transportation (VDOT) aggregate designation
21B	VDOT aggregate designation
AASHO	American Association of State Highway Officials
AASHTO	American Association of State Highway and Transportation Officials
AC	asphalt concrete
AIMS2	Second generation Aggregate Imaging Measurement System
ASTM	ASTM International
ATPB	asphalt-treated permeable base
AV	air voids
Caltrans	California Department of Transportation
CBR	California Bearing Ratio
Cc	coefficient of curvature
CH	constant head
COV	coefficient of variation
CR	cement ratio
CTB	cement-treated base
Cu	coefficient of uniformity
DI	diabase
DOT	department of transportation
EP	effective porosity
ESAL	equivalent single axle load
FC	fines content
FH	falling head
FHWA	Federal Highway Administration
G/S	gravel-to-sand ratio
GI	group index
GM	silty gravel
GP	poorly graded gravel
GP-GM	poorly graded gravel with silt
GR	granite
ID	identification
JMF	job mix formula
L/S	ratio of longest to shortest dimension
LL	liquid limit
MD	Micro-Deval
MDD	maximum dry density
MEPDG	*Mechanistic-Empirical Pavement Design Guide*
N/A	not applicable
OGA	open-graded aggregate
OMC	optimum moisture content
PI	plasticity index
PMED	Pavement ME Design

PS	permanent strain
PTF	Pavement Testing Facility
PTF-2	second-generation PTF
PTF-3	third-generation PTF
PTM	pavement testing machine
RAP	reclaimed asphalt pavement
RM	resilient modulus
RMSE	root-mean-square error
S	specimen
SANRA	South African National Roads Agency
SB	subbase
SC	clayey sand
SG	subgrade
SM	silty sand
SN	structural number
SpG	specific gravity
SSD	saturated surface dry
TFHRC	Turner-Fairbank Highway Research Center
TSR	tensile strength ratio
UCS	unconfined compressive strength
USACE	U.S. Army Corps of Engineers
USCS	Unified Soil Classification System
VDOT	Virginia Department of Transportation
WSDOT	Washington State Department of Transportation

Variables

a	cross-sectional area of reservoir tube
A	specimen cross-sectional area
a_2	structural layer coefficient of base material
a_3	structural layer coefficient of subbase material
d	characteristic diameter
D_{10}	diameter in which 10 percent of particles are finer
D_{30}	diameter in which 30 percent of particles are finer
D_{50}	diameter in which 50 percent of particles are finer
D_{60}	diameter in which 60 percent of particles are finer
D_{85}	diameter in which 85 percent of particles are finer
D_{max}	maximum particle size
E	elastic modulus
G_{mb}	bulk specific gravity
G_{mm}	maximum specific gravity
G_{sa}	apparent specific gravity
G_{sb}	bulk specific gravity (oven dry)
G_{se}	the effective specific gravity
h	drainage layer thickness
H	head difference
h_0	initial head of water

h_1	final head of water
i	hydraulic gradient
k	hydraulic conductivity
K_o	coefficient of lateral earth pressure at rest
k_1	regression coefficient
k_2	regression coefficient
k_3	regression coefficient
$k_{20\ (CH)}$	20 °C temperature corrected constant head permeability
$k_{20\ (FH)}$	20 °C temperature corrected falling head permeability
k_{sat}	the saturated coefficient of permeability
L	length
m	material properties factor
M_r	resilient modulus
M_{rs}	summary resilient modulus
N_e	effective porosity
P_{200}	percentage of fines
p_a	atmospheric pressure
Q	volume of drained water
QS	quick shear
q_u	unconfined compressive strength
R^2	coefficient of determination
Re	Reynold's number
R_T	ratio of water viscosity at test temperature and 20 °C
S	slope of the drainage layer
S_1	slope factor for drainage layer
t	time
T	time factor related to time to drain
t_{50}	time to drain 50 percent of water
T_w	temperature of water
U	percent drainage
v	Poisson's ratio
V	velocity
W	drainage layer width
w_e	effective moisture content
w_{opt}	optimum moisture content
γ_d	dry unit weight
γ_{dmax}	maximum dry density
$\gamma_{d,max}$	maximum dry unit weight
γ_w	water unit weight
Δp	pressure loss over length
Θ	bulk stress
λ	friction factor
μ	absolute viscosity
ρ	*density of water*
σ_1	principal stress
σ_2	principal stress

σ_3	confining stress
σ_d	deviatoric stress
σ_{dmax}	maximum deviatoric stress
σ_{max}	maximum axial stress
τ_{max}	maximum shear stress
τ_{oct}	octahedral shear stress

CHAPTER 1. INTRODUCTION

For more than 3 decades (1986–present), the Federal Highway Administration (FHWA) has conducted accelerated pavement experimentation and testing at the Turner-Fairbank Highway Research Center's (TFHRC) Pavement Testing Facility (PTF). Due to the obsolescence of the original loading machines and the deterioration of the facility, FHWA designed and constructed a new, improved third-generation Pavement Testing Facility (PTF-3) to replace the second-generation PTF (PTF-2). PTF-3 includes a new outdoor laboratory building, 2 pavement test machines (PTMs), and 11 test lanes with 44 test sites (22 fully instrumented). The new facility presented a unique opportunity to expand the scope of the PTF program and its research objectives beyond simply evaluating asphalt binders and mixtures to include the geotechnical aspects of pavements for a more holistic approach to pavement design and performance. Adams, Nicks, and Carvalho (2024) provide a recount of the history of the PTF from its inception to the current pavement field, along with the fundamental design requirements, experimental plan, and instrumentation program for PTF-3.

DESIGN REQUIREMENTS

One of the fundamental design requirements for PTF-3 was to improve surface drainage across the pavement field (Adams, Nicks, and Carvalho 2024.). Drainage characteristics of the pavement subsurface layers play an important role in the resilience of pavements, particularly in extreme climatic events, such as floods and hurricanes. PTF-2 had drainage issues, evidenced by trapped water within the aggregate base layer, often up to the elevation of the surface pavement layer. As a result, premature distresses, such as early cracking and rutting, were observed in some lanes, and asphalt delamination occurred due to long-term moisture damage.

Forensic trenches across some of the PTF-2 pavement lanes revealed anomalous moisture trapped directly beneath the thin 4-inch asphalt layers. Permeability and effective porosity (EP) testing of the PTF-2 base layer material, an American Association of State Highway and Transportation Officials (AASHTO) A-1-a material, locally designated by the Virginia Department of Transportation (VDOT) as aggregate 21A (VDOT 2020), revealed that the time to drain for 50 percent of the water at the PTF was nearly half a year given the existing 150-ft longitudinal length and 0.5-percent cross-slope of the PTF-2 pavement field. The sieve analysis of the 21A base material revealed that it had a fines content (i.e., material passing the No. 200 sieve) of about 13 percent, leading to the suspicion of potential thaw weakening of the base material over time, which may have also contributed to the early distress in some of the test sections.

These observations and findings shed light on how free-draining road-base materials are defined within the context of pavement design. As such, an effort was made to apply to the PTF-3 design the pavement engineering saying: "three of the most important aspects of road design—drainage, drainage, and drainage."[1] Therefore, FHWA explicitly emphasized the importance of drainage in the design of the new PTF-3 pavement field.

[1]D. Fohs. 1989. TFHRC, McLean, VA. Don Fohs, former chief of FHWA's Materials Division, taught staff many practical aspects of pavement design. The three Ds are often overlooked in current practice.

Improvements were made to facilitate surface drainage by changing the cross slope to a 1.0-percent grade in the west-to-east direction instead of the north-to-south 0.5-percent longitudinal slope along the 150-ft length of the pavement lanes grade direction used in PTF-2. The selection of the 1.0-percent cross slope was an optimization between generating surface water flow and facilitating the movement of the PTMs across the pavement field, given their operational limits.

To eliminate the distance of surface water across the new pavement field, several edge drains were installed along the length of the pavement field to capture the surface water. The need for edge drains fed into the concept of different pavement pits separated by barrier walls. The primary function of the barrier walls was originally to capture surface water and serve as a barrier between pavement pits. The function quickly expanded to also serve as a method for instrumentation cable management and as a reference elevation across the pavement field for all future experiments (Adams, Nicks, and Carvalho 2024.). Edge drains at the top of each barrier wall flow southward at a 2-percent grade into a drainage system at a swale on the south-end pavement field.

The pavement field in PTF-3 is composed of four pits, designated as pits A, B, C, and D, each separated by the barrier walls. Pits A, B, and C (figure 1) are designated for longer term experiments, whereas pit D (figure 2) is designated for shorter term experiments.

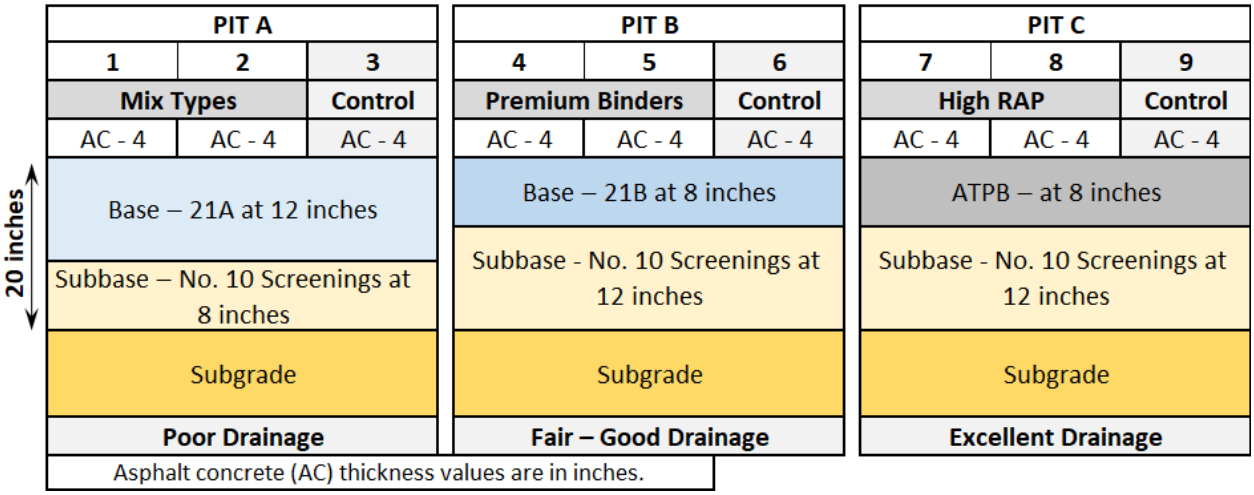

Source: FHWA.
AC = asphalt concrete; ATPB = asphalt-treated permeable base; RAP = reclaimed asphalt pavement.

Figure 1. Illustration. Conceptual pavement cross sections for the time-to-drain experiments (Adams, Nicks, and Carvalho 2024).

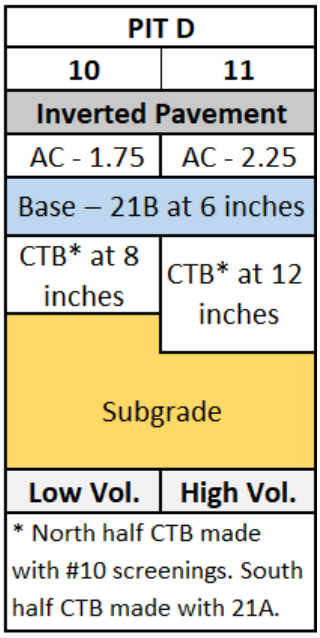

Source: FHWA.
CTB = cement-treated base.

Figure 2. Illustration. Conceptual pavement cross sections for inverted pavement experiments (Adams, Nicks, and Carvalho 2024).

RESEARCH OBJECTIVES

During the design and planning of PTF-3, several root (i.e., primary) and stem (i.e., secondary) research objectives were outlined. Root objectives included the following:

- Evaluating the geotechnical aspects of pavements.
- Assessing pavement resilience (e.g., time to drain).
- Comparing different pavement structures (e.g., layer thicknesses, inverted pavements) and design methodologies (e.g., *Guide for Design of Pavement Structures* (AASHTO 1993), *Mechanistic-Empirical Pavement Design Guide: A Manual of Practice* (MEPDG) (AASHTO 2020a), and AASHTOWare® Pavement™ ME Design™ (PMED) (AASHTO 2020b)).
- Evaluating state-of-the-art asphalt mixture designs and pavement response and performance.

These four objectives were the primary research goals for PTF-3; however, several secondary research objectives were defined, including validating nondestructive evaluation technologies for quality assurance (e.g., intelligent compaction), evaluating pavement preservation techniques, assessing instrumentation technologies, and quantifying the robustness and installation procedures of operational systems (Adams, Nicks, and Carvalho 2024).

One of the leading research objectives for the longer term experiments in pits A, B, and C was to evaluate the impact of drainage on pavement performance, particularly the time to drain (i.e., pavement resilience), with the requirement of selecting base materials with different permeabilities. Earlier design and construction practices aimed to build a strong and stiff pavement, which now appears insufficient. A fine balance exists between pavement strength and permeability properties to achieve the desired performance. This study was conducted to understand the balance between the strength and permeability of pavement subsurface layers.

As a starting point, the base material in pit A was constructed with the same 21A material used in PTF-2 to serve as a reference for comparison to past PTF experiments. The base material in pit B was then selected to have at least an order of magnitude higher permeability than in pit A. The base material in pit C was selected for excellent drainage.

The short-term experiments in pit D were selected to evaluate the concept and performance of inverted pavements. Four sections are considered in pit D, with varying thicknesses of cement-treated base (CTB) and asphalt-wearing course, meant to simulate low- versus high-volume roadways. In addition, different CTB materials were evaluated; the north half of pit D was made with cement-treated No. 10 screenings, while the south half was made with a cement-treated 21A.

REPORT ORGANIZATION

This report documents the laboratory characterization of the geotechnical materials as part of the PTF-3 research program and objectives, including the challenges and thought processes leading to the selection of the pavement subsurface layers i.e., base, subbase (SB), and subgrade (SG) placed during its reconstruction. Chapter 2 summarizes an overview of the background of pavement design methodologies from a geotechnical perspective, along with a synthesis of the literature on chemically treated bases, inverted pavements, and the use of waste material in pavements. The selected unbound and stabilized materials and their material and engineering properties are described in chapter 3 and chapter 4, respectively. Chapter 5 presents the expected number of equivalent single axle loads (ESALs) required before pavement failure in each pit, based largely on their level 1 inputs. Chapter 6 discusses the challenges faced throughout the material selection process and specification. Finally, key conclusions, research needs, and next steps are summarized in chapter 7, along with lessons learned in designing and constructing an accelerated pavement test facility.

CHAPTER 2. BACKGROUND

Before diving into the details of design and material characterization, a literature review was performed to understand current practices for flexible and inverted pavement design and base stabilization techniques, including asphalt, CTBs, and the use of quarry byproducts in pavements.

OVERVIEW OF FLEXIBLE PAVEMENT DESIGN METHODOLOGIES

Pavement design methodology has been studied for decades as pavements continually evolve to meet current infrastructure needs. Pavement design methods developed by AASHTO use layer coefficients that were initially developed during the American Association of State Highway Officials' (AASHO) Road Test in 1956 (Highway Research Board 1962). Most of AASHO's six test loops used crushed dolomitic limestone as the base material, as this material was the standard base used by the Illinois Division of Highways. AASHO used three additional base materials in select test sections to evaluate the potential of these materials compared to traditional crushed stone bases: CTB, bituminous-treated base, and uncrushed gravel base. Although stabilized and unbound subbase and base were used, AASHO only evaluated the pavement performance of the Road Test loops at the surface level (i.e., no cores were taken to assess individual layer performance or properties).

The 1972 *AASHTO Interim Design Guide of Pavement Structures* (Interim Design Guide) (AASHTO 1972) provided no guidance on the calculation of the structural layer coefficient of the base material (denoted as a_2 in the Interim Design Guide) for unbound and stabilized granular materials, and thus the structural number (SN), for base materials was different from the AASHO Road Test (Van Til et al. 1972). For unbound granular materials, the a_2 coefficient was therefore recommended based on the crushed stone used in the AASHO Road Test, while for stabilized granular materials, a_2 is defined based on 7-d compressive strength for cement stabilization and Marshall stability for asphalt-treated base materials (ASTM International (ASTM) D6927 (2022a)). For the structural layer coefficients of the subbase material (denoted as a_3 in the Interim Design Guide), a_3 was a function of other critical material properties (e.g., California Bearing Ratio (CBR), *R*-value, and triaxial strength). For all a_2 and a_3 calculations, nomographs were provided by Van Til et al. (1972) to approximate structural layer coefficients as a function of material properties.

The 1986 *AASHTO Guide for Design of Pavement Structures* introduced resilient modulus (RM) as the recommended test for soil characterization and structural layer coefficient calculation and included commentary on subsurface drainage considerations during pavement design to ensure adequate drainage (AASHTO 1986). Empirical equations to calculate a_2 for unbound granular bases and a_3 for granular subbase layers as a function of RM were offered as an alternative to the 1972 nomographs (AASHTO 1972). No empirical equations are provided for stabilized base materials, and the 1972 nomographs are repeated and recommended for use. The 1986 Design Guide does not provide a drainage design methodology, but it details the anticipated relationship between desired drainage level and overall pavement performance (AASHTO 1986). Excellent drainage is defined as a pavement that can remove water within 2 h; good drainage equates to 1 d; fair drainage equates to 1 w; poor drainage equates to 1 mo; and very poor drainage is for

pavements that will not drain. All 1986 Design Guide commentary on drainage is only valid for unbound base and subbase materials.

From a geotechnical materials perspective, no major changes were made between the 1986 AASHTO Design Guide (AASHTO 1986) and the 1993 *AASHTO Guide for Design of Pavement Structures* (AASHTO 1993). The 1993 AASHTO Design Guide continued to relate RM to other material properties (i.e., CBR and *R*-value) for unbound base and subbase materials; however, for stabilized base materials, the 1972 nomographs are recommended for selecting a_2 and a_3 structural layer coefficients (AASHTO 1972). From a drainage perspective, the 1993 Design Guide added substantial commentary on the effects of drainage on roadbed soil strengths compared to the 1986 Design Guide (AASHTO 1993, 1986). A scaling factor was included in the SN equation to account for the deleterious effects of moisture on pavement layer properties; however, scaling factors are only applied to untreated base and subbase layers. Asphalt-treated permeable bases (ATPBs) are referenced as an option to account for drainage; however, only a recommended material gradation and some additional references are provided for users.

Although the AASHTO Design Guides were an integral step forward in pavement design methodologies, recommended empirical relationships are based on pavements built and tested at the AASHO Road Test in the 1950s (Highway Research Board 1962), where typical pavements used neat asphalt binders, unbound granular bases, and natural sand-gravel subbase layers. Modern pavements are being built with reclaimed materials, modified binders, chemically stabilized soils, etc. AASHTO's MEPDG was introduced as an alternative to prior design guides where the design methodology was to interface materials, load-deflection relationships, construction, climate, traffic, and many other factors into the design of pavements (AASHTO 2020a). Today, the AASHTOWare PMED, along with the accompanying commercially available software, builds on the MEPDG and is used to support day-to-day pavement design functions (AASHTO 2020b).

PMED uses empirical equations to estimate material properties used in the design of unbound and chemically stabilized soils. For unbound pavement layers, both physical properties (e.g., dry density, moisture content) and engineering properties (e.g., RM) are required inputs. Inputs can be directly measured and inserted into the design framework (level 1 input), estimated using an empirical relationship (level 2 input), or estimated using an assumed constant (level 3 input).

Table 1 summarizes PMED material property requirements and whether they should be directly measured or estimated using level 2 or 3 inputs. Although level 1 inputs are recommended in most cases, level 2 relationships and level 3 inputs are provided for each material property if users cannot determine a level 1 input. The coefficient of lateral earth pressure is another material input property per PMED (AASHTO 2020b).

Table 1. Unbound aggregates and subgrade material properties for PMED (AASHTO 2020b).

Material Property	Level 1 Input	Level 2 Input	Level 3 Input
RM	X (AASHTO T 307 (2021a))	X	X
Poisson's ratio	N/A	N/A	X
K_o	N/A	N/A	X
Maximum dry density	X (AASHTO T 180 (2022a))	X	X
Optimum moisture content	X (AASHTO T 180 (2022a))	X	X
Specific gravity	X (AASHTO T 100 (2022b))	X	X
Saturated hydraulic conductivity	X (AASHTO T 215 (2023a))	X	X
Soil water characteristic curve parameters	X (ASTM D6836 (2016a))	X	X
Gradation	X (AASHTO T 88 (2022c))	X	X
Atterberg limits	X (AASHTO T 89 (2022d) and T 90 (2022e))	X	X

K_o = coefficient of lateral earth pressure at rest; N/A = not applicable.
Notes: Level 1 input is directly measured material property; level 2 input is empirical correlation used to estimate material property; level 3 input is assumed constant used to estimate material property; X denotes which input is used for the material property of interest.

For chemically stabilized soils, the flexural strength (i.e., modulus of rupture), elastic modulus (E), and density are required design inputs. Table 2 summarizes which material properties should be directly measured (level 1 input) and which properties can be estimated using an empirical equation (level 2 input) or assumed constant (level 3 input). As with unbound soils, PMED (AASHTO 2020b) does provide recommended level 2 relationships and level 3 inputs for each material property if a user does not have the capability of conducting tests to determine a level 1 input. Carey et al. (2022) included extended commentary on the accuracy of MEPDG- and PMED-recommended level 2 inputs for E of soil cement.

Table 2. Chemically stabilized soil design guidance for material properties for PMED (AASHTO 2020b).

Material Type	Material Property	Level 1 Input	Level 2 Input	Level 3 Input
Cement-treated aggregate	Elastic modulus	X (ASTM C469 (2022b))	X	X
	Flexural strength	X (AASHTO T 97 (2022f))	X	X
Lime-cement-fly ash	Resilient modulus	N/A	X	X
Soil-cement	Resilient modulus	X (AASHTO T 307 (2021a))	X	X
Lime-stabilized soil	Resilient modulus	X (AASHTO T 307 (2021a))	X	X
All chemically stabilized soils	Unit weight	N/A	N/A	X
	Poisson's ratio	N/A	X	X
	Thermal conductivity	X (ASTM E1952 (2023a))	N/A	X
	Heat capacity	X (ASTM D2766 (2009))	N/A	X
	Surface short-wave absorptivity	N/A	X	X

Notes: Level 1 input = directly measured material property; level 2 input = empirical correlation used to estimate material property; level 3 input = assumed constant used to estimate material property; X denotes which input is used for material property of interest.

In addition to traditional stabilized and unbound soils considered during flexible pavement design, ATPB has become an alternative base layer material due to its improved drainage capabilities. In the current version of PMED, ATPB was omitted from the global calibration process but was considered during the design of rigid pavements (i.e., concrete pavements) (AASHTO 2020b). Research conducted through FHWA's Long-Term Pavement Performance program has shown that including an ATPB layer can meaningfully reduce the fatigue life of a flexible pavement (AASHTO 2010). However, if desired, users can treat an ATPB layer as a high-quality aggregate base layer when analyzing the trial design with a representative RM of 65,000 psi.

In 2004, FHWA conducted a survey of State department of transportation (DOT) pavement design procedures that revealed that more than 50 percent of State DOTs used the AASHTO 1993 Design Guide (FHWA 2004; AASHTO 1993). However, with the introduction of the MEPDG (AASHTO 2020a) in the mid-2000s, several States altered their pavement design procedures to align with this new methodology. A subsequent review of State DOT pavement design practices by Timm et al. (2014) reported that 68 percent of States used the 1993 AASHTO Design Guide as their primary pavement design guidance. However, a later survey by Koerner, Koerner, and Koerner (2018) showed that 38 percent of States used the MEPDG, while 21 percent used the AASHTO 1993 Design Guide. The remaining 41 percent of State DOTs used either a State-specific design method or earlier versions of AASHTO design guides. Additionally, a survey of members of the AASHTO Committee on Materials and Pavements

conducted in 2018 showed that 40 percent of State DOTs have implemented the MEPDG in some form, and another 35 percent are considering implementation (Geary 2018). Based on these surveys, the two methodologies overwhelmingly used for pavement design in the United States are the 1993 AASHTO Design Guide and the MEPDG, with the MEPDG becoming the primary design methodology (AASHTO 1993, 2020a). With the evolution to PMED, it would be interesting to see how these pavement design trends change.

OVERVIEW OF ATPB IN PAVEMENT DESIGN

ATPB is a mixture of open-graded aggregates (OGAs) and a small percentage of asphalt binder intended for use as a stabilized base course with excellent permeability. ATPB has been used as a pavement base layer placed directly under the asphalt concrete (AC) layer to improve the pavement structure drainage by removing water that enters through the pavement surface and draining the water before it reaches the unbound layers and causes damage (Harvey et al. 1999; Harrigan 2002). A subdrain system is required when ATPB is used. Several DOTs have implemented ATPB (e.g., Oregon DOT (Zhou et al. 1992); Maine DOT (1999)). Many agencies also have developed mixture selection guides for properties such as gradation, binder content, binder type, laboratory tests, and construction methods (e.g., California DOT (Caltrans) (2019), FHWA (Garcia and Hansen 2001), Indiana DOT (2013), and Washington State DOT (WSDOT 2023).

The Caltrans DOT conducted extensive ATPB research in the late 1990s to supplement its design methodologies (Harvey et al. 1999). Commonly observed problems were asphalt binder stripping, loss of cohesion and stiffness, fine migration, and edge-drain clogging. The study recommended the following:

- Improving the ATPB material resistance to water damage.
- Increasing the gravel factor to two.
- Adding a filter layer beneath the ATPB to minimize the intrusion of fines.
- Maintaining the drains to prevent water from saturating the ATPB layer.
- Calibrating the design procedure using the heavy vehicle simulator.

If a supplemental base layer drainage is not needed, Harvey et al. (1999) recommended that an ATPB not be used.

Florida DOT (FDOT) investigated ATPB in a small number of projects, and similar issues were observed (Webb at al. 2007). The FDOT study recommended increasing the asphalt binder content to 3 percent, maintaining functional drainage systems, and placing ATPB over an impermeable dense graded layer.

Other States have reported using ATPB successfully as a base layer. A 13-yr study of an ATPB layer used during reconstruction of two roads in Vermont showed that ATPB layered roads reduced fatigue and transverse cracking; ride quality was comparable to conventionally built pavements 1 yr after construction (Kipp, Walters, and Ahearn 2013). Additionally, construction of the ATPB road resulted in a 5-percent reduction of the average bid price.

OVERVIEW OF INVERTED PAVEMENT DESIGN METHODOLOGY

Inverted pavement systems use an unbound granular base aggregate placed between a CTB and a thin asphalt surface layer (Papadopoulos and Santamarina 2019). Typically, the asphalt layer is 2–3 inches thick, the unbound aggregate layer is 6–8 inches thick and compacted to at least 100-percent modified Proctor density (AASHTO 2022a), and the CTB layer is 6–12 inches thick with approximately 4-percent cement by weight (Tutumluer and Barksdale 1995). The South African construction specification followed for inverted pavements provides a range of target unconfined compressive strengths (UCS) for CTB of 200–500 psi (South African National Roads Agency (SANRA) 1998). The main design difference between inverted pavements and traditional pavements is the sequence of the different material layers.

Since the 1970s, South Africa has implemented inverted pavement design for heavy traffic loads on a large scale (Buchanan 2010). In the United States, inverted pavements have been successfully implemented in Georgia (Frost 2017), Virginia (Weingart 2010), Tennessee (Xi et al. 2022), Louisiana (Ozer and Al-Qadi 2021), North Carolina (Underwood, Guddati, and Samu 2020) and New Mexico (Johnson 1961).

Inverted pavements provide many potential positive impacts. From a pavement performance standpoint, the unstabilized base layer can achieve higher compaction above a stiff, stabilized layer, leading to better confinement and reduced permanent deformations. Additionally, the likelihood of reflective cracking is meaningfully reduced or eliminated since the CTB layer is below the well-compacted unbound aggregate layer (Tutumluer and Barksdale 1995). From an economic perspective, inverted pavements have repeatedly been reported as having lower initial construction costs and lifecycle savings. For example, South Africa reported upward of 20-25 percent in lifecycle savings compared to traditional pavement systems (SANRA 1998). Inverted pavement sections built in the United States have similar economic benefits. A project in Virginia reported initial construction costs of an inverted pavement section decreased by 22 percent compared to a conventional pavement section (Weingart 2010), and a project in Georgia reported a lifecycle cost analysis where inverted pavements had project savings of $139,000 per lane mile compared to conventional pavement sections (Cardosa 2008).

INCLUSION OF WASTE MATERIAL IN PAVEMENT DESIGN

The inclusion of recycled and waste materials in pavements has significantly increased with the push for greener and sustainable construction practices (Bamigboye et al. 2021; Meininger and Stokowski 2011) as well as the reduction in quality pavement materials (Ghaaowd et al. 2022). Materials evaluated within pavement subsurface layers include rubber tires (Peng et al. 2023), municipal solid waste incineration ash (Vizcarra, Casagrande, and Goretti da Motta 2018), construction and demolition waste (Aytekin, Mardani, and Ünsever 2023), and reclaimed asphalt pavement (Puppala et al. 2017). One material of particular interest for use within the PTF-3 is quarry byproduct materials (i.e., stone dust), namely the No. 10 screenings created during the production of traditional aggregates.

Stone dust has been evaluated in several studies as a stabilizing agent that can be added to traditional roadway materials for optimized properties. Optimal replacement percentages of stone dust range in literature from 30 to 60 percent (Cakuru et al. 2021; Sridharan et al. 2006). In some

cases, stone dust and cement have been successfully added to soil for pavement base layers to improve mechanical properties. Two different studies in Nigeria examined the optimal ratios of stone dust, cement, and soil needed to meet the strength requirements for cement-stabilized pavement base materials of 218–435 psi at 7 d per the Nigerian General Specifications (Federal Republic of Nigeria 2013). Arinze, Agunwamba, and Mama (2018) reported soil/stone dust/cement ratios (CRs) of 54:40:6 percent and 40:50:10 percent by weight met the specifications for flexible pavement base material. Etim et al. (2021) used a much lower quantity of stone dust (86:8:6 percent soil/dust/CR by weight) to meet the strength requirements of flexible pavement base materials. From an economic perspective, ratios with a higher stone dust content are preferred since more waste material is used.

Although stone dust has been successfully used as a soil stabilizing material, the PTF-3 uses No. 10 screenings as the subbase material. For one lane of the inverted pavement experiments, the No. 10 screenings are stabilized with a small cement dosage. Select literature has evaluated the potential of cement-stabilized quarry fines as a subsurface pavement layer. Nweke and Okogbue (2017) determined that a minimum cement content of 3 percent by weight yielded a material that satisfied Nigerian highway construction requirements of 218–435 psi at 7 d for road materials; however, the material did have a high liquid limit, which can be an indicator of potential expansion. Ghaaowd et al. (2022) compared cement-stabilized stone dust to traditional cement-stabilized aggregates and found the stone dust was a comparable base material when considering permeability, UCS, M_r, and quick shear strength.

CHAPTER 3. SELECTED GEOTECHNICAL MATERIALS

The design requirements for both the time-to-drain and the inverted pavement experiments vary despite having some similarities in their input design parameters (table 1 and table 2, respectively). This section describes the process of selecting the materials for all pavement pits in PTF-3. The iterative process required and the challenges encountered along the way will be discussed in more detail in chapter 6, "Design Challenges and Lessons Learned."

TIME-TO-DRAIN EXPERIMENTS

The simplified flowchart shown in figure 3 illustrates the general steps considered in the selection of the pavement base layer materials in pits A, B, and C (figure 1).

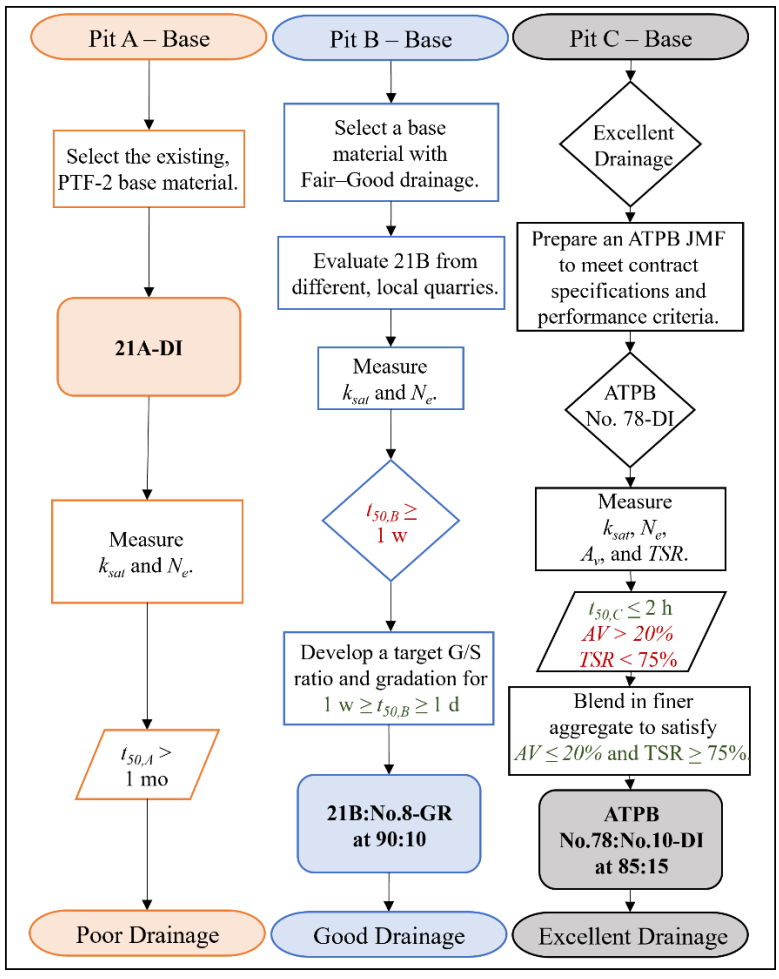

Source: FHWA.
DI = diabase; K_{sat} = the saturated coefficient of permeability; N_e = effective porosity; $t_{50,A}$, $t_{50,B}$, $t_{50,C}$ = time to drain 50 percent of water for pits A–C, respectively; G/S = gravel to sand; GR = granite; JMF = job mix formula; AV = air voids; TSR = tensile strength ratio.

Figure 3. Flowchart. Procedures for material selection for the long-term PTF experiments.

Essentially, the base material in pit A was known to have poor drainage quality. According to AASHTO (1993), the drainage quality of construction materials is based on the time to 50 percent drainage (t_{50}) and can be qualitatively categorized as very poor (t_{50} > 1 mo), poor (t_{50} = 1 mo), fair (t_{50} = 1 w), good (t_{50} = 1 d), and excellent (t_{50} < 2 h). The challenge was finding materials from local quarries that met the desired degree of drainage quality for pit B (i.e., fair to good) and pit C (i.e., excellent), which will be expounded on in chapter 6. Note that the construction specification for all base and subbase material in the time-to-drain experiment was to compact to 95 percent of their maximum dry unit weight per a modified Proctor test according to AASHTO T 180 (AASHTO 2022a).

Pit A Base Material: Poor Drainage

The existing 21A material used in PTF-2 was selected for PTF-3 to serve as a basis for comparison with the previous experiments. The mineralogy of the 21A is diabase (DI); hence, the nomenclature used throughout is 21A-DI. Figure 4 shows an oven-dried representative sample of the 21A-DI base material. Table 3 provides the grain size specifications.

Source: FHWA.

Figure 4. Photo. 21A-DI (oven dried).

Table 3. Gradation specifications for PTF-3 unbound materials.

Sieve No.	Particle Size (inch)	Passing (percent)			
		21A[+]	21B[+]	No. 8 [++]	No. 10[++]
2-inch	2.0	100	100	—	—
1-inch	1.0	94–100	85–95	—	—
3/4-inch	0.75	—	—	—	—
1/2-inch	0.50	—	—	100	—
3/8-inch	0.375	63–72	50–69	85–100	100
No. 4	0.187	—	—	10–30	85–100
No. 8	0.093	—	—	0–10	—
No. 10	0.0787	32–41	20–36	—	—
No. 16	0.0465	—	—	0–5	—
No. 40	0.0165	14–24	9–19	—	—
No. 100	0.006	—	—	—	10–30
No. 200	0.0029	6–12	4–7	—	—

[+]Per VDOT (2020).
[++]Per AASHTO M 43 (2022g).
—Not specified.

Pit B Base Material: Fair—Good Drainage

In the preliminary stages of this work, a base optimization study was performed to understand the balance between permeability, stiffness, and strength for the 21A-DI with different amounts of fines content (FC), fine-sand content, and coarse material (Gebrenegus et al. 2022). The results reinforced the notion that lower FC and fine-sand content, or higher coarse content, improved drainability with relatively small differences in stiffness (i.e., RM). Because of the impracticality of modifying the 21A to achieve the desired drainage quality, VDOT 21B aggregates (table 3), which are specified to be coarser, with lower FC than 21A (VDOT 2020), were first proposed for the fair–good permeability pit B.

Chapter 6 discusses that the choice was not as simple as selecting 21B. A custom blend of 90 percent 21B and 10 percent No. 8 aggregates by weight was produced by a local granite (GR) quarry in Lorton, VA. The nomenclature for this material used herein is 21B:No.8-GR (VDOT 2020). A specific target gradation was created based on a 90:10 blend (table 4), with allowable ranges for each sieve size comparable to the VDOT-specified limits on unblended 21B.

Table 4. Percent passing for 90:10 blended aggregate base for pit B.

Sieve Size	90:10 21B:No. 8 (percent)
2-inch	100
1-inch	91–100
3/8-inch	48–60
No. 10	24–36
No. 40	15–23
No. 200	8–12

Figure 5 shows an oven-dried representative sample of the 21B:No.8-GR base material selected for pit B.

Source: FHWA.

Figure 5. Photo. 21B:No.8-GR at 90:10 mix ratio (oven dried).

Pit C Base Material: Excellent Drainage

An ATPB was selected for pit C because of its inherently high permeability. The gradation specifications used by WSDOT were used as a general guide, with a slightly coarser gradation specified in the PTF-3 contract (table 5). A No. 78 stone was initially evaluated for the ATPB because it met the WSDOT 3/4-inch gradation requirements (table 5); No. 78 has better stability and requires a less compactive effort than the more conventional No. 57 stone (Meyers 2021). Again, as will be discussed in chapter 6, the material selection was not as simple as specifying a No. 78 ATPB. Like 21B:No.8-GR, a blend of No.78 was needed to meet the requirements for stability and moisture susceptibility. As such, the No. 78 (table 5) was blended with No. 10 screenings (table 3) at a mix ratio of 85:15 percent by volume and treated with a target of 3.5 percent highly modified, polymer grade PG64E-22 (AASHTO M 320 (2023b)) asphalt binder (figure 6). Both aggregates in the blend were of diabase DI mineralogy acquired from a local quarry in Chantilly, VA. As such, the nomenclature used throughout is ATPB-No.78:No.10-DI.

Table 5. Gradation specifications for PTF-3 ATPB.

Sieve Size	Percent Passing			
	Grading 3/4+ WSDOT (2023)	PTF-3 ATPB	No. 78 (AASHTO 2022g)	No. 10 (AASHTO 2022g)
1.5-inch	—	—	—	—
1-inch	—	100	—	—
3/4-inch	100	88–100	100	—
1/2-inch	90–100	70–90	90–100	—
3/8-inch	40–80	—	40–75	100
No. 4	0–30	—	5–25	85–100
No. 8	0–20	0–15	0–10	—
No. 16	0–10	—	0–5	—
No. 100	—	—	—	10–30
No. 200	0–4	0.5–4.5	—	—

—Not specified.
+Minimum asphalt binder content is 3.5 percent.

Source: FHWA.

Figure 6. Photo. ATPB-No.78:No.10-DI at 85:15 mix ratio.

Subbase Material

The same SB was used in pits A, B, and C to isolate the influence of the base materials and their corresponding times to drain. To evaluate sustainability practices within PTF-3, a quarry byproduct material designated as No. 10 screenings (table 3) was selected (figure 7). The material was of GR mineralogy and, therefore, is designated as No.10-GR throughout.

Source: FHWA.

Figure 7. Photo. No.10-GR (oven dried).

INVERTED PAVEMENT EXPERIMENTS

Inverted pavement experiments were designed to serve as short-term studies in PTF-3 (figure 2). Lane 10 represents low-volume road design, while lane 11 represents a higher volume road design.

Pit D Base Material

The base layer of the pit D inverted pavement was constructed using the same 21B:No.8-GR blend as pit B (figure 5); however, the compaction during construction was higher, with a target unit weight of 100 percent of the maximum dry unit weight per the modified Proctor (i.e., AASHTO T 180 (AASHTO 2022a)).

Pit D Subbase Materials

Two different CTBs were explored for the inverted pavements: one with a conventional road base material and the other with the No. 10 quarry byproduct (AASHTO 2022g). Each lane is divided into halves, with the north half consisting of a No.10-GR aggregate—denoted as CTB-No.10-GR herein (figure 8)—and the south half consisting of a 21A-GR—denoted as CTB-21A-GR (figure 9) (VDOT 2020). Both materials were specified to have about 4 percent type IL portland-limestone cement by weight to target a UCS of 350 psi for the CTB. The actual cement contents of the delivered CTB-No.10-GR and CTB-21A-GR, as determined by the quarry using Virginia Test Method-40 (VDOT 2000), were 3.7 and 4.2 percent, respectively.

Source: FHWA.

A. Fresh CTB-No.10-GR.

Source: FHWA.

B. Cured CTB-No.10-GR.

Figure 8. Photos. CTB-No.10-GR.

Source: FHWA.

A. Fresh CTB-21A-GR.

Source: FHWA.

B. Cured CTB-21A-GR.

Figure 9. Photos. Cement-treated 21A-GR.

SUBGRADE

The subgrade across the pavement field, originally classified as an A-4 material in PTF-1 (Anderson et al. 1988), remained as part of PTF-3 (figure 10); however, the top 0.5 ft of the subgrade was reconditioned and then recompacted to 95 percent of its maximum dry unit weight per a new standard Proctor test (AASHTO T 99 (AASHTO 2022h)). Note that changing the grade across the 156-ft-wide pavement field to a 1-percent cross slope required the excavation of the subgrade to a progressively deeper depth of 1.56 ft between barrier walls 1 and 5, where the top of barrier wall 1 was built at the existing elevation of the second-generation pavement field.

Note that a Class Ⅱ Type E (FHWA 2014) polypropylene nonwoven geotextile separator was placed between the boundary of the subgrade and subbase across all lanes.

Source: FHWA.

Figure 10. Photo. Subgrade soil (oven dried).

SUMMARY OF SELECTED PTF-3 GEOTECHNICAL MATERIALS

Table 6 presents all materials used in the construction of the PTF for each pavement pit, layer, and mineralogy, along with sample identifications (IDs) used throughout this report.

Table 6. Locations, mineralogy, and sample IDs for all examined materials.

Material	Pit	Layer	Mineralogy	Sample ID
21A[+]	A	Base	DI	21A-DI
21B[+] blend with No.8[++] (90:10 target ratio)	B, D	Base	GR	21B:No.8-GR
ATPB-No.78[++] blend with No.10[++] with 3.5-percent asphalt binder*(85:15 target ratio)	C	Base	DI	ATPB-No.78:No.10-DI
No. 10[++]	A, B, C	Subbase	GR	No.10-GR
CTB—No. 10[++] with 4-percent cement	D (north half)	Subbase	GR	CTB-No.10-GR
CTB—21A[+] with 4-percent cement	D (south half)	Subbase	GR	CTB-21A-GR
Subgrade	A, B, C, D	Subgrade	N/A	SG

[+]Per VDOT (2020).
[++]Per AASHTO M 43 (2022g).
*PG 64E-22 per AASHTO M 332 (AASHTO 2023c).
N/A = not applicable.

A cross section of the as-designed time-to-drain and inverted pavement experiments are illustrated in figure 11.

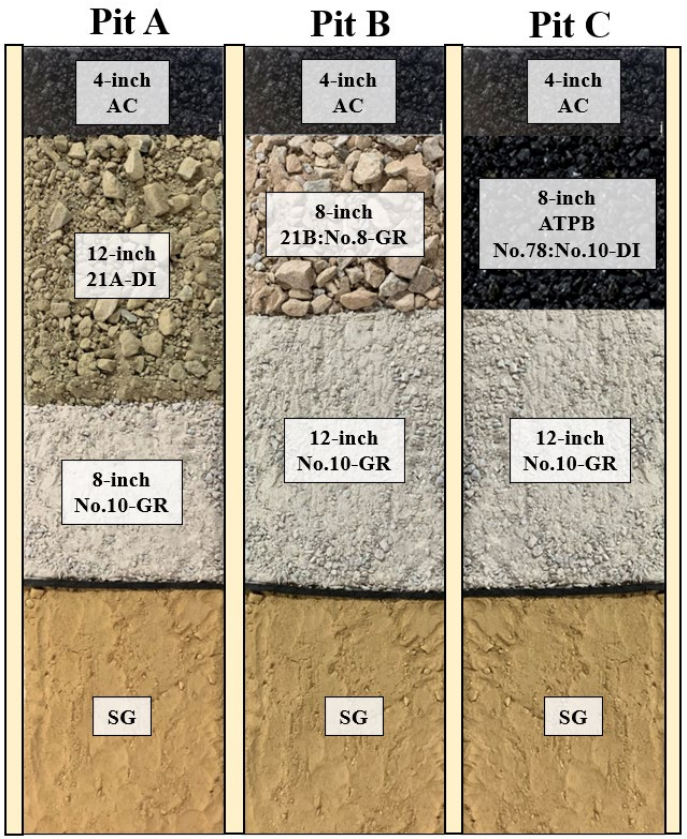

Source: FHWA.
Note: Dimensions shown are design targets, not as-builts.

A. Time-to-drain pits A, B, and C.

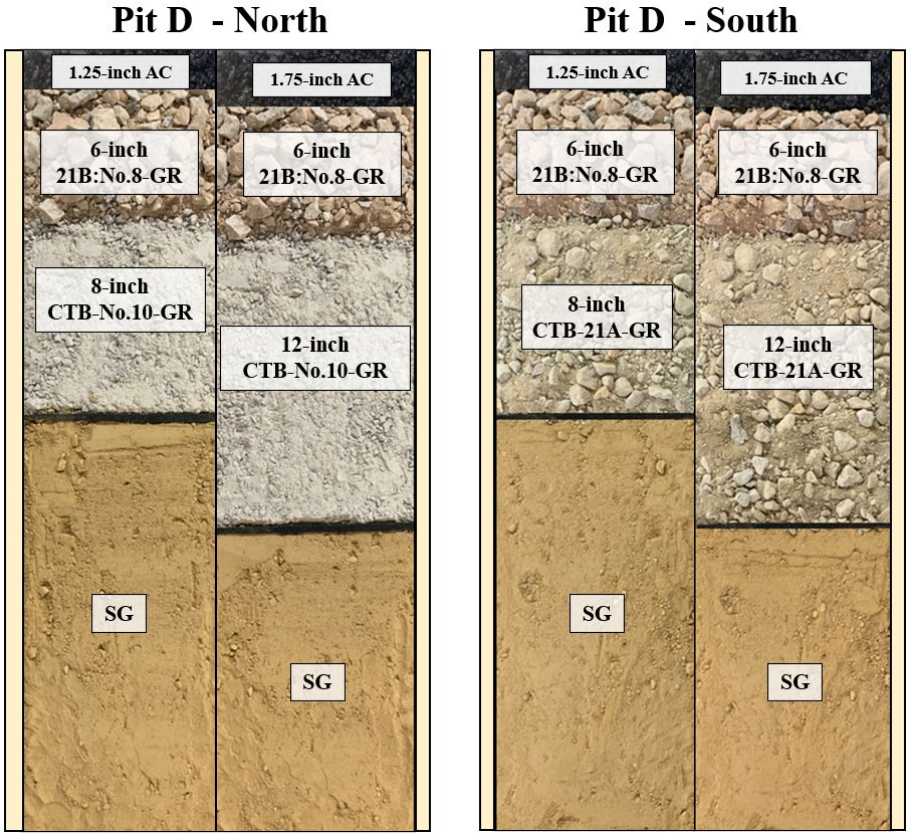

Source: FHWA.
Note: Dimensions shown are design targets, not as-builts.

B. Inverted pavement pit D.

Figure 11. Illustrations. PTF-3 targeted (not as built) pavement cross sections and thicknesses.

CHAPTER 4. SELECTED MATERIAL CHARACTERIZATION

As outlined in figure 3 and described in chapter 6, selection of the materials used to reconstruct the new pavement field was an iterative process. The process began with the design-development phase of the project, whereby laboratory samples obtained from various quarries were prepared and tested in the laboratory to ascertain their feasibility. A second round of testing occurred during the preconstruction phase, with the collection of production samples from the quarries or the asphalt paving plant to ensure the selected materials could be produced to meet the PTF's design objectives. A final round of sampling and testing occurred during construction, either during the placement of the new pavement layers or from onsite stockpiles. The results presented herein represent the best possible characterization of the materials placed at PTF-3 (table 7).

Table 7. Sample collection locations for PTF-3 material characterization.

Layer	Sample ID	Pit	Phase[+]	Sample Collection Location
Base	21A-DI	A	Construction	Stockpile from pavement field excavation
	21B:No.8-GR	B, D	Construction	Onsite stockpile delivered by the quarry
	ATPB-No.78:No.10-DI	C	Preconstruction	Asphalt plant preproduction
Subbase	No.10-GR	A, B, C	Construction	Onsite stockpile delivered by the quarry
	CTB-No.10-GR*	D	Preconstruction	Quarry
	CTB-No.21A-GR*	D	Preconstruction	Quarry
Subgrade	SG	A, B, C, D	Construction	In situ from four locations across the pavement field

[+]Preconstruction is defined as the phase where the quarry/plant prepared initial batches of the material to be delivered for construction; construction is defined as the phase during which the materials were delivered or excavated onsite.
*The Proctor and saturated permeability tests were conducted on materials collected from the quarry and mixed in the FHWA Geotechnical Laboratory during the design stage.

Regardless of the sample collection location, the first step before any laboratory testing was to oven dry the unbound materials for 24 h; the material used for the Atterberg limits (ASTM 2017a) was dried at 140 °F (60 °C), while the material for all other tests was oven dried at 110 °C. The dry aggregates were blended and quartered per method B of AASHTO R 76 (2020c). The research team then performed various tests to characterize the pavement subsurface layers' physical, mechanical, and hydraulic properties. A summary of the tests performed to characterize the materials, along with their corresponding standard test procedures and IDs, is shown in table 8.

Table 8. Material characterization tests and standards.

Properties	Test	Standard Test Method(s)
Physical	Washed/dry sieve	ASTM C117 (2023b)/C136 (2019)
	Hydrometer analysis	AASHTO T 88 (2022c)
	Standard Proctor	AASHTO T 99 (2022h)
	Modified Proctor	AASHTO T 180 (2022a)
	Moisture density of CTB	AASHTO T 134 (2019)
	Aggregate specific gravity and absorption	AASHTO T 84 (2022i)/85 (2022j)
	Soil-specific gravity and absorption	AASHTO T 100 (2022b)
	Atterberg limits	ASTM D4318 (2017a)
	Maximum specific gravity of ATPB	AASHTO T 209 (2023d)
	Bulk specific gravity of ATPB	AASHTO T 331 (2003e)
	Superpave™ gyratory compactor	AASHTO T 312 (2022k)
	Aggregate shape	AASHTO T 381 (2022l)
Mechanical	RM	AASHTO T 307 (2021a)
	Quick shear	AASHTO T 307 (2021a)
	CBR	AASHTO T 193 (2022m)
	Micro-Deval	AASHTO T 327 (2022n)
	Unconfined compressive strength of CTB	ASTM D1633 (2017b)
	Tensile strength ratio of ATPB	AASHTO T 283 (2022o)
Hydrologic	Constant head permeability	AASHTO T 215 (2023a)
	Falling head permeability	USACE (1970)
	Effective porosity	—

—User-defined.
USACE = U.S. Army Corps of Engineers.

GRADATION

One of the primary specifications in the selection of unbound and stabilized materials is their gradation. Materials must meet the specified gradation(s) for a project, which often includes tolerances per sieve size based on the number of tests performed (VDOT 2020). Along with the practical application of sieve analysis, the gradation properties provide insight into the material's engineering properties and guide the dimensions and procedures used in other ASTM and AASHTO test standards.

While typically performed more for subgrade materials, hydrometer analysis distinguishes the amount of clay and silt particles that can impact a material's hydrologic and mechanical properties. For some base and subbase materials, hydrometer analysis may be required to determine the smaller particle sizes necessary as inputs in pavement design to estimate the saturated coefficient of permeability (k_{sat}).

Methods

Samples of each material were initially washed to accurately determine the fines content (i.e., percentage passing the 0.0029-inch (No. 200) sieve) per ASTM C117 (2023b). This step is particularly important as a simple dry sieve could significantly underestimate the percentage of fines. Dry sieving was then performed on the remaining aggregates per ASTM C136/136M (2019). Hydrometer analysis was conducted per AASHTO T 88 (2022c) to determine the gradation of the particles finer than 0.0029 inch; the measured apparent specific gravity of the soil was used for each material. The gradations of the stabilized materials were determined based on their aggregate constituents without any asphalt or cement binder.

Results

Figure 12 shows the gradation curves for all materials.

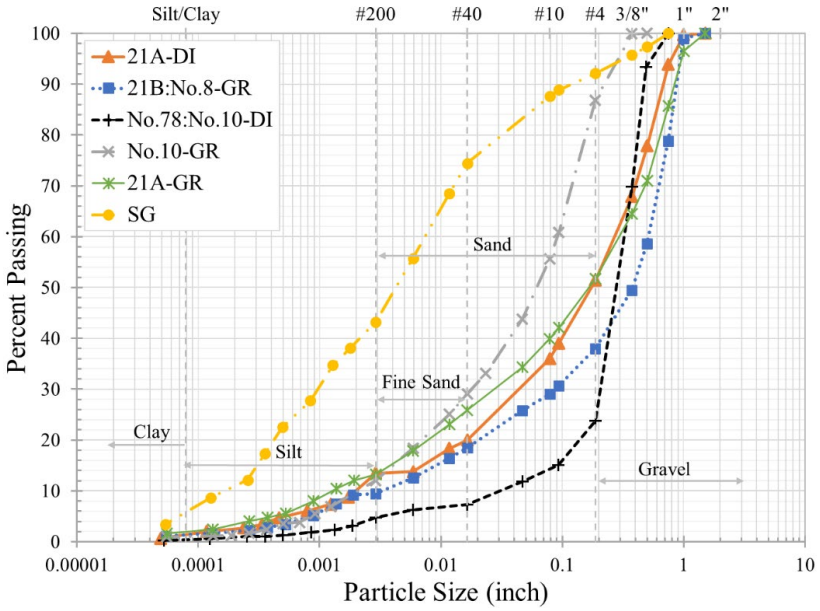

Source: FHWA.

Figure 12. Graph. PTF gradation curves.

The gradation data was used to determine the percentage of fines, sands, and gravels to classify the materials per the Unified Soil Classification System (USCS) (ASTM D2487 (2017c) and AASHTO M 145 (2021b), respectively) (table 9). The gravel-to-sand ratio (G/S), which has been shown to play a key role in the stability of unbound pavement materials, was also determined (Xiao and Tutumluer 2012; Qamhia and Tutumluer 2021; Hatipoglu, Cetin, and Aydilek 2020).

As desired, the materials for the time-to-drain experiments progressively got coarser and less well-graded from 21A-DI in pit A to ATPB-No.78-No.10-DI in pit C, even though they have the same AASHTO classification (table 9). For the inverted pavement experiments, the CTB constituents ranged from sand (No.10-GR) to gravel (21A-GR), which allowed for a good comparison of performance between a sandy CTB and a gravelly CTB in pit D.

Table 9. Gradation parameters.

Category	Sample ID					
	21A-DI	**21B:No.8-GR**	**No.78:No.10-DI**	**No.10-GR**	**21A-GR**	**SG**
D_{max} (inch)	1.5	1.5	0.75	0.5	1.5	0.75
D_{85} (inch)	0.6115	0.8270	0.4555	0.1804	0.7379	0.0660
D_{60} (inch)	0.2848	0.5172	0.3349	0.0913	0.3084	0.0078
D_{50} (inch)	0.1761	0.3818	0.2941	0.0636	0.1700	0.0045
D_{30} (inch)	0.0554	0.0877	0.2123	0.0181	0.0314	0.0010
D_{10} (inch)	0.0021	0.0035	0.0346	0.0024	0.0013	0.0002
C_u	135.6	147.8	9.7	38.3	237.2	44.4
C_c	5.1	4.2	3.9	1.5	2.5	0.7
gravel[+] (percent)	48.6	62.1	76.2	13.1	48.2	7.9
sand[+] (percent)	38.0	28.5	19.0	74.8	38.5	48.9
fine sand[+] (percent)	6.5	9.1	2.6	17.0	12.7	31.2
fines[+] (percent)	13.5	9.4	4.8	12.0	13.2	43.2
silt[+] (percent)	12.2	7.2	4.4	11.0	11.4	38.0
clay[+] (percent)	1.2	2.2	0.4	1.0	1.9	5.3
G/S	1.3	2.2	4.0	0.2	1.3	0.2
USCS classification	GM	GP-GM	GP	SM	GM	SC
AASHTO classification	A-1-a	A-1-a	A-1-a	A-1-b	A-1-a	A-4(1)

[+]Per ASTM D2487 (2017c).
D_{10}, D_{30}, D_{50}, D_{60}, D_{85} = diameter in which 10, 30, 50, 60, and 85 percent of particles are finer, respectively; D_{max} = maximum particle size; C_u = coefficient of uniformity; C_c = coefficient of curvature; GM = silty gravel; GP = poorly graded gravel; GP-GM = poorly graded gravel with silt; SM = silty sand; SC = clayey sand.
Note: AASHTO classification refers to the USCS (ASTM D2487 (2017c); AASHTO M 14 (2021b)).

The subgrade used across the entire pavement was classified as an AASHTO A-4(1) material, which generally agrees with the previous A-4(0) subgrade classification for PTF-2 (Bonaquist 1993). Regardless of the slight increase in the group index (GI), computed per AASHTO M 145 (2021b), the GI was still low for SG (table 9), indicating SG is a relatively good material for construction purposes (GI values of zero and above greater than 20 indicate good and very poor materials, respectively). However, as indicated in AASHTO M 145, detailed pavement structure design requires strength and performance tests performed under field conditions.

ATTERBERG LIMITS

Atterberg limits define the moisture contents under which fine-grained soils transition between different states of consistency. The liquid limit, plastic limit, and plasticity index are the most used Atterberg limits in engineering design and construction and were used to classify the material in conjunction with gradation.

Atterberg limits on the soil passing the No. 40 sieve for each unbound material were determined per ASTM D4318 (2017a) using the dry preparation procedure. The Liquid Limit Method A (Multipoint Method) and Plastic Limit Specimen Preparation Procedure 1 were followed. The samples for this test were collected from material that was oven dried to 60 °C. All the materials exhibited nonplastic behavior, except for the subgrade, which had a liquid limit of 31 and a plasticity index of 10, indicating the fines within the SG classified as a low-plasticity clay.

SPECIFIC GRAVITY AND ABSORPTION

The specific gravity (SpG) is a fundamental soil property and is a relative measure of the soil's density compared to water. SpG is needed for calculating void ratios, porosity, and the degree of saturation and is a direct input into the PMED (AASHTO 2020b). Therefore, using measured values rather than assumed values will provide a more accurate assessment of the material's properties.

The SpG expressed as either bulk (G_{sb}) (oven dry), G_{sb} (saturated surface dry (SSD)), or apparent (G_{sa}) was determined for both the fine and coarse aggregates used in the base and subbase materials. The apparent SpG of soils was also found for the subgrade. Absorption was also measured for all materials as a byproduct of the test.

Methods

For the unbound base and subbase materials, SpG and absorption were determined in accordance with AASHTO T 84 (AASHTO 2022i) and AASHTO T 85 (AASHTO 2022j) for fine and coarse aggregates, respectively. Coarse aggregates are defined as materials retained on the No. 4 (0.187-inch) sieve, while fine aggregates are those passing the No. 4 (0.187-inch) sieve. A weighted average of the coarse and fine aggregate fractions was then taken to determine each material's average SpG and absorption.

The ATPB specimens were prepared using a Superpave gyratory compactor per AASHTO T 312 (AASHTO 2022k). The specimen's maximum specific gravity (G_{mm}) and bulk specific gravity (G_{mb}) were then measured per AASHTO T 209 (AASHTO 2023d) and AASHTO T 331 (AASHTO 2023e), respectively. A PG 64E-22 AASHTO (2023c) polymer-modified binder, with a job mix formula (JMF)-specified specific gravity of 1.03, was used. The effective specific gravity (G_{se}) of the ATPB was also calculated based on the G_{mm}, the binder's specific gravity, and the binder percentage (WSDOT 2024).

Finally, for the subgrade soils, SpG tests were performed in accordance with AASHTO T 100 (2022b). Although this test only provides the apparent SpG compared to AASHTO T 84 (2022i), this method was selected due to the high percentage of fines in the subgrade (table 9) and the difficulty in fully mixing and saturating the sample required per AASHTO T 84 (2022).

Results

Table 10 presents the results of SpG tests for the unbound materials. DI is heavier than GR, which is reflected in the SpG values. The absorption percentage was also higher for DI relative to GR. For the ATPB, the G_{mm}, G_{mb}, and G_{se} were 2.756, 2.255, and 2.937, respectively.

Table 10. Specific gravity and absorption.

Sample ID	*Gsb* (Oven-Dry)	*Gsb* (SSD)	*Gsa*	Absorption (percent)
21A-DI	2.910	2.941	3.003	1.0
21B:No.8-GR	2.634	2.649	2.675	0.6
No.78:No.10-DI	2.893	2.919	2.969	0.8
No.10-GR	2.651	2.665	2.690	0.5
21A-GR	2.606	2.625	2.657	0.7
SG	—	—	2.699	—

—Value not calculated.

MOISTURE-DENSITY RELATIONSHIPS

Proctor compaction tests were performed for unbound and stabilized aggregates to determine the maximum dry density (MDD) and optimum moisture content (OMC). The target compaction level for each pavement subsurface layer was based on the standard or modified MDD and OMC of the material, as appropriate; hence, these parameters were used for quality control and assurance during the construction of PTF-3. The MDD and OMC were also used as the basis of compaction for all subsequent laboratory testing in this work.

Methods

Moisture-density relationships were developed for the unbound base and subbase aggregates per the modified Proctor method (AASHTO T 180, Method D (2022a)); the standard Proctor method (AASHTO T 99, Method C (2022h)) was used for the subgrade. Any particles retained on the 3/4-inch sieve were removed (i.e., scalped) before testing. If the percentage of scalped oversized fractions was higher than 5 percent, then the MDD and OMC were corrected based on the measured moisture content and an assumed *Gsb* of the oversized (coarse) particles.

For the CTBs, moisture-density relationships were initially determined on samples immediately after treatment of the aggregates with 4.5-percent content by weight per method B of AASHTO T 134 (2019). Note that AASHTO T 134 imparts the same compaction energy as the standard Proctor test (AASHTO T 99 (2022h)); however, any material retained on the 3/4-inch sieve is removed and replaced by an equivalent amount of aggregate between the 3/4-inch and No. 4 (0.187-inch) sieves. This practice was required for CTB-21A-DI but not for CTB-No.10-DI. Preliminary compaction testing of the CTB-No.10-DI and CTB-21A-DI with 0 and 4.5-percent cement content by weight found that the MDD and OMC of the CTBs were largely independent (less than 1 percent) of the cement content (Ghaaowd et al. 2022); hence, additional testing was not performed on the updated 4.0-percent cement content that was eventually selected for the PTF.

Results

Figure 13 shows the measured moisture-density relationships for the unbound and cement-treated materials.

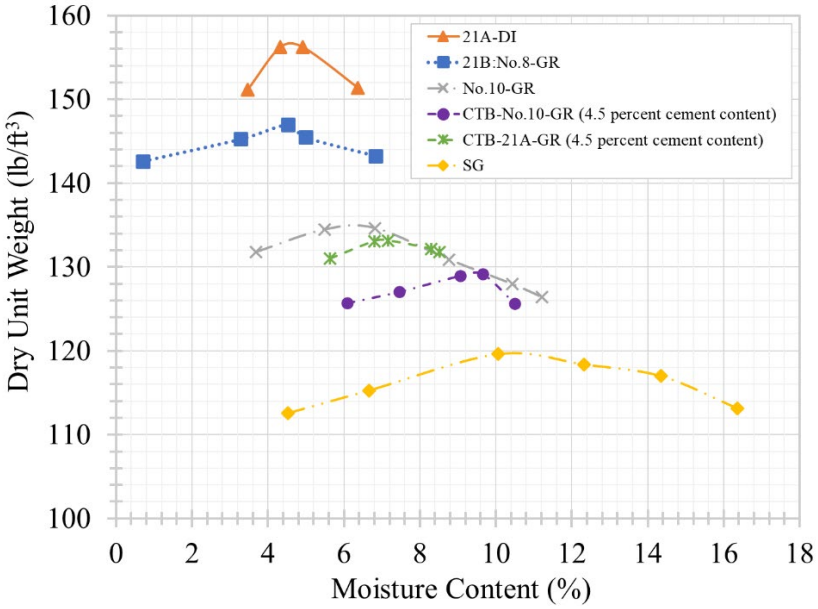

Source: FHWA.

Figure 13. Graph. Moisture to dry unit weight relationships.

Table 11 summarizes the MDD (γ_{dmax}) and OMC (w_{opt}) for each sample. Higher values of $\gamma_{d,max}$ and lower values of w_{opt} were obtained for the unbound base and subbase materials tested per modified Proctor compared to the CTBs and subgrade tested per standard Proctor.

Table 11. Moisture-density results.

Sample ID	AASHTO Standard	Oversized Particles (percent)	Before Oversize-Aggregate Correction		After Oversize-Aggregate Correction		Percent Compaction
			γ_{dmax} (lb/ft^3)	w_{opt} (percent)	γ_{dmax} (lb/ft^3)	w_{opt} (percent)	
21A-DI	T 180 (2022a)	6	154.6	4.8	156.7	4.6	95
21B:No.8-GR	T 180 (2022a)	21	141.6	5.7	147.0	4.5	95–100[++]
No.10-GR	T 180 (2022a)	N/A	135.0	6.3	—	—	95
CTB-No.10-GR[+]	T 134 (2019)	N/A	129.2	9.5	—	—	100
CTB-21A-GR[+]	T 134 (2019)	N/A	133.2	7.1	—	—	100
SG	T 99 (2022h)	N/A	119.5	11.5*	—	—	95

[+]Samples prepared at 4.5-percent cement content; results are assumed equal to samples prepared at 4.0-percent cement per Ghaaowd et al. (2022).
[++]Pit A had 95-percent compaction, and pit D had 100 percent.
*Target moisture content for laboratory tests was +2 percent of OMC (i.e., 13.5 percent).
—Oversize-aggregate (greater than or equal to three-quarter inch) correction not required.

To replicate anticipated field conditions, all base and subbase specimens were prepared at their OMC to a target dry unit weight based on their measured MDD and specified percentage of compaction (table 11). The subgrade, however, was tested 2 percent wet of optimum to better replicate the in situ moisture content at its depth, particularly since the mechanical properties can be significantly impacted by moisture (Ooi, Archilla, and Sandefur 2004; Nazarian et al. 2014; Narzary and Ahamad 2020). The average in situ water content of the collected samples was 12.6 percent, with a standard deviation of 2 percent.

DRAINAGE BEHAVIOR

The drainage behavior of the pavement was a key consideration in the design of PTF-3 and in the material selection for the time-to-drain experiments. Understanding the impact of drainage on pavement performance is critical in advancing the resilience of pavements. The hydraulic properties that describe drainage behavior that were of interest in this work were the saturated coefficient of permeability (k_{sat}) and effective porosity (N_e). These properties are direct inputs to determine the time to drain at 50 percent (t_{50}) and the drainage quality of the base and subbase materials.

Time to drain refers to the time required for a certain percentage of the unbound water to be removed from a pavement layer (AASHTO 1993). The fundamental equation to compute time to drain involves two factors: a time factor (T) and a material factor (m), as shown in equation 1 (Christopher, Schwartz, and Boudreau 2006).

$$t = T \times m \times 24 \quad (1)$$

Where:

t = time to drain (hours).
T relates to both pavement geometry (i.e., slope, width, and thickness of the drainage layer) and target drainage level (i.e., 50 percent for t_{50}).
m relates to material properties (i.e., permeability and N_e) of the layer.

The Casagrande and Shannon (1952) approach was used to determine t_{50}, as shown in equation 2.

$$t_{50} = \left(1.2 - \frac{0.4}{S_1^{\frac{1}{3}}}\right)\left[2US_1 - S_1^2 \ln\left(\frac{S_1+2U}{S_1}\right)\right] \times \frac{N_e W^2}{kh} \quad (2)$$

Where:

S_1 = a slope factor equal to h/WS.
h, W, and S = thickness, width, and slope of the base/subbase layer, respectively.
U = percent drainage (e.g., 0.5 for 50-percent drainage).
k = the coefficient of permeability.
N_e = the effective porosity (i.e., drainable porosity).

Coefficient of Permeability and Effective Porosity

Two of the key parameters in equation 2 are k and N_e, in which a higher k will reduce t_{50}, while a higher N_e will increase t_{50}. Several methods exist to determine k, typically constant head (CH) or falling head (FH) test methods, using either a rigid or flexible wall permeameter. CH tests with a rigid wall permeameter are more common for granular base materials, whereas FH tests using a flexible wall permeameter are suggested for finer soil materials like subgrade.

Methods

The coefficient of permeability of the base and unbound subbase was measured on specimens following a CH, FH, and EP sequential testing methodology. The SG was tested following an FH and EP testing scheme. In all cases, unscalped samples were tested.

The sample preparation procedure followed method B of AASHTO T 215 (2023). The unbound base materials (i.e., 21A-DI and 21B:No.8-GR) were compacted in three layers by a vibratory hammer in 6-inch diameter by 4.6-inch high acrylic, rigid wall permeameter mold to their respective, target MDD and OMC (table 11). No.10-GR and SG were compacted similarly, except in seven layers. The number of compaction layers was based on the D_{max} per AASHTO T 215 (2023). Note that a 5.9 x 10^{-4}-inch pore-size filter paper, a No. 100 mesh, and a perforated plate with 0.06-inch perforations were added to the top and bottom of the mold to encase the specimen and prevent loss of fines.

The specimens were weighed, and representative samples of the material before and after compaction were ovendried to determine the actual dry unit weight and moisture content. For ATPB-No.78:No.10-DI, a 6-inch diameter by 4.5-inch long test specimen was prepared using a Superpave gyratory compactor per AASHTO T 312 (2022k). Specimens were compacted to their lock point, in which no further vertical displacement happened during the gyration, and the number of gyrations reached 75. Perforated plates with 0.36-inch perforations were used rather than the other filters to ensure the coefficient of permeability measurements were not affected by the permeability of the filters. Once the permeameter was assembled, it was placed in a water tub and saturated from the bottom up overnight, as shown in figure 14-A.

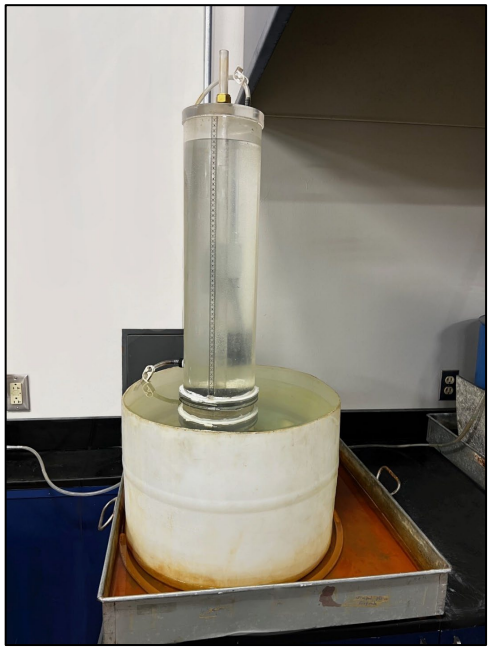

Source: FHWA.

A. CH-FH permeameter.

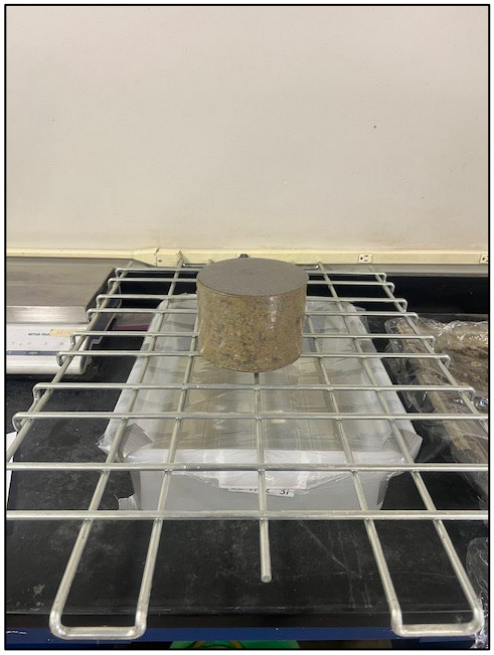

Source: FHWA.

B. Specimen drainage for EP.

Figure 14. Photos. CH-FH permeability and EP test setup.

CH tests were performed first per AASHTO T 215 (2023a). The coefficient of permeability corrected for the viscosity of water at 68 °F (20 °C) determined using the CH ($k_{20\,(CH)}$) for each hydraulic gradient was determined using equation 3.

$$k_{20\,(CH)} = R_T\left(\frac{Q \cdot L}{A \cdot t \cdot H}\right) = R_T\left(\frac{Q}{At}\right)\left(\frac{L}{H}\right) = R_T\left(\frac{V}{i}\right) \quad (3)$$

Where:

R_T = the ratio of water viscosity at test temperature to water at 68 °F (20 °C) (equation 4).
Q = volume of drained water.
L = length of the specimen.
A = cross-sectional area of the specimen.

t = time for elevation drop.
H = head difference between the inlet and outlet.
V = velocity.
i = hydraulic gradient (equal to H/L).

$$R_T = \frac{2.290\left(0.9842^{T_W}\right)}{T_w^{0.1702}} \tag{4}$$

Where T_w is the average temperature of the test water (readings were taken at the start and end of measurements).

CH tests for each material were performed at a minimum of three hydraulic gradients (i), starting with the lowest head of bubble emergence. Note that the CH test procedure (method B of AASHTO T 215 (2023a)) does not specify the minimum number of tests to run nor what increments to adjust subsequent heads. For granular bases, Jones and Jones (1989) reported that laminar flow, a key assumption in Darcy's law, does not occur at hydraulic gradients greater than 0.05; however, the U.S. Army Corps of Engineers (USACE 1986) defined turbulent flow for hydraulic gradients greater than 4.5 for dense sands.

Therefore, hydraulic gradients for the 21B:No.8-GR (pit B) and ATPB experiments ranged from 0.05 to 0.5, while the remainder of the materials were tested under hydraulic gradients ranging from 0.05 to 4.50. Curves were established using a temperature-corrected V, equal to $R_T(Q/At)$, as a function of i. The overall $k_{20\,(CH)}$ was then determined as the slope of the best-fit trendline through the measured data points (with the intercept forced to zero).

The laminar flow assumptions were verified by comparing the computed Reynold's number (Re) per equation 5. Jones and Jones (1989) reported the following two equations to verify the linear relationship between the computed Reynolds number and a friction factor (λ) (equation 6).

$$Re = \frac{\rho V d}{\mu} \tag{5}$$

$$\lambda = \frac{\Delta p d}{2\rho V^2} \tag{6}$$

Where:
ρ = density of water.
V = velocity.
d = characteristic diameter (assumed equal to D_{max}).
μ = absolute viscosity.
Δp = pressure loss over length.

Plotting the log of *Re* and log λ should provide a linear relationship for laminar flow per Jones and Jones (1989). In all tested specimens, the relationship was linear. Note that the hydraulic diameter through porous media is much smaller than the assumed D_{max} for *d*; however, since *d* influences *Re* and λ equally, the relationship will be the same regardless of the selected *d*.

After completing the CH measurements, an FH test was performed on the same specimen per the USACE (1970). The bubble tube was removed, and the chamber was filled with water, similar to the CH test. A plug was added to the top opening and removed at the start of the stopwatch. Readings were taken intermittently until the water level reached the tub's water level. Equation 7 (USACE 1970) was used to compute the coefficient of permeability for FH tests ($k_{20\,(FH)}$).

$$k_{20\,(FH)} = R_T \left(\frac{2.303 \cdot a \cdot L}{A \cdot t}\right) \log\left(\frac{h_o}{h_1}\right) \tag{7}$$

Where:

R_T = the ratio of the viscosity of water at test temperature to water at 20°C (Eq. 4),
a = cross-sectional area of the reservoir tube.
A = area of the specimen.
h_o = initial head of water.
h_1 = final head of water.

Note that with this setup, *a* was equal to *A*, effectively canceling those terms from equation 7.

Finally, after taking the final readings from the FH tests, an EP test was conducted to measure N_e. Christopher et al. (2006) defined N_e as the ratio of the volume of water that can drain under gravity from a sample to the total volume of the sample. No currently accepted AASHTO or ASTM standard exists for EP testing; as such, a simple method whereby the specimen within the permeameter was allowed to drain for 24 h, as shown in figure 14-B, with weight measurements taken before, after, and intermittently throughout the test. To ensure drainage and not evaporation of the water within the specimen, the tops of the specimens were wrapped in plastic.

N_e was calculated as the volume of drained water after 24 h by the total specimen volume. Alternatively, effective water content (w_e) within the specimen was also obtained by oven drying at the conclusion of the test, and N_e was calculated according to equation 8 (Federal Aviation Administration 2008).

$$N_e = 1 - \frac{\gamma_d}{(G_{sb})(\gamma_w)}(1 + G_{sb} w_e) \tag{8}$$

Where:

γ_d = dry unit weight of the soil.
G_{sb} = bulk specific gravity of solids.
γ_w = unit weight of the water.

FH tests using an asphalt permeameter were selected for the CTBs because of their anticipated low permeabilities (Quang and Chai 2015). No AASHTO or ASTM standard exists for cement-treated aggregate. As such, a FDOT method for measuring the permeability of compacted asphalt paving mixtures, designated as FM 5-565 (2015), was used as guidance. Ghaaowd et al. (2022) provide additional details on permeability testing of CTBs.

The CTB specimens were mixed at the 4-percent target cement content and optimum water content (table 11). Each specimen was then compacted in five layers in a 6-inch diameter by 4-inch high split Proctor mold to MDD (table 11) and cured in a humidity chamber at 69.8 °F (21 °C) and 95-percent humidity. After 24 h, the specimens were extruded, wrapped in plastic sheeting, and placed back into the humidity chamber for 7 d. Before testing, specimens were soaked in water overnight. After curing, the specimens were wrapped in a latex membrane and were tested in an asphalt permeameter (figure 15).

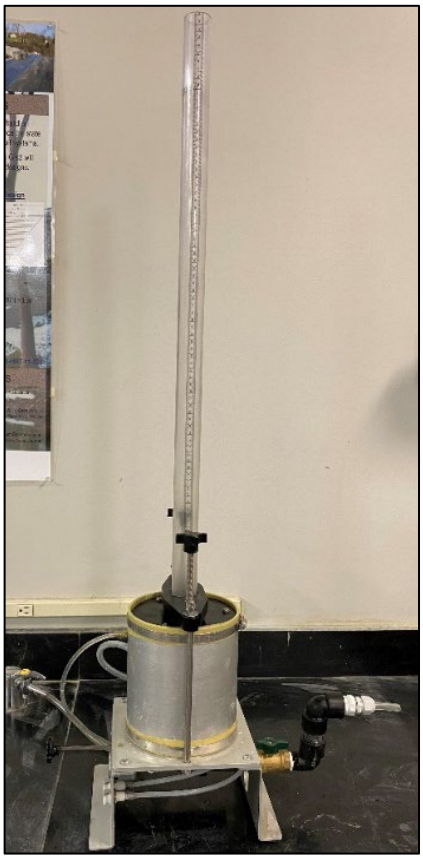

Source: FHWA.

Figure 15. Photo. CTB FH permeability test setup.

Results

Table 12 presents the saturation of the specimens at the beginning and end of the EP measurements. Most specimens were saturated during the testing. The time-to-drain layers drained as expected, with the ATPB on the complete opposite drainage spectrum (much higher) compared to the rest.

Table 12. Saturation at end of FH test and after 24 h of drainage.

Sample ID	Saturation (percent)	
	At End of FH Test	At End of 24-h Drainage
21A-DI	100	85.5
21B:No.8-GR (pit B)	100	83.3
21B:No.8-GR (pit D)	100	90.4
ATPB-No.78:No.10-DI	100	24.3
No.10-GR	96.0	80.1
SG	100	98.0

Table 13 presents the k_{20} and N_e results for all materials. No significant difference existed when the researchers compared the CH and FH methods with low-permeability materials. When comparing the two more permeable materials, the CH test tends to overestimate or the FH test underestimates the permeability. Note the drastic difference in permeability between the bases of pits B and D. Another specimen was compacted to determine the accuracy of the 100-percent compacted 21B:No.8-GR. Similar results were measured, opening discussion in compaction methodology that will be addressed in chapter 7.

Table 13. Coefficient of permeability and EP results.

Sample ID	$k_{20\,(CH)}$ (ft/day)	$k_{20\,(FH)}$ (ft/day)	N_e (percent)	
	Linear (AASHTO T 215 (2023a))	USACE (1970)	Measured	Calculated (equation 6)
21A-DI	1.739	2.227	4.3	2.7
21B:No.8-GR (pit B)	66.011	11.280	3.0	2.5
21B:No.8-GR (pit D)	0.007	0.006	1.2	−2.6
ATPB-No.78:No.10-DI	2,621.034	1,608.662	15.8	—
No.10-GR	1.713	0.995	3.6	4.5
CTB-No.10-GR	—	0.011	—	—
CTB-21A-GR	—	0.003	—	—
SG	—	0.008	0.8	−1.8

—Not calculated.

Presented in figure 16 and figure 17 are the permeability measurements for the CHs and FHs, respectively. The CH tests show a distinct vertical trend of velocity to gradient for highly permeable specimens, while the trend phases out horizontally when moving from more to least permeable (pit D). Interestingly, specimens 21A-DI and No.10-GR exhibit an identical relationship between velocity and gradient. The high drainage speed of the ATPB necessitated a 96-percent scaling of values for comparison purposes. For the FH tests, one representative measurement is shown for each material.

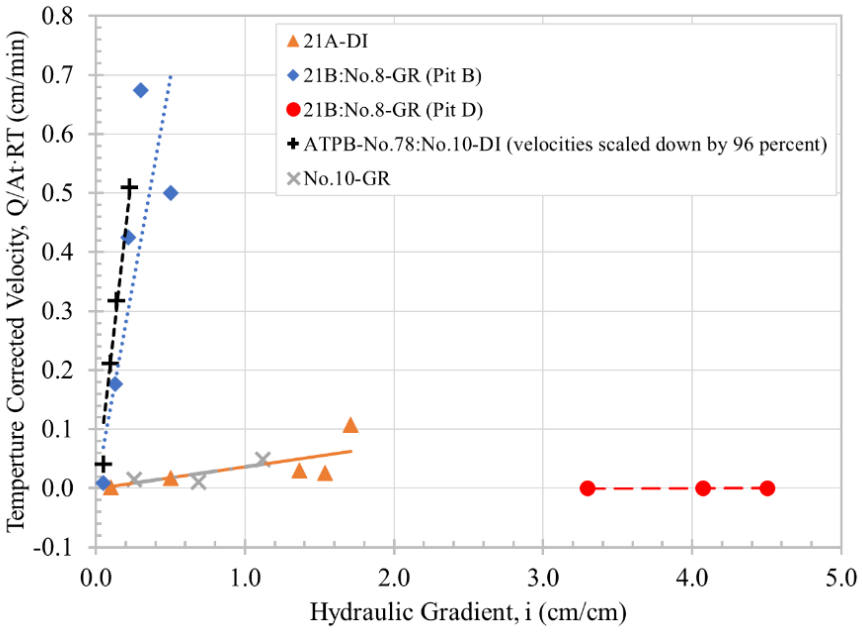

Source: FHWA.

Figure 16. Graph. CH trials.

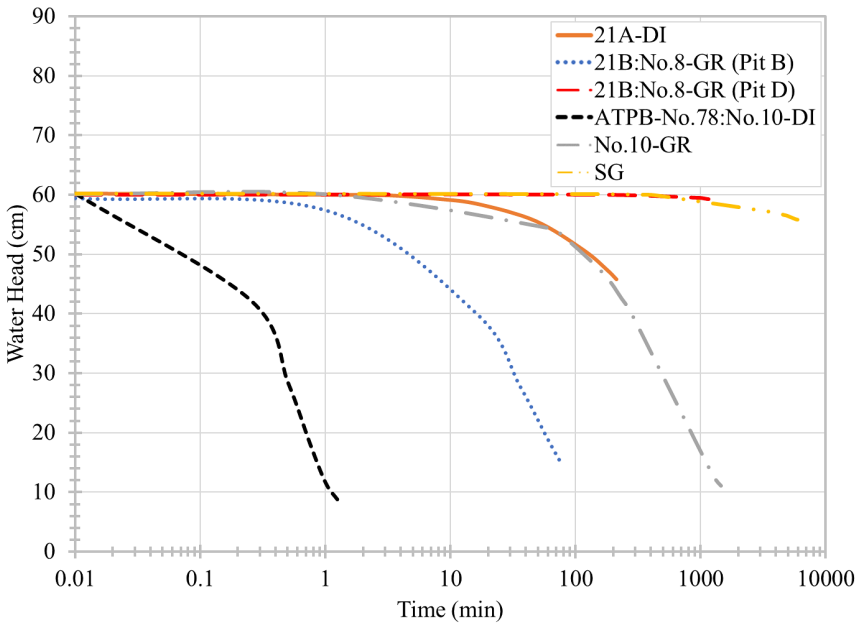

Source: FHWA.

Figure 17. Graph. FH permeability results.

Time To Drain

Permeability and EP test results are used to calculate t_{50} using equations 1 and 2 based on the measured (table 14) and calculated (table 15) effective porosity. As designed, pits A–C drainage qualities go from poor to good to excellent. For 21B:No.8-GR pit B, the drainage quality misses

the mark for good when computed with the FH permeability by 1 d; however, comparatively, the value is far better than the traditional pit A material. When comparing the N_e in equation 2, the lower measured or computed values provide a lower drainage quality than the higher effective porosity. Note that the CTB EP was not measured, and as such, the time to drain is not computed or presented.

Table 14. Test results for time to drain at 50-percent drainage using measured N_e.

	Linear (AASTHO T 215 (2023a)		USACE (1970)		Quality of Drainage[+]	
Sample ID	Days	Hours	Days	Hours	Linear	USACE (1970)
21A-DI	14	339.0	11	264.7	Poor	Poor
21B:No.8-GR (pit B)	0.3	8.2	2.0	48.1	Good	Fair
21B:No.8-GR (pit D)	921	22,098.1	1,055	25,318.3	Very Poor	Very Poor
ATPB-No.78:No.10-DI	0.05	1.1	0.07	1.8	Excellent	Excellent
No.10-GR	15	290.1	26	499.4	Poor	Poor
SG	N/A	N/A	602	14,450.7	N/A	Very Poor

[+]Per AASHTO (1993): very poor (t_{50} > 1 mo), poor (t_{50} within 1 mo), fair (t_{50} within 1 w), good (t_{50} within 1 d), and excellent (t_{50} > 2 h).

Table 15 Test results for time to drain at 50-percent drainage using calculated N_e.

	Linear (AASHTO T 215 (2023a)		USACE (1970)		Quality of Drainage[+]	
Sample ID	Days	Hours	Days	Hours	Linear	USACE (1970)
21A-DI	8.9	215	7.0	168	Poor	Fair
21B:No.8-GR (pit B)	0.3	6.7	1.6	39	Good	Fair
21B:No.8-GR (pit D)	—	—	—	—	N/A	N/A
ATPB-No.78:No.10-DI	N/A	N/A	N/A	N/A	N/A	N/A
No.10-GR	N/A	N/A	N/A	N/A	N/A	N/A
SG	N/A	N/A	—	—	N/A	N/A

[+]Per AASHTO (1993): very poor (t_{50} > 1 mo), poor (t_{50} within 1 mo), fair (t_{50} within 1 w), good (t_{50} within 1 d), and excellent (t_{50} > 2 h).
—Using calculated N_e-provided negative values = not reported.

CYCLIC STRENGTH BEHAVIOR

Pavement layer design is influenced by evaluating the resilient modulus of materials as it directly impacts the pavement's ability to withstand traffic loads over time. Measuring the modulus of a material is an important parameter used directly in pavement layer design within the MEPDG and AASHTO design guides (AASHTO 2020a, 2020b). Two typical methods of measure are used: mechanistic and empirical. The latter was discussed in the preceding section. For a direct measure, repeated loading and unloading experienced by pavements are simulated in the laboratory on compacted specimens to understand the cyclic behavior of the materials, which, in turn, provides a resilient modulus (M_r).

After the completion of M_r testing, quick shear (QS) measurements can be conducted on the same specimen, providing shear strength. The QS test is a supplementary measurement, offering extra insight into the material's behavior under shear stress but not fundamentally driving design decisions.

Another measure, with no official methodology, is the strain experienced by a material. Collectively called permanent deformation/strain, it occurs when a material no longer returns to its original volume. Like M_r testing, repeatedly loading a specimen at high axial and confining stresses subjects the material to loading similar to the load path of a wheel. With sufficient cycles, the material will consolidate, and the before-and-after change in height defines a permanent strain.

Resilient Modulus

The E of unbound pavement materials is generally characterized in terms of its M_r (Christopher, Schwartz, and Boudreau 2006); the M_r refers to the ratio of the applied cyclic stress to the recoverable (elastic) strain after many cycles of repeated loading and is a direct measure of a material's stiffness. M_r is the single most important unbound material property in most current pavement design procedures, independent of size or shape. Outside of the elastic response of materials is the nonrecoverable strain that is accumulated over repeated loadings, referred to as the permanent strain (PS) or permanent deformation.

M_r is measured in the elastic recoverable range of the loading–unloading sequence. Pavement layers experience constant confinement and fluctuating load conditions throughout their life. The RM test simulates the loading conditions in the laboratory with different applied confining and axial stresses. By fitting the data at each of these different stress states, a model can be developed to determine a summary M_r (M_{rs}) at a known or specified stress state corresponding to in-service pavement conditions.

Methods

RM tests were performed on 6-inch diameter by 12-inch-long specimens in accordance with AASHTO T 307 (2021a) (figure 18). All tests were performed on unscalped specimens. Unbound materials were compacted with a vibratory hammer in six lifts to their target, corrected MDD and OMC (table 11). The ATPB sample was compacted fresh to its target density in six lifts. The target density was similar to the Superpave gyratory compacted permeability specimen. The ATPB material for every lift was placed in the oven at 284 °F (140 °C) before compaction to minimize any heat dissipation during the process.

The target densities of the CTB-No.10-GR and CTB-21A-GR were based on the same density as the specimens prepared by the quarry for UCS testing. In this case, CTB-21A-GR particles retained on the 3/4-inch sieve were scalped without replacement, leading to a lower density compared to the MDD obtained from standard compaction testing (table 11). Both CTBs were cured for 28 d before the RM test. The measured dry density of CTB-No.10-GR and CTB-21A-GR were 127.0 lb/ft^3 and 126.0 lb/ft^3, respectively.

RM testing started with a conditioning sequence of 500 cycles under a σ_3 of 15 psi or 6 psi followed by 15 sequences of a haversine-shaped load form using different confining and axial

loads depending on the material (base/subbase or subgrade). A computed M_r as a function of the load sequences was fitted using the generalized MEPDG stress-dependent constitutive model (Transportation Research Board 2004), as shown in equation 9.

$$M_r = k_1 p_a \left(\frac{\theta}{p_a}\right)^{k_2} \left(\frac{\tau_{oct}}{p_a} + 1\right)^{k_3} \quad (9)$$

Where:

k_1, k_2, k_3 = regression coefficients.
ρ_a = atmospheric pressure.
Θ = bulk stress
τ_{oct} = octahedral shear stress

The stress values σ_1, σ_2, σ_3 are principal stresses and σ_d is the deviatoric stress (equal to $\sigma_1 - \sigma_3$). This model is used to determine M_{rs} for a given stress state. For base and subbase aggregates, M_{rs} was selected at the stress state corresponding to a σ_3 of 5 psi and a maximum axial stress, σ_{max}, of 15 psi (i.e., load sequence 6 of the RM test); for the subgrade, M_{rs} corresponds to σ_3 and σ_{max} of 2 and 6 psi, respectively (i.e., sequence 13 of the RM test). Note that the actual confining and axial stresses are slightly different for each sequence than the nominal values presented in AASHTO T 307 (2021a).

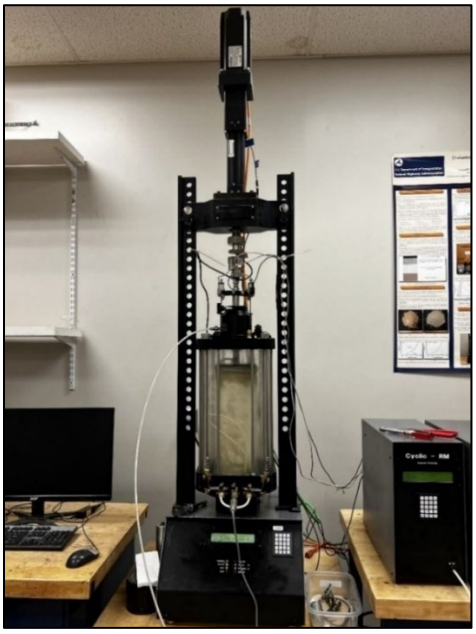

Source: FHWA.

Figure 18. Photo. RM testing apparatus.

Results

Table 16 summarizes the MEPDG model parameters extracted from the nonlinear regression fitting, as well as the M_{rs} computed for all examined materials (AASHTO 2020a). As expected,

the stabilized specimens exhibited the highest stiffness relative to the other materials, while SG produced the lowest. Of note is the coefficient of determination measure, R^2, for the resulting RM model per equation 9 (table 16); low R^2 values, such as those seen for 21B:No.8-GR, suggest outliers or anomalous data points may exist that need further investigation. The root mean square error (RMSE) is presented as a measure of the accuracy of the regression fitting between the measured and predicted M_r. Larger numbers, such as those seen in 21B:No.8-GR and the ATPB, show the weight that anomalous data points have on M_{rs}.

Table 16. RM and QS test results.

Sample ID	M_{rs} and Model Parameters						σ_{dmax} (psi)	τ_{max} (psi)
	k_1	k_2	k_3	M_{rs} (psi)	R^2	RMSE (psi)		
21A-DI	979.3	0.6409	0.0940	23,591.3	0.994	1,051.0	74.7	37.4
21B:No.8-GR (pit B)	3,336.5	0.4993	−1.2412	43,001.8	0.217	19,880.9	93.2	46.6
21B:No.8-GR (pit D)	4,320.4	1.1799	−2.8687	47,750.4	0.532	30,843.7	153.2	76.6
ATPB-No.78:No.10-DI	2,653.5	0.5770	−0.0452	57,828.0	0.818	15,125.6	166.6	83.3
No.10-GR	878.8	0.7116	−0.4140	18,238.8	0.988	1,081.1	44.2	22.1
CTB-No.10-GR	2,646.5	-0.0271	1.5757	70,840.4	0.971	3,319.8	417.2	208.6
CTB-21A-GR	3,225.6	0.1819	0.6005	68,333.4	0.900	4,528.2	271.7	135.9
SG	2,406.5	0.1481	−6.2688	11,384.9	0.667	7,215.2	25.1	12.6

Regardless, the results suggest that along with differences in drainage, the base materials in the time-to-drain experiments also got progressively stronger, with 21A-DI in pit A the weakest and ATPB-No.78:No.10-DI the strongest (table 16). Interestingly, the M_{rs} of No.10-GR is close to that of the conventional 21A-DI, suggesting that this type of quarry byproduct may be a suitable replacement as a base material in terms of stiffness. In fact, comparing the VDOT RM results for State calibration into MEPDG (Hossain and Lane 2015), both materials are within the range of 10,610 to 30,034 psi. This result is further supported by the results of the inverted pavement materials, where CTB-No.10-GR had a similar stiffness to CTB-21A-GR (table 16).

Table 17 and table 18 present the measured PS at the end of each cycle and the measured M_r per sequence number. With a few errant readings, the PS increases with each subsequent sequence. Expectedly, the PS at the end of the tests was the lowest for the stabilized materials. A peculiar distinction is measured between the 95-percent compacted pit B and 100-percent compacted pit D 21B:No.8-GR. The PS of pit B is less than pit D, yet the measured M_r is much higher in pit D, suggesting the density and M_r correlate but not PD. Further testing would need to validate this result as anomalous or case dependent. The sequences of the SG specimen show how the combination of the confining and axial stresses directly influences the stiffness of the material.

Table 17. Measured base and subbase PS and RM of each testing sequence.

Sequence No.	Stress (psi)		21A-DI		21B:No.8-GR (Pit B)		21B:No.8-GR (Pit D)		ATPB-No.78:No.10-DI		No.10-GR		CTB-No.10-GR		CTB-21A-GR	
	σ_3	σ_{max}	PS (%)	M_r (psi)	PS (%)	M_r (psi)	PS (%)	M_r (psi)	PS (%)	M_r (psi)	PS (%)	M_r (psi)	PS (%)	M_r (psi)	PS (%)	M_r (psi)
0	15	15	0.196	38,250	0.075	49,710	0.125	80,162	0.052	97,714	0.215	33,567	0.051	62,814	0.034	79,231
1	3	3	0.133	13,832	0.016	105,360	0.031	141,640	−0.007	42,295	0.130	12,618	0.025	47,699	0.009	60,189
2	3	6	0.141	16,477	0.020	25,820	0.037	30,538	−0.004	39,956	0.148	13,222	0.028	54,357	0.010	49,828
3	3	9	0.157	16,702	0.035	29,918	0.053	22,481	0.003	45,019	0.188	13,574	0.030	53,554	0.012	52,012
4	5	5	0.160	19,297	0.041	72,401	0.063	61,368	0.009	52,742	0.190	16,195	0.030	52,442	0.014	53,233
5	5	10	0.170	21,393	0.047	34,213	0.081	37,673	0.015	51,026	0.205	17,219	0.032	53,442	0.017	56,858
6	5	15	0.199	23,962	0.062	31,934	0.104	36,067	0.024	53,384	0.266	17,455	0.037	65,448	0.021	66,607
7	10	10	0.211	27,955	0.076	45,935	0.124	94,296	0.039	74,006	0.280	24,620	0.041	55,317	0.027	71,134
8	10	20	0.243	35,624	0.095	53,104	0.146	59,389	0.051	84,524	0.324	25,857	0.051	76,657	0.034	77,962
9	10	30	0.323	36,296	0.126	43,900	0.188	58,102	0.073	76,546	0.485	25,326	0.067	106,000	0.043	91,945
10	15	10	0.321	33,783	0.127	61,725	0.189	171,170	0.074	58,035	0.479	29,782	0.062	54,919	0.041	74,542
11	15	15	0.326	36,473	0.129	54,995	0.191	90,497	0.077	70,727	0.483	29,920	0.065	70,890	0.043	75,178
12	15	30	0.350	43,985	0.145	55,205	0.206	75,617	0.093	114,160	0.525	32,433	0.078	103,000	0.051	93,309
13	20	15	0.352	44,372	0.149	81,986	0.209	177,510	0.098	121,900	0.526	36,289	0.077	69,729	0.052	74,573
14	20	20	0.357	46,215	0.151	70,862	0.210	106,590	0.101	139,310	0.529	35,278	0.080	78,164	0.053	87,065
15	20	40	0.403	54,307	0.174	60,416	0.235	85,926	0.117	103,420	0.612	39,486	0.104	136,000	0.069	114,300

Table 18. Measured subgrade PS and RM of each testing sequence.

Sequence No.	Stress (psi)		SG	
	σ_3	σ_{max}	PS (percent)	M_r (psi)
0	6	4	0.245	12,318
1	6	2	0.241	19,866
2	6	4	0.247	12,335
3	6	6	0.319	12,318
4	6	8	0.417	10,649
5	6	10	0.518	10,534
6	4	2	0.446	46,454
7	4	4	0.446	15,392
8	4	6	0.451	10,569
9	4	8	0.468	10,044
10	4	10	0.500	8,953
11	2	2	0.398	32,795
12	2	4	0.398	12,543
13	2	6	0.408	8,238
14	2	8	0.432	6,986
15	2	10	0.502	6,569

QS Test

Immediately following the RM test, a QS test was performed on the same specimen. The QS test is a rapid, triaxial shear test performed under a specified confining stress. The test provides a measure of the maximum deviatoric stress (and thus maximum shear stress) of the materials under the test conditions.

Methods

QS tests were performed per AASHTO T 307 (2021a), whereby an axial strain rate of 1 percent per minute was applied to the sample under 5 psi of confining pressure. The σ_{dmax} was then determined as the peak of the resulting deviatoric stress–strain curve. Like RM testing, subgrade soils should be tested under a different stress state than base materials; however, for a more direct comparison between materials, the QS tests on the subgrade were performed under the same 5 psi of confining stress (versus 4 psi per AASHTO T 307).

Results

Figure 19 presents the deviatoric stress as a function of axial strain from the QS tests, and table 16 summarizes the peak σ_{dmax} and τ_{max} measured for all materials.

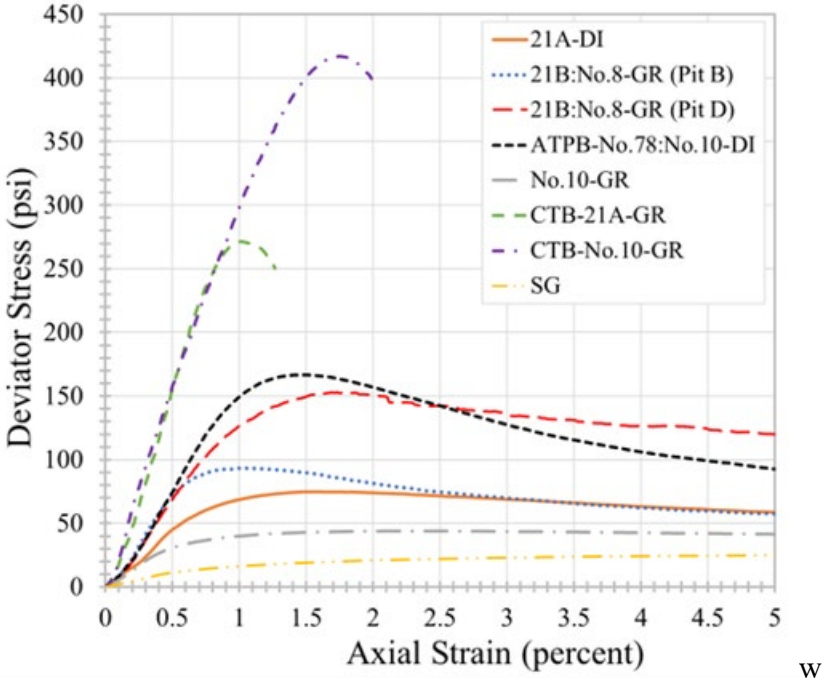

w

Source: FHWA.

Figure 19. Graph. QS test results at confining stress of 5 psi.

MONOTONIC STRENGTH BEHAVIOR

Monotonic strength behavior is the ability of a material to resist the application of continuous stress in a uniaxial direction, and it suggests how the material will perform under constant, static loading. Unlike cyclic load tests, samples in monotonic tests may be confined in terms of their compaction mold, but no confining pressure is applied, only normal stress.

CBR

CBR is a commonly used test method to determine the strength of unbound materials such as base aggregates for pavement construction. This test involves preparing a specimen within a mold, which is then subjected to a standardized rate of penetration by a piston for a predetermined penetration (AASHTO T 193 (2022m)). Although CBR is not a direct measure of the rutting potential and performance of base aggregates under dynamic traffic loading (Tanyu, Ullah, and Akmaz 2021), transportation agencies are familiar with the value, with higher CBR values indicative of a stronger material. Moreover, relationships between CBR and M_r for unbound and subgrade materials have been established as a level 2 input within MEDPG (AASHTO 2020a).

Methods

All CBR tests were performed in accordance with AASHTO T 193 (2022m) using the load frame shown in figure 20. Materials retained on the 3/4-inch sieve were scalped and replaced with materials retained between the 3/4-inch and No. 4 sieve (0.187-inch) sizes. Scalping only

pertained to 21A-DI and 21B:No.8-GR; unscalped samples were also tested to compare the impact of scalping for these two materials.

All base and subbase materials were compacted to their target MDD and OMC (table 11). For the scalped samples (i.e., 21A-DI and 21B:No.8-GR), the target compaction level was based on the uncorrected, maximum dry unit weight and OMC. The level of sample compaction is a disconnect from the CBR standard (AASHTO T 193-22 (2022m)), where another Proctor test should be done with an equivalent amount of material passing the 3/4-inch sieve and retained on the No. 4 sieve to those scalped above the 3/4-inch sieve. The unscalped samples were compacted to their uncorrected MDD and OMC (table 11).

Compaction was performed in five lifts via a vibratory hammer to achieve a specimen dimension of 6-inch diameter and 4.6-inch height. All tests were performed under soaked conditions after submerging the samples in water for 4 d (96 h) before testing; swell height during this period was measured using a digital dial gauge. Additional CBR tests were also performed on unsoaked samples for comparison. In either case, a surcharge with a total weight of 10 lb (4.54 kg), the minimum required per AASHTO T 193 (2022m), was placed on all materials to simulate the in situ overburden. The minimum 10 lb of surcharge is acceptable for the base materials, where the only overburden is the AC surface layer; however, additional weight could have been placed on the No.10-GR and SG specimens to account for their increased overburden in the field, which would likely result in a lower CBR than measured in this work.

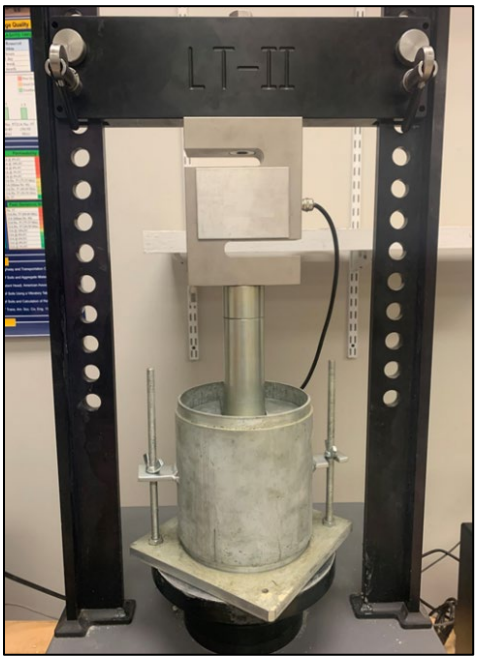

Source: FHWA.

Figure 20. Photo. Test setup for CBR test.

Results

Figure 21 presents soaked and unsoaked CBR test results up to 0.3-inch penetration for the unscalped samples. The comparative results for the scalped and unscalped 21A-DI and 21B:No.8-GR samples are plotted in figure 22. In cases where initial penetration took place without a proportional increase in resistance to penetration, the origin for penetration was corrected using an 80-point forward-moving average to extend the best-fit line in the straight portion of the stress–strain curve.

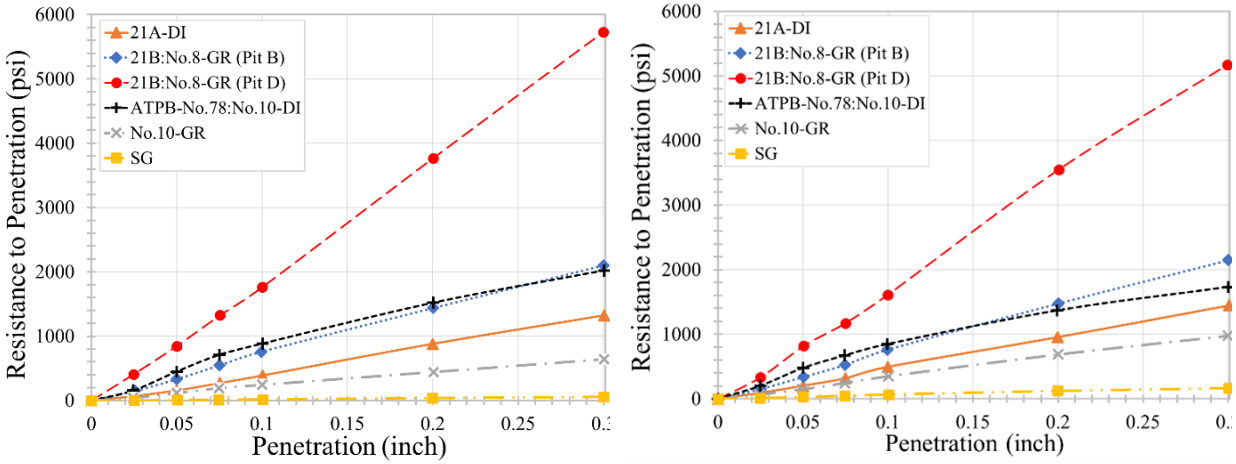

Source: FHWA.

A. Soaked.

Source: FHWA.

B. Unsoaked.

Figure 21. Graphs. CBR test results for unscalped samples.

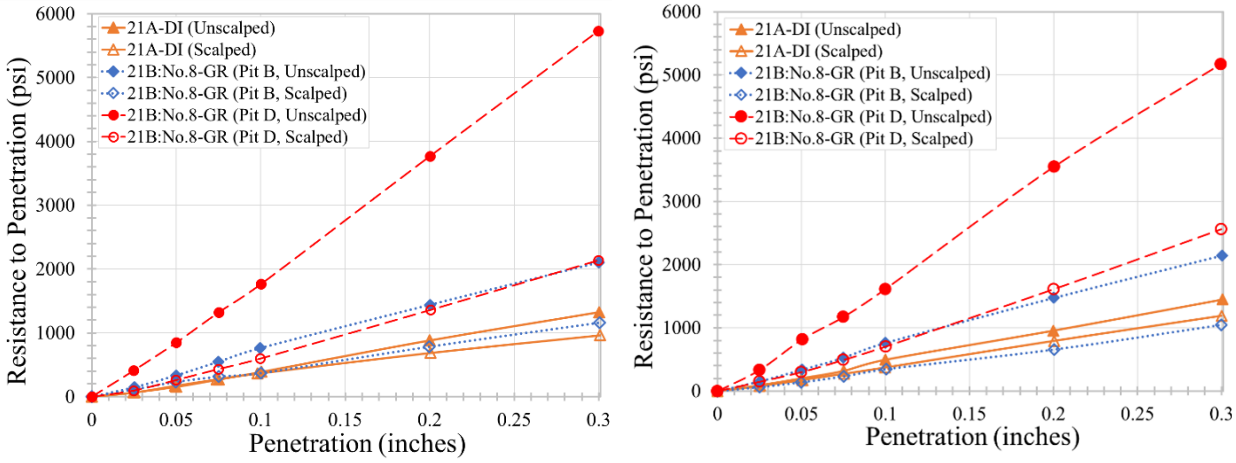

Source: FHWA.

A. Soaked.

Source: FHWA.

B. Unsoaked.

Figure 22. Graphs. CBR test results for scalped versus unscalped samples.

Based on the test results, CBR values at the corrected 0.2-inch penetration were consistently higher than at 0.1-inch penetration and were thus selected (table 19). Table 19 also summarizes the measured swell height after 96 h for all tested materials.

Table 19. CBR results and swell height for tested materials.

Sample ID	Sample Condition	Soaked		Unsoaked
		Swell Height (percent)	CBR (percent)	CBR (percent)
21A-DI	Unscalped	0.7	67.3	70.2
	Scalped	0.2	47.7	59.5
21B:No.8-GR (pit B)	Unscalped	0.01	101.7	105.9
	Scalped	0.03	59.3	49.6
21B:No.8-GR (pit D)	Unscalped	0.0	274.4	260.8
	Scalped	0.0	109.9	132.2
ATPB-No.78:No.10-DI	Unscalped	0.0	106.5	92.5
No.10-GR	Unscalped	0.3	30.7	48.9
CTB- No.10-GR	Unscalped	—	—	—
CTB-21A-GR	Unscalped	—	—	—
SG	Unscalped	1.7	3.0	8.7

—Test not performed.

Scalping and replacing particles greater than three-quarter inch resulted in a significant decrease in CBR regardless of the soaking condition, particularly for 21B:No.8-GR. The lowest CBR was obtained for SG, which is an indication of SG's susceptibility to moisture and, consequently, a decrease in strength under saturated conditions. When comparing the soaked and unsoaked conditions, the coarse-grained aggregates were less affected by moisture; however, the No.10-GR increased by 59 percent, and the SG increased by 190 percent. Interestingly, the CBR of the scalped and unsoaked 21B:No.8-GR pit D decreased, unlike the rest, suggesting that either excess pore water pressures caused a decrease in strength for this specimen or the gradation of the unscalped soaked specimen was coarser than its counterpart.

ATPB-Specific Test: Tensile Strength Ratio (TSR)

The ATPBs selected for pit C have a limited amount of asphalt binder to improve the stability of the OGAs without compromising their drainability quality. However, the long-term exposure of ATPBs in the field due to repeated traffic loading and environmental changes can potentially result in stripping of the low-asphalt content (Harvey et al. 1998). To evaluate the resistance of the ATPB to moisture-induced damage, the TSR, defined as the ratio of the average conditioned tensile strength that is retained after the moisture and freeze–thaw conditions (AASHTO T 283 (2022o)) to the average dry tensile strength, was measured.

Methods

FHWA's Asphalt Binder and Mixtures Laboratory performed TSR tests for ATPB-No.78:No.10-DI specimens per AASHTO T 283 (2022o). TSR tests were performed for ATPB-No.78:No.10-DI specimens per AASHTO T 283. The ATPB-No.78:No.10-DI with the desired JMF (table 5) was prepared using a Superpave gyratory compactor. The ATPB cylinder was then subjected to indirect tensile strength tests under two different conditions: dry and conditions whereby the sample was subjected to vacuum saturation and a freeze cycle, followed by a warm-water soaking cycle. At the end of the test, the TSR of the ATPB under conditioned (i.e., wet) to dry conditions was computed; a minimum ratio of 75 percent was required to meet the minimum threshold for ATPB (WSDOT 2023).

Results

Figure 23 presents the TSR results for duplicated specimens. The conditioned tensile strength averaged 80.4 psi, while the dry strength was 90.5 psi, resulting in a TSR of 85.5 percent, which exceeded the 75-percent threshold by a considerable margin.

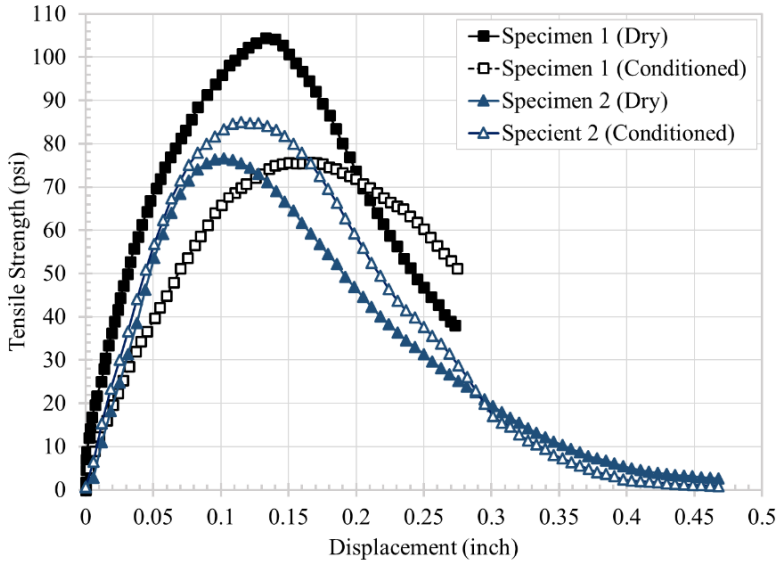

Source: FHWA

Figure 23. Graph. TSR test results for ATPB-No.78:No.10-DI materials.

CTB-Specific Test: UCS

Treating soils with cement can improve mechanical properties, such as UCS (Abu Farsakh, Dhakal, and Chen 2015; Ardah, Abu-Farsakh, and Chen 2016; Ghaaowd et al. 2022). UCS is also a parameter for CTB materials used in pavement design (AASHTO 2020a). For PTF-3, a UCS of around 350 psi after 7 d of curing was targeted. In this study, the two selected materials for pit D, CTB-No.10-GR and CTB-21A-GR, were tested for UCS. The UCS values are level inputs in MEPDG to predict the modulus of elasticity and RM of chemically stabilized pavement layers for MEPDG-based pavement designs (AASHTO 2020a).

Methods

The UCS was measured per ASTM D1633 (2017b) on Proctor specimens with a heigh-to-diameter ratio of 1.15. The material retained on the 3/4-inch sieve was first scalped. Three specimens per CTB were compacted in split molds following ASTM D559, Method B procedures (i.e., 3 layers, 25 blows per layer with a 5-lb, 12-inch drop height hammer) (ATSM 2017d). During the design stage, CTB specimens were prepared at the quarry. Unlike design work in the laboratory, the quarry works on a commercial scale. To ensure adequate sampling, multiple specimens were prepared rather than relying on a single specimen. One day after compaction, the specimens were demolded, wrapped in plastic wrap to mitigate moisture loss, and cured at room temperature for up to 7 d. After curing, the specimens were submerged in water for 4 h before testing. Due to the surface condition of specimens, neoprene pad caps and steel retainer rings were used per ASTM C1231/C1231M (2023c) to create a smooth testing surface so the load could be evenly applied during testing. The specimens were loaded at a displacement rate of 0.05 inch per minute. The testing setup is shown in figure 24.

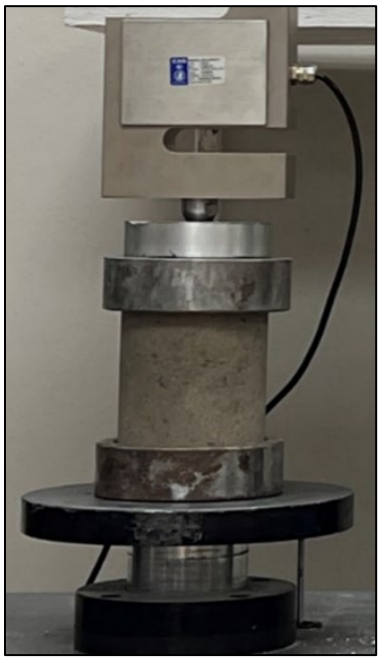

Source: FHWA.

Figure 24. Photo. UCS testing.

Results

Figure 25 and table 20 report the 7-d UCS data for CTB-No.10-GR and CTB-21A-GR; three specimens for each CTB mix design. Even though the target densities were not met, both CTBs were within the targeted range of UCS for PTF-3.

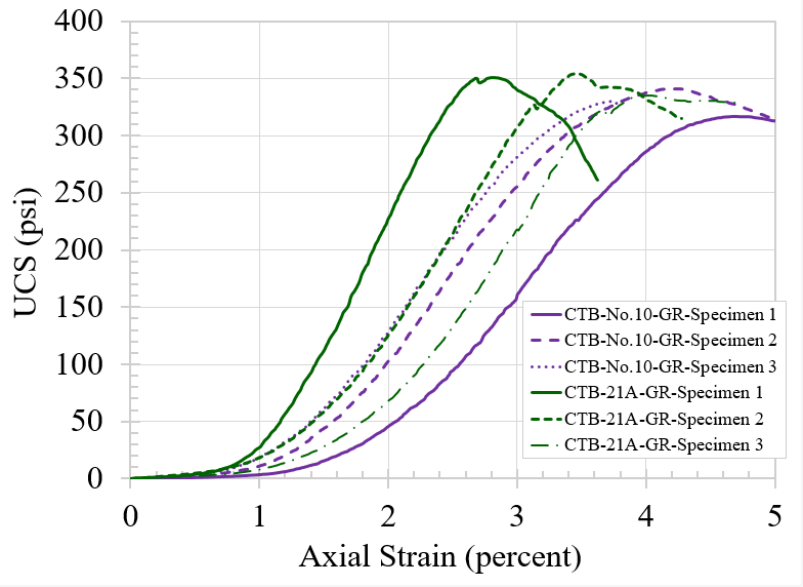

Source: FHWA.

Figure 25. Graph. UCS test results for CTBs.

Table 20. CTB UCS results.

Sample ID	Cement Content (percent)	UCS (psi)	Average (psi)	Standard Deviation (psi)	COV (percent)
CTB-No.10-GR-S01	3.7	316.7	329.1	9.7	3.0
CTB-No.10-GR-S02		340.5			
CTB-No.10-GR-S03		330.0			
CTB-21A-GR-S01	4.2	350.8	346.8	8.5	2.4
CTB-21A-GR-S02		354.5			
CTB-21A-GR-S03		335.0			

COV = coefficient of variation.

The comparison of both materials showed that the 7-d strengths were similar (table 20). These results demonstrate the comparable performance of the byproduct No. 10 screenings relative to the conventional 21A.

AGGREGATE SHAPE

The particle shape of unbound and bound materials is a physical characteristic that can significantly affect the performance of pavement systems (Masad et al. 2007). Hence, aggregate shape factors were characterized for all base and subbase aggregates considered in this work.

Methods

Characterization of shape factors (e.g., angularity, texture, sphericity, flatness, and elongation) for each base and subbase aggregate was performed in accordance with AASHTO T 381 (2022l). Measurements were taken by using a second-generation Aggregate Imaging Measurement

System (AIMS2). Before testing, the samples were washed and sieved to the required size fractions for AIMS2 testing. A stockpile analysis was performed using a weighted average based on the material's gradation to determine the shape factors. Table 21 illustrates the range of classifications for angularity, sphericity, and surface texture shape factors per AASHTO R 91 (2022p).

Table 21. Shape factor index classifications.

Shape Factor	Low	Medium	High
Angularity	≤3,300	3,300–6,600	6,600–10,000
Sphericity	≤0.3	0.3–0.7	0.7–1.0
Surface texture	≤260	260–550	550–1,000

Results

Shape factors from the AIMS2 test for unbound aggregates are presented in table 22. The materials ranged from low to medium angularity; however, given the coefficient of variation (COV) and acceptable range of results provided by AASHTO R 91 (2022p), any differences are considered insignificant. All materials exhibited a medium classification for sphericity and met the 30-percent flat and elongated 5:1 maximum threshold of 30 percent (VDOT 2020).

Table 22. Summary of shape factors for base and subbase aggregates.

Shape Factors		Sample ID				
		21A-DI	21B:No.8-GR	No.78:No.10-DI	No.10-GR	21A-GR
Angularity	Average index	3425.4	3213.3	3008.0	3336.2	2718.3
	Classification	Medium	Low	Low	Medium	Low
Sphericity	Average index	0.61	0.66	0.73	0.60	0.65
	Classification	Medium	Medium	High	Medium	Medium
Flat and elongated values	L/S ≥ 1:1	38.3	52.8	79.7	13.1	48.3
	L/S ≥ 2:1	29.6	37.9	31.3	12.3	35.4
	L/S ≥ 3:1	13.9	12.5	2.4	7.1	11.7
	L/S ≥ 4:1	5.4	2.6	0.0	3.1	4.5
	L/S ≥ 5:1	2.2	0.6	0.0	1.6	0.5
Surface texture	Average index	378.3	274.4	601.8	251.9	270.8
	Classification	Medium	Medium	High	Low	Medium

L/S = longest/shortest dimensions.

ABRASION RESISTANCE

The base and subbase materials examined in this study are crushed products from rocks with different mineralogy. Tests were performed to evaluate their abrasion resistance and durability.

Methods

Abrasion resistance was determined in accordance with AASHTO T 327 (2022n) using a Micro-Deval device. In this test, a 3.3-lb sample of washed and oven-dried material was placed in a Micro-Deval apparatus with 0.53 gal of water and 11.0 lb of an abrasive charge. The jar was then revolved at 100 rotations per minute for at least 9,500 revolutions. After testing, samples were washed from the jar and wet sieved through a No. 4 sieve superimposed on a No. 16 sieve. Then, sample fractions retained on each sieve were oven dried, and the total mass loss was determined.

Results

Table 23 summarizes the resistance to degradation for each material, expressed as a percentage of mass loss. As expected, aggregates with GR mineralogy had higher abrasion degradation values than aggregates with DI mineralogy. Based on the limits of satisfactory performance of aggregates presented in AASHTO T 327 (2022n), the Micro-Deval mass loss of all base and subbase aggregates tested were well below the maximum thresholds of 25 and 30 percent, respectively.

Table 23. Micro-Deval results.

Sample ID	Micro-Deval Abrasion Loss (percent)
21A-DI	6.2
21B:No.8-GR	10.6
No.78:No.10-DI	6.5
No.10-GR	18.8
21A-GR	13.2

SUMMARY OF MATERIAL LABORATORY MEASUREMENTS

This chapter presented the initial PTF-3 design and construction values for various geotechnical tests. The data presented characterized PTF-3 in terms of the geotechnical material's physical properties, drainage behavior, and strength behavior. Tests typical of roadway design—such as Proctor, gradation, and RM—were presented, as well as the hydraulic conductivity with a comparative CH, FH methodology, and the effective porosity. The time-to-drain experiments showed how well the drainage and stiffness of 21B:No.8-GR was over its counterpart, 21A-DI, with the ATPB-No.78:No.10-DI exceeding both as expected.

The values obtained from select tests were presented as key inputs for MEPDG (AASHTO 2020a) and AASHTOWare PMED (AASHTO 2020b) in the next chapter.

CHAPTER 5. PAVEMENT FOUNDATION DESIGN SUMMARY

The material characterization performed resulted in data that can be directly used as level 1 inputs or leveraged as level 2 or level 3 inputs in the MEPDG 2020 (AASHTO 2020a) analysis software AASHTOWare PMED (AASHTO 2020b). Material and engineering properties not incorporated within level 1 inputs were also measured in this study for use in level 2 correlations and for future refinement and research into their impact on pavement response and performance. Within PMED, level 1 inputs are treated as level 3 inputs. Level 3 inputs can be *default* values or *user* (level 1) defined, measured data, whereas empirical relations from select tests define level 2 inputs.

Knowing the defaults and limitations within PMED is important before inputting key laboratory data. Table 24 shows the fundamental default inputs for flexible pavements. These values are computed from the selection of the structure type, either nonstabilized or subgrade material, and then the material classification. Select gradations of each material percent passing also exist, ranging from 3.5-inch to the No. 200 (0.003-inch) sieve. As shown in table 24, many parameters stay the same or change minimally across the different layers. The hydraulic conductivity is quite different from the measured laboratory test values (table 13), yet PMED states that the shown k_{20} values are recommended based on global default values (AASHTO 2020b).

PMED is limited by using stabilized base/subbase layers under flexible pavements such as the ATPB. The ATPB layer should be treated as a high-quality, crushed stone base layer (AASHTO 2020a), leaving the engineer to determine what a high-quality, crushed stone base is. PMED includes four possible inputs: crushed gravel, crushed stone, permeable aggregate, or river-run aggregate. When comparing the inputs, the only value to change in the defaults is the M_{rs} values, ranging from 15,000 to 30,000 psi, which is much less than the measured ATPB M_{rs}. Instead, the ATPB defaults are based on their A-1-a classification (AASHTO 2021b). The final defaults left untouched are the soil-water characteristic curves (ASTM D6836 (2016a)), which were not measured.

Table 24. Default inputs for flexible pavement layers (AASHTO 2020b).

Layer	Pit	Sample ID	H (inch)	K_o	ν	M_{rs} (psi)	γ_d (lb/ft^3)	w_{opt} (percent)	G_{sa}	k_{20} (ft/day)	Atterberg Limits	
											LL	PI
Base	A	21A-DI	6	0.5	0.35	40,000	127.6	7.4	2.7	1.3	6	1
	B	21B:No.8-GR	6	0.5	0.35	40,000	127.6	7.4	2.7	1.3	6	1
	C	ATPB-No.78:No.10-DI	6	0.5	0.35	40,000	127.6	7.4	2.7	1.3	6	1
Subbase	A	No.10-GR	6	0.5	0.35	38,000	123.4	9.3	2.7	0.06	11	1
	B–C		6									
Subgrade	A–C	SG	N/A	0.5	0.35	15,000	118.4	11.8	2.7	0.0002	21	5

LL = liquid limit; PI = plasticity index; ν = Poisson's ratio.

TIME-TO-DRAIN EXPERIMENTS

This section presents a hierarchy of pavement foundation design inputs for the time-to-drain experiments.

Level 1 Inputs

Table 25 presents a summary of key level 1 inputs (i.e., measurements) for the time-to-drain experiments. Only the key parameters shown and the gradation of the material can be input. Note that the coefficient of lateral earth pressure (K_o) and Poisson's ratio (ν) were kept as the default values since they were not measured. The hydraulic conductivity input used was $k_{20\ (CH)}$ for all except subgrade using $k_{20\ (FH)}$. The γ_d and w_{opt} inputs were those used for the RM test (AASHTO 2020b).

Table 25. Key level 1 results and defaults for the time-to-drain experiments (pits A–C).

Layer	Pit	Sample ID	*H* (inch)	K_o+	ν+	M_{rs}* (psi)	γ_d (lb/ft³)	w_{opt} (%)	G_{sa}	k_{20} (ft/day)	Atterberg Limits	
											LL	PI
Base	A	21A-DI	12	0.5	0.35	23,591.3	148.9	4.6	3.003	1.739	0	0
	B	21B:No.8-GR	8	0.5	0.35	43,001.8	139.7	5.0	2.675	66.011	0	0
	C	ATPB-No.78:No.10-DI	8	0.5	0.35	57,828.0	133.0	—	2.969	2,621.034	0	0
Subbase	A	No.10-GR	8	0.5	0.35	18,238.8	135.0	6.3	2.690	1.713	0	0
	B–C		12									
Subgrade	A–C	SG	—	0.5	0.35	11,384.9	119.5	13.5	2.699	0.008	31	10

*Values represent conditions under σ_3 = 5 psi, σ_{max} = 15 psi for base/subbase, σ_3 = 2 psi, and σ_{max} = 6 psi for subgrade.
—Data not available/applicable.
+Defaults.

Carvalho et al.[1] performed two analyses (table 26) to determine the estimated number of ESALs over the pavement life—one using the AASHTO 1993 Pavement Design method and one using PMED (AASHTO 1993, 2020b). The results for bottom-up cracking (i.e., alligator cracking) were based on the M_{rs} (table 16) inputs from the time-to-drain experiments and other parameters. Based on the analysis performed, table 26 shows the AASTHO 1993 method overestimates, or the PMED underestimates the total EASLs at 30-percent cracking. PMED requires a design threshold of cracking, in this case 30 percent, to predict ESALs at failure. This cracking threshold is the amount the pavement surface is expected to crack. Details on the asphalt inputs and other analyses, including inputs such as environmental conditions, axle configuration, traffic capacity, and design life, are presented by Carvalho et al.[1] While many factors play a role in the calculations, pit A, with a thicker base, cracked earlier or with the same amount of ESALs as pit B with a thinner base, highlighting the significance of blending VDOT 21B with a quarry byproduct.

[1]Report by Carvalho, R., et al. is under development.

Table 26. Predicted number of ESALs (in millions) at failure for the time-to-drain experiments (Carvalho et al.[1]).

Layer	AASHTO (1993)	PMED for 30-percent cracking (AASHTO 2020b)
Pit A	11.2	4.5
Pit B	38.4	10
Pit C	73.8	14.9

Level 2 and Level 3 Inputs

Level 2 inputs for key PMED design parameters were also estimated based on the measured data, whereas level 3 inputs are based on the material classification (AASHTO 2020b). K_o and ν are not inputs but defaults.

For all materials, M_{rs} was based on the measured CBR values under soaked scalped (where applicable) or soaked unscalped conditions (table 19) using the relationship presented in MEPDG (AASHTO 2020a) (equation 10); however, for the subgrade, M_{rs} was estimated based on the relationship presented in AASHTO (1993) for materials with CBR between 2 and 10 percent (equation 11). Another level 2 estimate of M_{rs} is to use the percentage of fines (P_{200}) and the plasticity index (PI) to estimate the CBR as shown in equation 12, then use that CBR value in equation 10. Equation 12 provided CBR values of 75 for all materials, as the PI was zero, except for the SG, which was 0.62. Figure 26 shows the difference between the measured and estimated M_{rs} in this study.

$$M_{rs}(psi) = 2{,}555CBR(\%)^{0.64} \quad (10)$$

$$M_{rs}(psi) = 1{,}500CBR(\%) \quad (11)$$

$$CBR(\%) = \frac{75}{1+0.278(P_{200}PI)} \quad (12)$$

[1]Report by Carvalho, R., et al. is under development.

The level 3 inputs for M_{rs} were simply determined from the AASHTO classification of each material type. For instance, base aggregates with A-1-a and A-1-b classifications have M_{rs} values of 40,000 and 38,000 psi, respectively (AASHTO 2020a). These global level 3 values (table 27) are higher than the experimentally determined level 1 inputs (table 25). Although the manual recommends M_{rs} 16,500 psi for subgrade under flexible pavements, PMED provides a default of 15,000 psi (AASHTO 2020b). Another discrepancy noted is in the preparation of RM specimens, in which the recommended density and OMC should come from AASHTO T 180 (2022a) for all materials; however, the standard for preparing subgrade soils remains according to AASHTO T 99 (2022h). In fact, AASHTO T 99 is a listed acceptable laboratory material characterization testing method (MEPDG 2020a), yet PMED suggests T 180 (2022a) for subgrade soils. In this analysis, the target density and moisture content per AASHTO T 99 (2022h) were used.

Table 27. Key level 2 and level 3 inputs and defaults for the time-to-drain experiments (pits A–C).

Layer	Pit	Sample ID	*H* (inch)	K_o+	ν+	M_{rs} (psi)			γ_d (lb/ft^3)		w_{opt} (percent)		G_{sa}+	k_{20} (ft/day)		Atterberg Limits	
						CBR	P_{200} and *PI*	Level 3	Level 2	Level 3	Level 2	Level 3		Level 2	Level 3	LL	PI
Base	A	21A-DI	12	0.5	0.35	30,314	40,498	40,000	127.5	127.6	7.4	7.4	2.7	0.4	1.3	6	1
	B	21B:No.8-GR	8	0.5	0.35	34,845	40,498	40,000	127.8	127.6	7.3	7.4	2.7	2.7	1.3	6	1
	C	ATPB-No.78:No.10-DI	8	0.5	0.35	50,687	40,498	65,00–75,000	127.2	127.6	7.6	7.4	2.7	1170	1.3	6	1
SB	A	No.10-GR	8	0.5	0.35	22,864	40,498	38,000	124.2	124.0	9.1	9.3	2.7	0.03	0.06	11	1
	B–C		12														
SG	A–C	SG	N/A	0.5	0.35	4,500	928	16,500	121.3	119.0	10.6	11.8	2.7	0.0001	0.0002	21	5

+Defaults.

To estimate the level 2 and level 3 inputs of the ATPB, the sieve data of the constituents, namely No.78:No.10-DI, is used. No clearly defined level 3 M_{rs} value for ATPB is included in MEPDG (2020a) except for the recommended equivalent annual modulus (i.e., the modulus accounting for seasonal variations), ranging from 65,000 to 75,000 psi, which is 12–30 percent higher than the measured resilient modulus, respectively.

PMED internally computes level 2 inputs for γ_d, w_{opt}, and k_{20} for a given material using the sieve data (figure 12) and AASHTO classification (table 9). For level 3 values, only the AASHTO classification is needed, and all other values are default. The Atterberg limits and specific gravity are based on the material classification.

The findings indicate that current design practice overestimated M_{rs} for 21A-DI and No.10-GR while both underestimating and overestimating the subgrade. 21B:No.8-GR (pit B) measured versus level 2 and level 3 M_{rs} were within a 20-percent range, whereas the ATPB was within a 30-percent range. In all cases, the level 2 and level 3 γ_d and w_{opt} were much lower or higher, respectively, than the measured values (table 11), except for the SG, which was accurate for level 3 but too high for level 2. The hydraulic conductivity of the bases increased from pit A to pit C with the level 2 sieve and classification inputs, highlighting the importance of gradation, as the level 3 classification alone shows no change. The level 3 k_{20} for the ATPB is significantly underestimated by up to three orders of magnitude relative to both level 1 and level 2. Lastly, the Atterberg limits are computed based on their classification, with no option for *no plasticity* unless defined by the user (i.e., level 1); however, the base/subbase PI of 1 is more suggestive of computational stability within PMED (AASHTO 2020b). Using a PI of 1 in equation 12, rather than zero, would have value but is not explicitly stated, nor was it pursued. Table 27 highlights the value and significant differences in using directly measured (level 1) inputs (table 25) for design rather than relying on classification and gradation alone.

Figure 26 presents the M_{rs} from all levels, highlighting the importance of using measured over default or estimated values. For comparison, 65,000 psi is plotted for the M_{rs} of the ATPB level 3. Using equation 10 and equation 11 provides the highest correlation to the measured values. If looking at only the traditional road base, 21A-DI, the gradation and classification overestimate by wide margins. Simply put, the CBR (equation 10) estimation is about 29 percent more than measured.

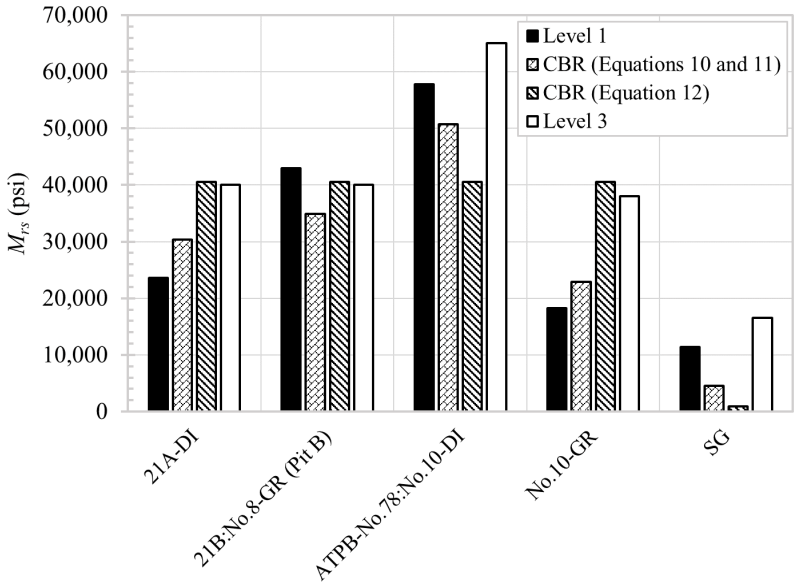

Source: FHWA.

A. Different M_{rs} values per time-to-drain materials.

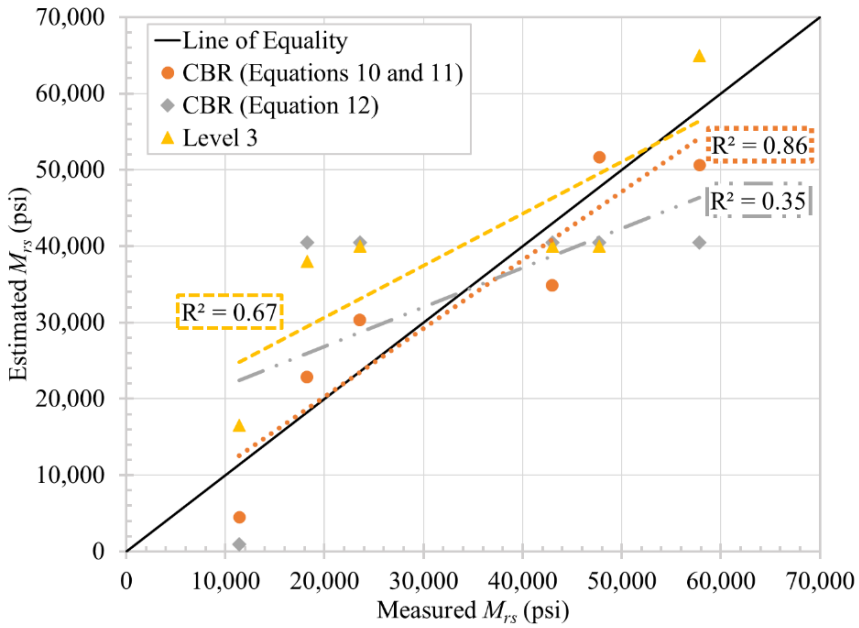

Source: FHWA.

B. Comparison of computed M_{rs} to measured.

Figure 26. Graphs. Measured and estimated M_{rs} based on level 2 and level 3.

INVERTED PAVEMENT EXPERIMENTS

MEPDG (2020a) has numerous CTB inputs for rigid and semi-rigid pavements but does not allow cement-stabilized soils to be placed under unbound aggregates. No supplementary information exists on inverted pavements in MEPDG (2020a) or PMED (2020b). PMED does not have a design option specifically for inverted pavement types. As such, within this work, inverted pavement structures were evaluated similarly to the other flexible pavement structures.

Level 1 Inputs

Table 28 presents the level 1 inputs for all the materials in pit D, with the expected number of passes and ESALs at failure presented in table 29. Carvalho et al.[1] conducted only PMED (AASHTO 2020b) analysis. As expected, the thicker lane 11 is predicted to last longer than lane 10. With similar M_{rs}, a clearer distinction exists in how PMED seems to value the thickness of a layer over the modulus. Comparing only the thickness yields a 3 million predicted ESAL increase between lanes 10 and 11; however, only comparing the 2,500 psi difference between both CTBs, the difference is up to 0.3 million EASLs.

Table 28. Key level 1 results and defaults for the inverted pavement experiments (pit D).

Layer	Pit	Sample ID	*H** (inch)	K_o^+	ν^+	M_{rs}^{++} (psi)	γ_d (lb/ft^3)	w_{op} (%)	*Gsa*	k_{20} (ft/day)	Atterberg Limits	
											LL	PI
Base	D	21B:No. 8-GR	6	0.5	0.35	47,750.4	147.0	4.5	2.675	0.007	0	0
Subbase	D North	CTB-No.10-GR	8/12	0.5	0.35	70,840.4	129.2	9.5	2.690	0.011	0	0
	D South	CTB-21A-GR	8/12	0.5	0.35	68,333.4	133.0	7.1	2.657	0.003	0	0
Subgrade	D	SG	N/A	0.5	0.35	11,384.9	119.5	13.5	2.699	0.008	31	10

*L10 of subbase = 8-inch and L11 of subbase = 12-inch.
$^{++}$Values represent conditions under σ_3 = 5 psi and σ_{max} = 15 psi for base/subbase and σ_3 = 2 psi and σ_{max} = 6 psi for subgrade.
$^{+}$Defaults.

Table 29. Predicted number of ESALs at failure for the inverted pavement experiments (Carvalho et al.[1]).

Pit D Location	ESALs per PMED for 30-Percent Cracking (no. in millions)
L10 North	15.4
L10 South	15.1
L11 North	18.3
L11 South	18.1

[1]Report by Carvalho, R., et al. is under development.

Level 2 and Level 3 Inputs

To reiterate, similar to the ATPB, both CTBs were treated as unbound subbases based on their AASHTO classification (table 9) and gradation (figure 12) for the level 2 and level 3 inputs presented in table 30.

Table 30 encapsulates the level 2 and level 3 inputs alongside default values used for the inverted pavement experiment. Remarkably, the base layer's M_{rs} value mirrors the trend of a high modulus as measured in the level 1 results. The level 2 and level 3 M_{rs} estimations do not significantly deviate for the subbase, but no confidence in the base values exists because the base values are far lower than the measured values. The hydraulic conductivity shows a slight increment from level 2 to level 3 for the base and CTB-21A-GR, whereas the subgrade displays a minimal conductivity consistent with the nature of the material. The coarse-grained material densities are estimated low and minimally change between the layers, whereas the moisture content is similar to measured CTB and subgrade. The unfortunate thing about all these inputs is that the thin base layer and CTBs cannot be properly accounted for or included within PMED (AASHTO 2020b).

Table 30. Key level 2 and level 3 inputs and defaults for the inverted pavement experiments.

Layer	Pit	Sample ID	*H* (inch)	K_o+	ν+	M_{rs} (psi)			γ_d (lb/ft^3)		w_{opt} (percent)		G_{sa}+	k_{20} (ft/day)		Atterberg Limits	
						CBR	P_{200} and *PI*	Level 3	Level 2	Level 3	Level 2	Level 3		Level 2	Level 3	LL	PI
Base	D	21B:No.8-GR	6	0.5	0.35	51,717	17,790	40,000	127.8	127.6	7.3	7.4	2.7	2.7	1.3	6	1
Subbase	D North Half	CTB-No.10-GR	8/12	0.5	0.35	—	40,498	38,000	121.3	124.0	10.6	9.3	2.7	0.03	0.06	11	1
	D South Half	CTB-21A-GR	8/12	0.5	0.35	—	40,498	40,000	128.3	127.6	7.1	7.4	2.7	1.47	1.28	6	1
Subgrade	D	SG	N/A	0.5	0.35	4,500	928	16,500	121.3	119.0	10.6	11.8	2.7	0.0001	0.0002	21	5

—Data not available.
+Defaults.

OTHER MEASURED PROPERTIES AND TRENDS

This work determined other properties relevant to pavement system performance besides the key design inputs in the current PMED (AASHTO 2020b). Table 31 summarizes these potentially pertinent parameters for the time-to-drain and inverted pavement experiments. The parameters common to the two experiments include σ_{dmax}, τ_{max}, and PS. EP is more related to the time-to-drain experiments, while TSR and UCS are specialized tests related to ATPB and CTBs, respectively.

Table 31. Other measured properties for flexible pavement design (all pits).

Layer	Pit	Sample ID	σ_{dma} (psi)	τ_{max} (psi)	UCS (psi)	PS (%)	TS (%)	N_e (%)
Base	A	21A-DI	74.7	37.4	N/A	0.403	N/A	4.3
	B	21B:No.8-GR	93.2	46.6	N/A	0.174	N/A	3.0
	D	21B:No.8-GR	153.2	76.6	N/A	0.235	N/A	1.2
	C	ATPB-No.78:No.10-DI	166.6	83.3	N/A	0.117	85.5	15.8
Subbase	A–C	No.10-GR	44.2	22.1	N/A	0.612	N/A	3.6
	D North	CTB-No.10-GR	417.2	208.9	329.1	0.104	N/A	—
	D South	CTB-21A-GR	271.7	135.9	346.8	0.069	N/A	—
Subgrade	A–D	SG	25.1	12.6	—	†0.502	N/A	0.8

—Data not available

†PS dependent on sequence number. See table 18.

The study found that σ_{dmax} increased exponentially to M_{rs} (figure 27). The G/S had an evident impact on the resilient modulus of the unbound material, as shown in figure 28. As expected, the G/S ratio had a clear impact on the permeability, as presented in figure 29, where permeability increases vastly. Note that figure 27 covers all M_{rs} specimens (unbound and stabilized), whereas figure 28 only presents the unbound specimens, and figure 29, had no CH test for the SG.

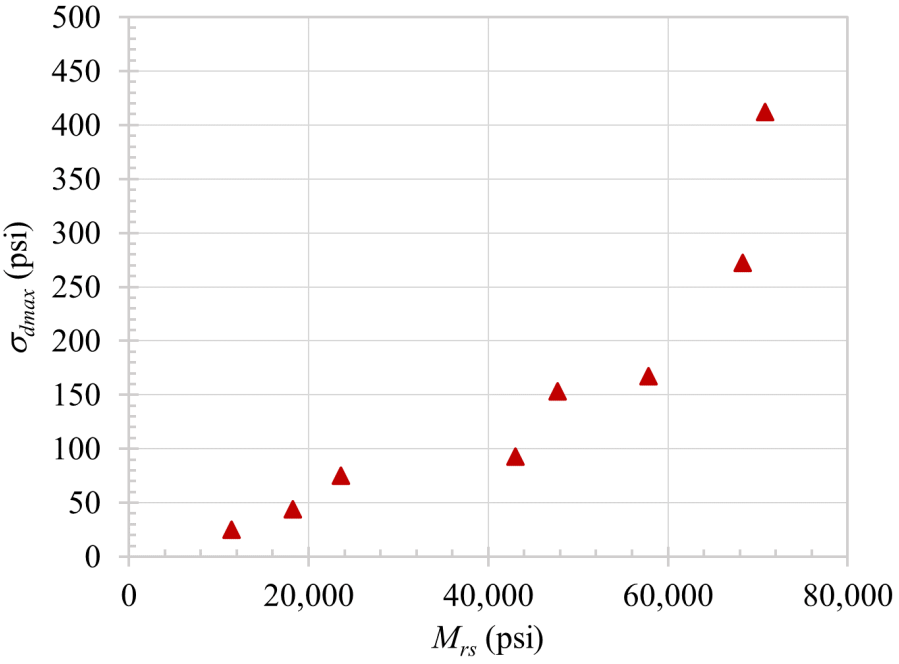

Source: FHWA.

Figure 27. Graph. Maximum deviator stress versus summary resilient modulus.

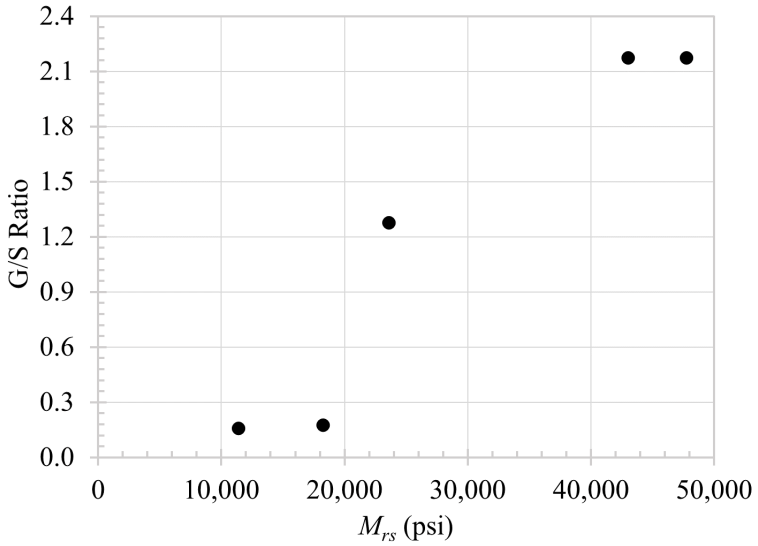

Source: FHWA.

Figure 28. Graph. Relationship between M_{rs} and G/S for the unbound material.

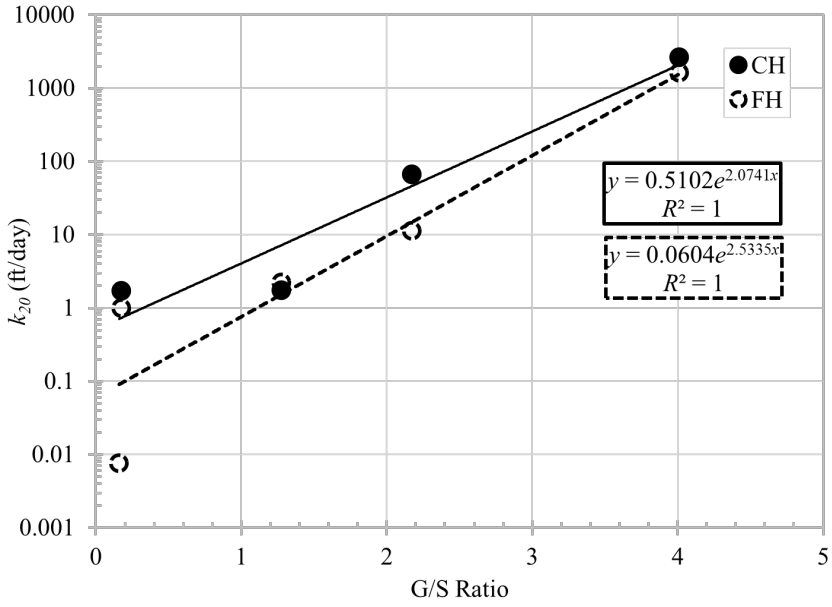

Source: FHWA.

Figure 29. Graph. Relationship between G/S and k_{20} for the unbound material.

CHAPTER 6. DESIGN CHALLENGES

PTF-3's design and development required an iterative process in the final selection of the materials used to build the pavement foundations. Several challenges, primarily related to material selection to meet the research objectives of the PTF (Adams, Nicks, and Carvalho 2024), were encountered as part of this process, which required engineering judgment. This chapter covers the primary design challenges faced during the material selection and characterization.

PRIMARY DESIGN CHALLENGES

While the existing 21A-DI material excavated from PTF-2 was reused as base layers in pit A, pits B, C, and D involved an extensive material selection process. This process required evaluating different base and subbase materials. The primary considerations in this selection process were the time-to-drain, stiffness, and practicality (i.e., availability and cost) concerns. This section discusses the challenges in selecting both unbound and stabilized materials that offered the desired drainage, stiffness, and other material characteristics for both the time-to-drain and the inverted pavement experiments.

Pit B: Material Selection for Permeability

The primary objective during the material selection process for pit B was to improve the permeability and drainage quality of the 21A-DI material previously used in PTF-2 and selected for pit A. As mentioned in chapter 3, the selected base material would need to have good to fair drainage.

Initially, FHWA explored reusing excavated 21A-DI after washing out the fines and fine sands. Initial tests of washed 21A-DI showed a significant increase in permeability (Gebrenegus et al. 2022); however, washing hundreds of tons of excavated material was impractical. In response, FHWA selected a similar, yet slightly coarser, VDOT 21B gradation as a good base layer candidate for pit B.

Samples of 21B were procured from three quarries (referred to herein as quarries A, B, and C) and then tested for their suitability. Quarry A had a granite mineralogy, while quarries B and C were DI. Sieve analysis and modified Proctor tests from the three quarries were performed on each 21B sample to determine the materials' gradation, MDD, and OMC. FH permeability tests were performed for each 21B sample as a screening tool at 95-percent MDD and OMC. The permeability results, G/S ratio, and percent fines for each sample are presented in table 32.

Table 32. Coefficient of permeability results for 21B from varying quarries.

Aggregate Source	Mineralogy	G/S Ratio	Fines (percent)	γ_{dmax} (pcf)	w_{op} (percent)	$k_{20\,(FH}$ (ft/day)
Quarry A	GR	2.31	10.0	144.2	4.7	27.7
Quarry B	DI	0.78	10.4	147.8	8.0	0.7
Quarry C	DI	2.46	8.1	157.0	5.2	85.5

The initial permeability tests showed that quarries A and C had a higher permeability than quarry B. Since quarry C offered the highest permeability during the trial and the DI mineralogy would yield stronger aggregates than GR, a preliminary decision was made to proceed with quarry C to the next round of testing. To further validate the results before making the final decision, FHWA procured and tested a second batch of quarry C's 21B. This batch was found to have a significantly finer gradation with a correspondingly low permeability compared to the initial batch tested. The differences in the batches highlighted day-to-day variability in quarry production as an essential consideration, which prompted FHWA to request and acquire daily quality control data from the selected quarries to ensure the material selected would meet the target drainage quality for pit B. To illustrate and evaluate quarry variability, heat maps were generated using the mean and standard deviation of each sieve for the 67, 106, and 66 daily quality control test results provided by quarries A, B, and C, respectively (figure 30).

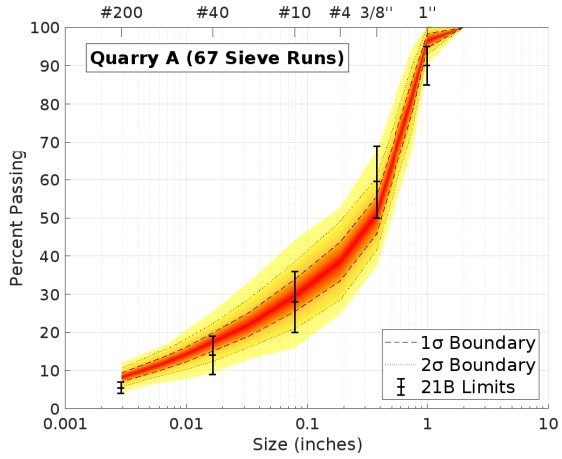

Source: FHWA.

A. Quarry A.

Source: FHWA.

B. Quarry B.

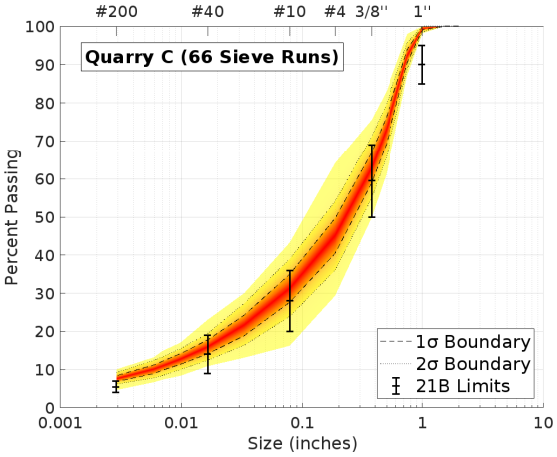

Source: FHWA.

C. Quarry C.

Figure 30. Graphs. Heat maps for 21B aggregate gradations from different quarries.

Quarry B had the lowest variability but the finest 21B blend (figure 30), matching the exceptionally low permeability result (table 32). In contrast, quarries A and C had wide variability, which had the side effect of producing very coarse (i.e., permeable) blends on some days while less permeable blends on other days.

Considering the quality control data, it became apparent that getting the ideal batch of aggregate was as important as selecting the right quarry. Determining what constituted the ideal batch of 21B became the primary objective. The G/S ratio was determined to be a concise surrogate for each procured sample's gradation (table 32). Plotting the 21B G/S ratio as a function of permeability for the tested aggregates clearly showed an exponential increase in permeability with increasing G/S ratio (figure 31).

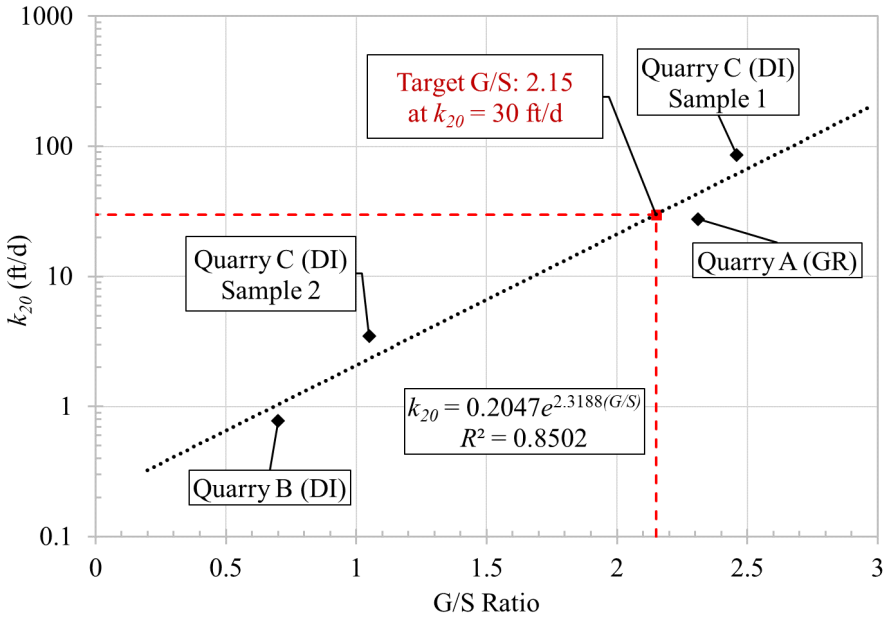

Source: FHWA.

Figure 31. Graph. Permeability as a function of G/S for 21B aggregates.

Based on the relationship between G/S and permeability, it was determined that the ideal 21B blend should have a minimum G/S of 2.15, corresponding to an expected permeability of 30 ft/d. The quality control data from quarries A and C suggested that they did sometimes produce batches of 21B that met such a target. In contrast, quarry B produced an exceptionally consistent 21B product that unfortunately never approached the target G/S ratio in the provided quality control data; hence, quarry B was removed from consideration.

Having eliminated quarry B based on its consistently finer than desired gradation, the next step was determining whether quarry A or C would be more likely to produce a 21B sample with the desired gradation. The mean and standard deviation for each sieve from quarry A's and C's combined quality control data were used to simulate an even larger dataset to conceptualize possible gradations that would meet the target 2.15 G/S ratio. A target gradation area was built from 1,000 valid simulated gradations (i.e., decreasing percent passing on each finer mesh sieve) with G/S greater than 2.15 and plotted with the real sieve data from quarry A and C (figure 32). Often, but not always, the quality control results from quarry A overlapped with the target region at the No. 4 sieve, which defines G/S. Contrastingly, quarry C's quality control tests only occasionally overlapped with the target region.

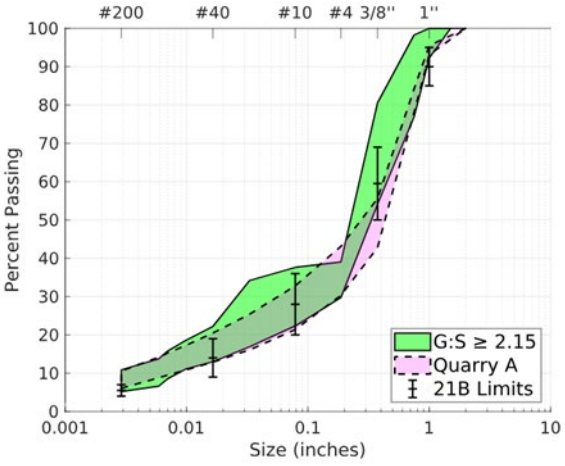

Source: FHWA.

A. Quarry A.

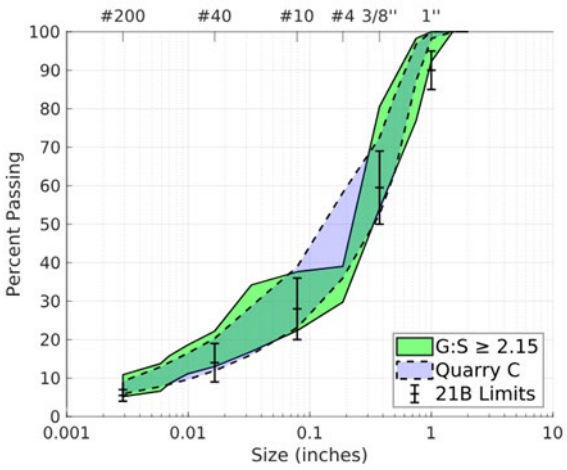

Source: FHWA.

B. Quarry C.

Figure 32. Graphs. Quarry A sieve data versus target gradation.

Ultimately, neither quarry A nor quarry C could provide a 21B having sufficient permeability for the experimental requirements with the high degree of confidence needed. Although quarry A could be expected to often meet the target gradation, the quarry was likely to deliver at least some 21B batches during construction that were too finely graded. After consulting with both quarries, FHWA determined that the best plan forward was to create a blended material based on a preexisting 21B that would more consistently fall within the target gradation region (i.e., G/S ratio ≥ 2.15).

Quarry A's 21B was selected as the starting point given that it was most likely to meet the criteria without significant modification; plus, the lighter GR mineralogy is considered easier to compact and more representative of base materials across the country than DI. Quarry A offered to blend its 21B granite with a No. 8 granite at a ratio of 90:10 by mass, coarsening the material to try to ensure a consistently high permeability.

To address the viability of this option, FHWA procured virgin 21B and No. 8 granite samples from quarry A and blended them at the 90:10 mass ratio. Table 33 shows a summary of the gradation, modified Proctor, and permeability results. Although the G/S ratio of the blended sample was lower than the target of 2.15, the permeability was nearly six times the 30 ft/d necessary. The more than satisfactory permeability and relative ease of production led to the selection of the 90:10 blend of 21B-GR with No. 8-GR from quarry A as the base material for pit B. A specific target gradation was created based on the 90:10 blend (table 34) (figure 33), with allowable ranges for each sieve size comparable to the VDOT-specified limits on unblended 21B. Deviation from the target gradation was allowed in accordance with local VDOT process tolerances on delivered materials, which range from 0.6- to 8-percent tolerance, dependent on sieve size and the number of laboratory tests performed.

Table 33. Screening results for 90:10 FHWA-blend of 21B-GR and No. 8-GR.

Aggregate Source	Mineralogy	G/S Ratio	Fines (percent)	γ_{dmax} (pcf)	w_{opt} (percent)	k_{s20} (ft/day)
Quarry A	GR	2.05	9.5	146.1	5.0	173.1

Table 34. Percent passing for 90:10 blended aggregate and VDOT 21B.

Sieve Size	90:10 21B:No. 8 Blend (percent)			VDOT 21B (percent)	
	Tested Gradation	Target Minimum	Target Maximum	Specification Minimum	Specification Maximum
2-inch	100	100	100	100	100
1-inch	97	91	100	85	95
3/8-inch	54	48	60	50	69
No. 10	30	24	36	20	36
No. 40	19	15	23	9	19
No. 200	10	8	12	4	7

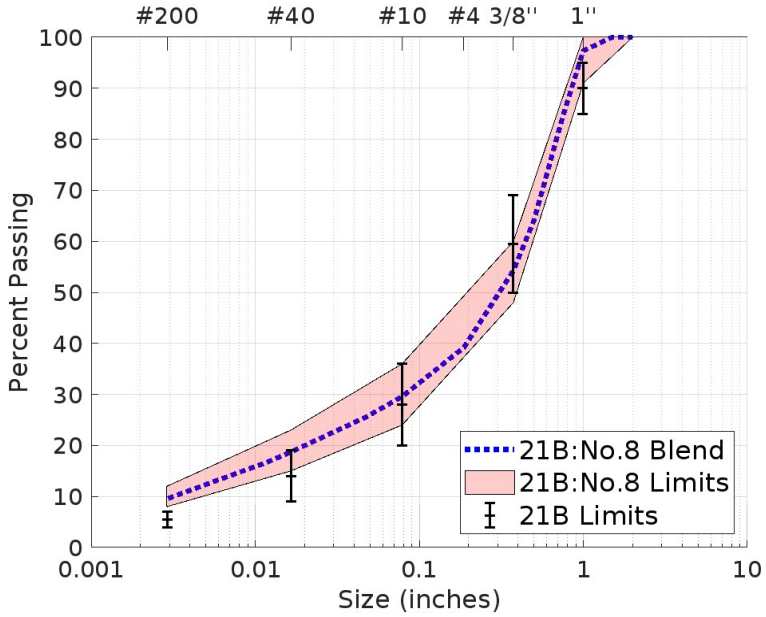

Source: FHWA.

Figure 33. Graph. Received 21B:No. 8 blend sieve data and limits.

The 21B:No.8-GR blend fell comfortably within the fair-to-good drainage target outlined in chapter 3, with a t_{50} of 2.6, given the parameters of pit B.

Pit C: Material Selection for ATPB

FHWA wanted excellent drainage quality for pit C, requiring the selection of a base course with a k_{20} greater than 1,000 ft/d (FHWA 1992). Therefore, an ATPB was identified for pit C. Note that the ATPB was the only non-Government-furnished geotechnical material, so the actual JMF, including source location and binder content, was determined by the contractor based on input from FHWA's Geotechnical Laboratory at TFHRC.

The ATPB gradation specified by WSDOT (2023) was used for the PTF because no local, regional, or Federal specification existed; however, the specs are broad enough that various materials would satisfy the requirements. A No. 78 stone that meets the gradation requirements (table 5) was initially evaluated for the ATPB because it has better stability and requires less compaction effort than the conventional No. 57 stone (Meyers 2021). The researchers found two different local sources for the No. 78 stones: one from a source with granite mineralogy (No.78-GR) and the other with DI mineralogy (No.78-DI). Ghaaowd et al. (2024) found that mixing both No. 78 materials with standard PG 64-22 asphalt binder up to 4 percent by weight resulted in AV larger than the 20-percent limit per WSDOT (2023); therefore, a slightly finer aggregate blend was needed.

The need for a finer aggregate blend was further corroborated through testing to identify potential issues with moisture susceptibility. The moisture susceptibility of the JMF was evaluated due to concern that the low asphalt binder content would be stripped from the aggregate in the presence of moisture (Harvey et al. 1998). Tensile strength ratio tests were first performed per AASHTO T 283 (2022o) for the No. 78-GR with 3 percent by weight of the PG 64S-22 binder, but the specimen failed during the conditioning stage; thus, the specimen was excluded. In response to this failure, the gradation was revised to enhance its resistance to moisture susceptibility by adding No. 10 screenings; in addition, the binder was upgraded to a polymer-modified binder, PG 64E-22. These changes aimed to reduce the AVs and improve moisture resistance. The new mix was a blend of No.78-DI and No.10-DI mixed at a target ratio of 85:15 by weight and designated as ATPB-No.78:No.10-DI.

The No.78:No.10-DI was mixed with 3.5 percent by weight of PG 64E-22 asphalt binder. The percentage of AVs after 75 gyrations was 18.2 percent, within the WSDOT (2023) limits. The $k_{20\,(CH)}$ was 2,621 ft/d (table 13), nearly three times higher than the FHWA 1992 requirement (1,000 ft/d). To verify the final JMF, six specimens were prepared and tested; three were tested dry, and the other three were tested after partial saturation and moisture conditioning with a freeze–thaw cycle. The TSR of No.78:No.10-DI was, on average, 88.8 percent, meeting the minimum threshold of 75 percent for ATPB (WSDOT 2023).

Aside from the design aspects, challenges also existed with the production and placement of the ATPB. The contractor had no experience placing ATPB in the field since the material is not common practice. Compared to traditional mixes, the asphalt plant was also not geared to produce mixes with binder contents of 3–4 percent. Additionally, because the PG 64E-22 asphalt binder costs more than PG 64S-22, the asphalt plant produced a trial JMF batch using 3.5 percent of PG 64S-22 with the No.78:No.10-DI blend as guide for the production mix used in Pit C.

Finally, the change of specimen height during the Superpave gyratory compaction was used to determine the loose asphalt layer thickness after placing and before compaction. The gyratory specimen height decreased by 18 percent after 75 gyrations. This result was used to calculate the loose ATPB lift thickness that would produce a 4-inch layer thickness in the field after compaction. The loose thickness was 4.85 inches and will be used by the contractor to place the ATPB in the field in the construction stage.

Pit D: Material Selection for Compressive Strength

The CTB is used as a subbase for the inverted pavement in pit D, one designated CTB-21A-GR and CTB-No.10-GR. No local guidelines are available for the inverted pavement design, which was a challenge for the Geotechnical Laboratory team at TFHRC. The team followed the South African inverted pavement design specification (Department of Transport 1996), in which the CTB UCS is required to be within the range of 200–500 psi to mitigate the reflective cracking. Therefore, the target UCS value was around 350 psi, and the CR corresponding to this target needed to be determined. To overcome this challenge, UCS tests per ASTM D1633 (2017b) were conducted for both CTBs at CR of between 2.0 and 6.0 percent (Ghaaowd et al. 2022). A linear relation between the UCS and CR for both CTBs was determined. The target CR was around 4 percent.

Similar to the challenge that the asphalt plant had with production of a nonstandard ATPB, the quarry was set up to produce a standard VDOT CTB mix with a target UCS of 650 psi per VDOT (2016) specifications for cement-treated aggregates, requiring several trial batches to meet the target UCS based on laboratory-prepared mixes. In the laboratory, AASHTO T 134 (2019) was used to determine the MDD and OMC of both CTBs; however, the test method calls for materials retained on the 3/4-inch sieve to be scalped and replaced by an equal percentage of aggregate between the 3/4-inch sieve and No. 4 sieve. Removal of the oversized material impacts the measured MDD and OMC of CTB-21A-GR, which led to discrepancies in the actual dry density and moisture content of the as-delivered material, as reported in table 35. Although the measured UCS specimen densities were less than the target, the densities all fell within the required strength range (table 20).

Table 35. The target and measured moisture and dry unit weight for the UCS specimens.

Sample ID	Moisture-Density Measurements			
	w (percent)		γ_d (lb/ft^3)	
	Target	Measured	Target	Measured
CTB-No.10-GR-S01	9.5	6.9	129.2	127.6
CTB-No.10-GR-S02		6.9		128.0
CTB-No.10-GR-S03		6.9		128.1
Average CTB-No.10-GR	N/A	6.9	N/A	127.9
CTB-21A-GR-S01	7.1	7.9	133.0	129.4
CTB-21A-GR-S02		8.1		128.0
CTB-21A-GR-S03		7.9		128.5
Average CTB-21A-GR	N/A	8.0	N/A	128.6

Additionally, the construction of PTF-3 was the first time that the No. 10 screenings were used in design, let alone a cement-stabilized material from the quarry. During the preconstruction phase, the quarry was visited to conduct trial batches. On the first visit, the quarry prepared a CTB-21A-GR trial mix; the measured CR was around 4.2 percent, and UCS specimens were prepared. The UCS at 7 d of curing was 292 psi, closer to the UCS design value and within the design range. The second visit to the quarry was to check the No.10-GR batch. The same procedures were followed; the CR was around 5 percent, and UCS was 553 psi at 7 d, higher than the 500 psi UCS maximum limit (Department of Transport 1996). The third visit to the quarry was to tune the CTB-No.10-GR CR and UCS at 7 d. The measured CR was around 3.7 percent, and the UCS was around 285 psi, within the UCS design range for construction of the inverted pavement test lanes.

CHAPTER 7. CONCLUSIONS

FHWA initiated the redesign of PTF-3 in 2018; construction was completed in October 2023. From a geotechnical perspective, two primary studies are fundamental to the objectives of this new facility:

1. Assessing the impact of drainage on pavement response and resilience through the time-to-drain experiments (pits A, B, and C).

2. Evaluating pavement design and sustainability through the inverted pavement experiments (pit D).

The use of a quarry byproduct (i.e., No. 10 screenings) in the subbase of pits A through C and as a constituent in one of the CTBs will allow FHWA to evaluate its application as a sustainable material in pavement applications.

A suite of laboratory tests was performed to select and characterize the unbound and bound materials comprising the pavement foundations in PTF-3. Based on that work, several observations, analyses, and conclusions can be drawn that may serve as potential predictors of future pavement response and performance at PTF-3 as a result of the foundation material properties and drainage characteristics. Based on lessons learned, this report shares the following recommendations to facilitate the experimental setup process:

- Use Government-furnished materials for the construction of the pavement foundation.

- Recognize the inherent variability of quarry-produced materials.

- Adopt and conform to uniform sample preparation techniques for the special test procedures to achieve consistent and realistic test results.

- Collaborate with the aggregate industry to minimize the risk in the delivery of the specific materials to meet the experimental objectives of PTF-3.

TIME-TO-DRAIN EXPERIMENTS

The time-to-drain experiments required identifying and selecting base materials with different drainage qualities: poor in pit A, good in pit B, and excellent in pit C. Figure 3 presents a simplified flowchart outlining this selection process. Ultimately, 21A-DI, 21B:No.8-GR, and ATPB-No.78:No.10-DI were selected for pits A, B, and C, respectively. No. 10-DI was selected as the subbase across all the time-to-drain pits to help isolate the influence of the base materials and their corresponding times to drain. All materials were compacted to 95 percent of their target MDD and OMC per AASHTO T 180 (2022a). The cross-sections in figure 34 illustrate the primary results within each pit.

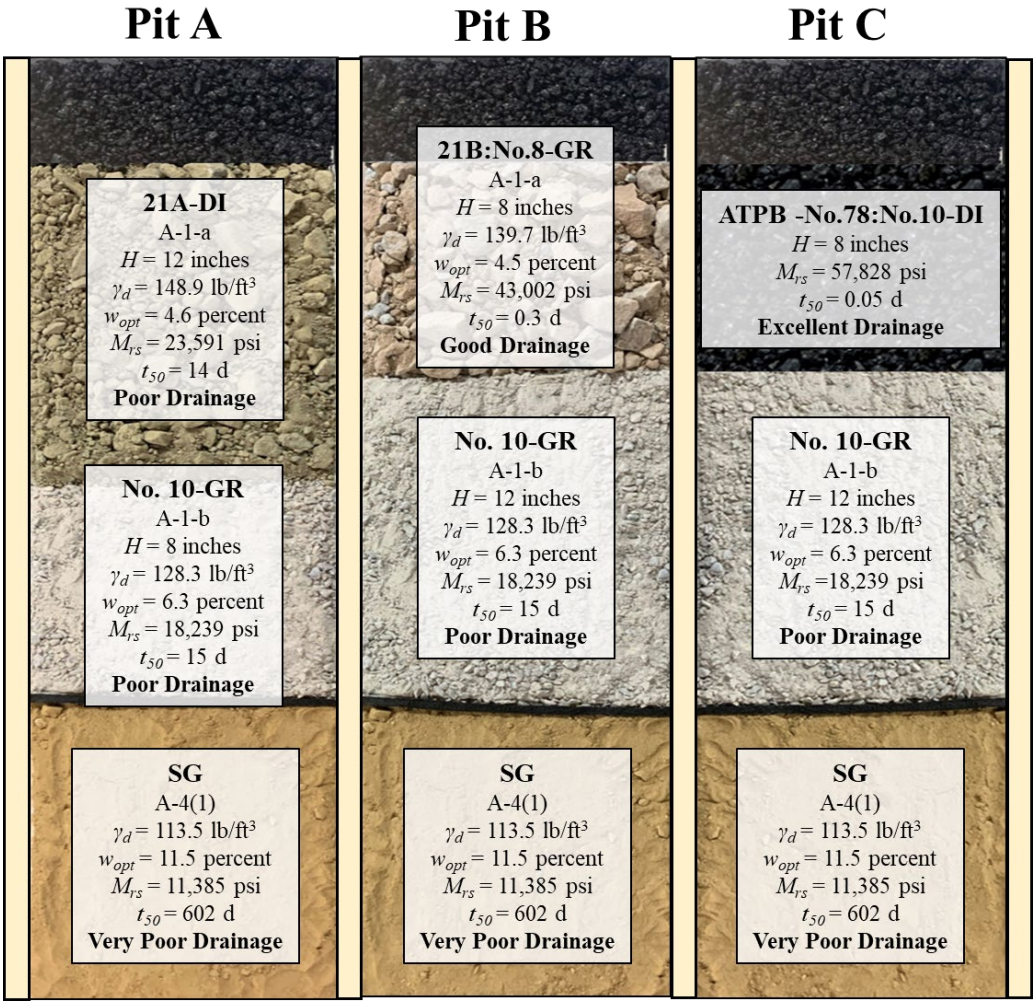

Source: FHWA.

Figure 34. Illustration. Key results by pits for the time-to-drain experiments.

Key findings from the material selection and laboratory characterization are as follows:

- Hydraulic conductivity is highly dependent on gradation, particularly the G/S ratio (figure 31). The relationship between *k* and G/S was found to be exponential and could potentially replace the current PMED (AASHTO 2020b) relationships.

- G/S also strongly influenced the M_r (figure 28). In fact, a better correlation was observed between M_{rs} and G/S than between M_{rs} and CBR (figure 26) in this study, suggesting additional calibrations within PMED (AASHTO 2022b) may improve predictions of M_{rs} for unbound base materials.

- Inherent variability in the gradations produced by quarries can be considerable, with some quarries having a tighter day-to-day production tolerance than others (figure 30). Product variability, both materially and spatially, impacts the characterization results performed on representative samples in the laboratory. The variability is further exacerbated by the gradation tolerances established by transportation agencies.

- Many of the laboratory test methods conducted in this work require scalping, or removal, of larger particles. Most notably, compaction testing per AASHTO T 180 (2022a) or T 99 (2022h) calls for the removal of particles greater than three-quarter inch and then correcting the resulting densities and moisture contents based on the scalped oversized particles to determine a field MDD and OMC. However, when selecting a target compaction level for laboratory testing, little guidance is provided to ensure the lab results mimic representative field conditions. For example, for the two base materials in pits A and B with this issue (21A-DI and 21B:No.8-GR, respectively), oversize particles ranged from 6 to 21 percent (table 11); by scalping the samples, the soaked CBR values were about 30–60 percent lower than the unscalped samples (table 19).

- Considering there is no standard test method to determine N_e, performing an EP test on the same specimen used for permeability testing is suggested, measuring both the volume of water drained as a function of time and the final moisture content after 24 h. This information can be used to verify saturation at the initial stage (table 12), determine N_e (table 13), and compute the time to drain, or t_{50}, for the sample (table 14).

INVERTED PAVEMENT EXPERIMENTS

The inverted pavement experiments required identifying and selecting the aggregate constituents within the CTBs. Different CTB thicknesses were installed in pit D, lanes 10 and 11, to evaluate low-volume versus high-volume pavement design and performance, respectively. A conventional base material, 21A-GR, was selected for the CTB in the south half of pit D, while the No.10-GR quarry byproduct was selected for the CTB in the north half. The same 21B:No.8-GR used in pit B was also used as the base material in pit D, except for its target compaction level (100 percent modified at OMC). The cross sections in figure 35 illustrate the primary results within each pit.

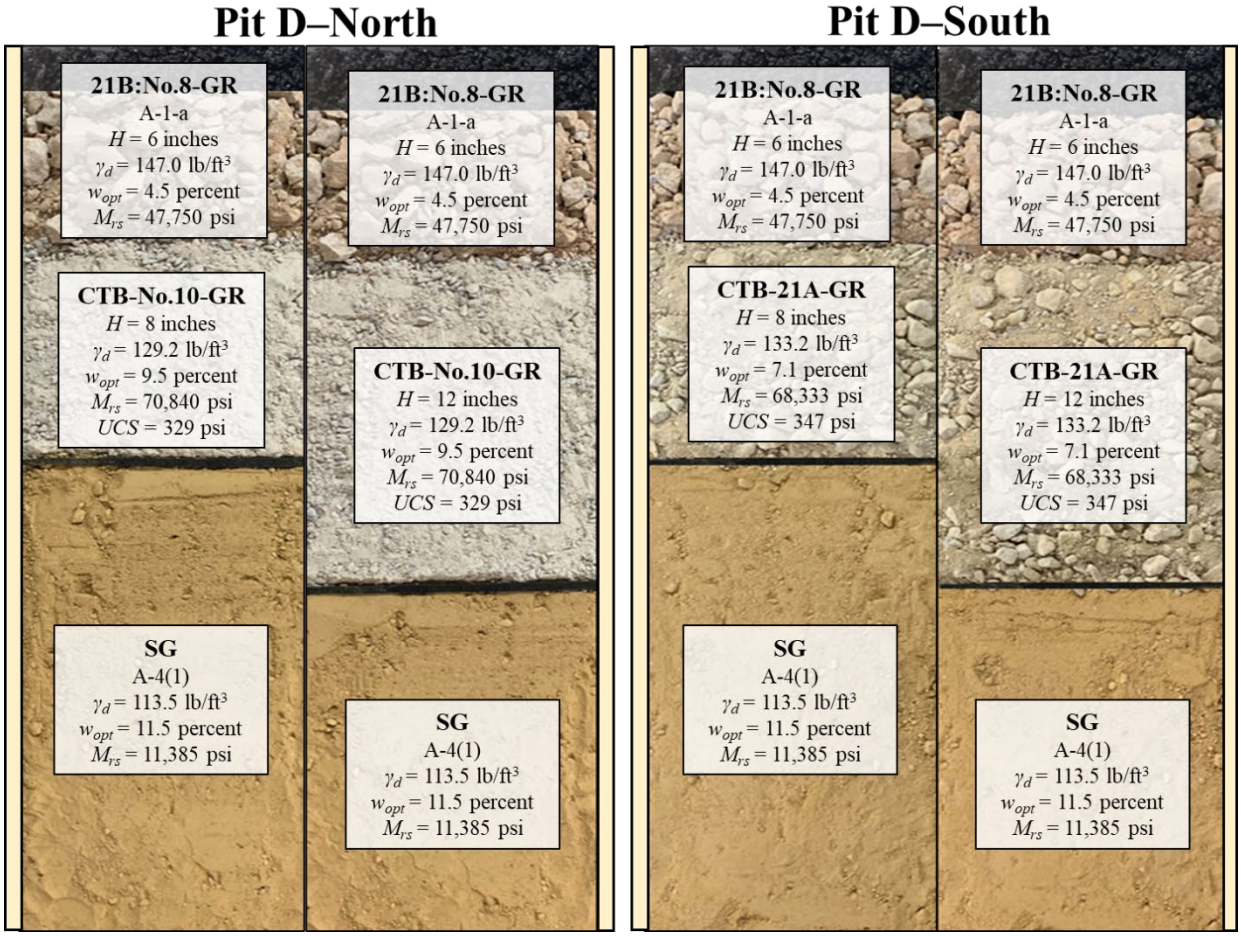

Source: FHWA.

Figure 35. Illustration. Key results by pits for the inverted pavement experiments.

Key findings from the material selection and laboratory characterization are as follows:

- The moisture-density relationships for CTBs are prepared per AASHTO T 134 (2019),
- which uses standard compaction energy akin to AASHTO T 99 (2022h), thus explaining why the MDD and OMC were lower and higher than the unbound materials, respectively (table 11), despite the approximate 4.0-percent cement content.
- The addition of cement to stabilize the selected aggregates (No.10-GR and 21A-GR) significantly decreased permeability (table 13) and increased stiffness and strength (table 16).
- CTB material properties appear to have relatively low variability compared to unbound aggregates, as evidenced by the moisture-density measurements (table 35) and UCS results (table 20), suggesting that the quarries produced a consistent CTB product for the pavement field.

- A disconnect exists between laboratory compaction testing of CTBs and field compaction efforts. While an oversize particle correction is taken to determine the MDD and OMC for unbound materials, the laboratory compaction test for CTBs instead replaces oversized particles with the same percentage of particles ranging between three-quarter inch and No. 4 (0.187-inch) sieves. How this practice impacts the compaction that can be achieved in the field or how it informs sample preparation for laboratory tests on CTB samples is not well understood.

- A comparison of the MDD and OMC of the treated CTBs and untreated specimens showed the CR of up to 4.5-percent cement did not have an obvious impact on the MDD and OMC.

- The addition of cement to stabilize the selected aggregates (No.10-GR and 21A-GR) led to a significant decrease in permeability (table 13) and an increase in stiffness and strength (table 16).

USE OF QUARRY BYPRODUCTS

Key findings and conclusions related to the use of a No. 10 screening (i.e., a quarry byproduct) within the pavement foundation include the following:

- The unbound No.10-GR is generally finer than the base materials, classified as a sandy versus gravel material (table 9); however, the measured k (table 13), t_{50} (table 14 and table 15), and M_{rs} (table 16) are comparable to the 21A-DI base material. Maximum shear stress (table 15) and CBR (table 18), however, was notably lower than 21A-DI. In addition, the No.10-GR experienced more total PS as compared to 21A-DI at the end of RM testing (table 17). For a subbase material that will experience a lower stress state than a base material, the initial laboratory characterization suggests this type of quarry byproduct is suitable for pavement design and construction.

- The characterization of the stabilized No.10-GR (i.e., CTB-No.10-GR) also indicates that this quarry byproduct may be a suitable replacement for traditional base materials in CTBs. For example, the stiffness and UCS of CTB-No.10-GR and CTB-21A-GR are nearly identical (table 15 and table 19, respectively), with CTB-No.10-GR considerably stronger in shear (table 15). Like the unbound No.10-GR, CTB-No.10-GR also experienced more total PS than CTB-21A-GR (table 16); however, the difference is considered negligible.

GEOTECHNICAL INPUTS IN PAVEMENT DESIGN

Key findings and conclusions related to PMED-based pavement design input parameters include the following:

- A considerable difference existed between the measured level 1 design inputs (table 24) and the level 2 and level 3 estimated inputs (table 26). The estimated OMC and dry density differed significantly, either too high or too low from the measured inputs.

- PMED (AASHTO 2020b) does not explicitly address the design of inverted pavements. Instead, the mechanical parameters for CTBs were input the same as if the material was unbound. Similarly, the ATPB layer was also treated as a high-quality aggregate base layer. For example, CBR was used to predict the level 2 M_{rs} for ATPB, and the sieve data and AASHTO classification of the constituents of the CTBs (i.e., CTB-No.10-GR and CTB-21A-GR) and ATPB (i.e., ATPB-No.78:No.10-DI) were also used to predict some of the level 2 and level 3 design parameters. Whether this approach is correct is up to the judgment of the pavement engineers since no adequate guidance for using stabilized materials in PMED is available.

- No consensus exists on whether and how to replicate in situ test density, particularly permeability, when conducting the different specialized tests. Material is not scalped over a 3/4-inch sieve during construction. Yet, within many standards, the material is scalped, which begs the question of whether scalped test results have any meaning or whether the materials are scalped simply because the molds are smaller. Take the permeability of 21B, for example. A major focus of this study was improving the permeability where more coarse aggregates were added, yet the standards would effectively negate the purpose of the 21B:No.8-GR blend and the whole time-to-drain experiment. Another difference between the standards and in the field is the compaction layers. While the standards provide guidance typically based on the D_{max} and mold height, within field compaction, the typical compaction layer can be anywhere from 4 to 12 inches (project specific). Research into when field and contract conditions should govern scalping, compaction, and layers is needed depending on the specific test requirements.

- The Casagrande and Shannon (1952) equation (equation 2) provides a peculiar relationship between N_e and k. Conceptually, the higher the N_e, the better k should be; however, for equation 2, the higher the porosity (table 13), the worse the calculated drainage times (table 14 and table 15). This counterintuitive outcome arises because the N_e represents the volume of water available to drain, while k dictates how fast it will drain, meaning that more water to drain at the same velocity will increase the time to drain.

LESSONS LEARNED

Regardless of the design challenges encountered, materials meeting the desired properties were selected for the PTF, allowing for the future evaluation of the materials' behavior and performance during loading in combination with the time-to-drain and inverted pavement experiments. Throughout the design and development process, several lessons were learned that can be applied by others in developing an accelerated pavement testing facility or a geotechnical testing program for the selection of unbound and stabilized materials:

- The gradation variability of conventional base materials, even among the same quarry, makes it advantageous to specify and procure the required gradation of material for the project rather than rely on the contractor to supply the materials. The base material for pit B serves as the best example; if the Government had simply specified a 21B, the contractor may have selected a quarry and product that did not meet the target drainage

quality. By furnishing the material for the PTF, the Government was able to minimize risk in achieving the experimental drainage requirements.

- Quarries may be able to produce custom blends of gradations if their production equipment allows for it; however, additional costs may be incurred. For a research facility, engineering the base and subbase materials (and perhaps the subgrade) is an important component in achieving the specific research objectives. For example, the base material for pit B required a custom blend of 90 percent 21B-GR and 10 percent No. 8-GR because the variability in 21B's gradation suggested the target drainage quality would not be met with high likelihood without spiking it with more coarse material.

- A more coherent dataset of properties representative of the material may be ensured by minimizing the number of unique samples for testing. For example, the permeability and EP tests were initially performed on separately prepared samples; however, EP tests can be performed immediately following CH or FH permeability tests on the same sample. Since EP tests require minimal labor, requiring it along with permeability tests would establish an estimate of the time to drain for the pavement during design rather than just relying on the measured k_{sat} or the default value in PMED (AASHTO 2020b).

- A single, measured test value cannot be assumed to be deterministic; variability exists due to the unpredictability in the actual gradation of a test sample prepared from a larger batch, stockpile, or quarry. For a research facility, replicates would provide a range and estimated variance for each measured parameter. In more real-world transportation projects, however, resources may be limited to a single test from a sample meant to represent the entire material. In that case, it would be prudent to also evaluate pavement design given a range of expected values based on local experience.

- Specific gravity should be measured during the early phase of lab testing and quarry-provided data obtained for comparison rather than using an assumed specific gravity for oversize corrections. In AASHTO T 180 (2022a), the recommended specific gravity is 2.65, while PMED (AASHTO 2020b) defaults to 2.7; regardless, the value plays an important role in determining compaction target density and can vary significantly.

FUTURE WORK

From the geotechnical aspects-of-pavements perspective, future work at the new pavement field will involve achieving the core research objectives as described in Adams, Nicks, and Carvalho (2024); conducting comparative analyses of different pavement structures and design methodologies; assessing pavement resilience (e.g., time-to-drain evaluations); and evaluating different pavement foundation systems, including sustainable construction technologies (e.g., inverted pavements). The accomplishment of these objectives requires collaboration between the interdisciplinary teams associated with the PTF research program; a combination of other data collected during construction, including in situ tests (e.g., nuclear density gauge, intelligent compaction, falling weight deflectometer, and lightweight deflectometer); and pavement performance information to better understand the role and influence of the pavement foundation on design and response.

Additional details on the planned research are as follows:

- **Conducting comparative analyses of different pavement structures and design methodologies.** Performing a sensitivity analysis between different mechanistic and empirical design models of pavement systems to understand the impact of different input values in design outcomes, including the significance of standard default input values. This effort also includes developing correlations between laboratory and field in situ test data in combination with pavement response information for refinements and improvements to design methodologies.

- **Assessing pavement resilience.** The resilience of pavements has become a relevant issue due to climate change. For this reason, the new pavement field was specifically designed with different pavement structures, each with different drainage capacities to evaluate the time to drain (i.e., t_{50}) and potentially revisit the AASHTO drainage criteria.

- **Advancing sustainable construction technologies.** The use of the No. 10 screenings, a quarry byproduct, as the subbase material and the inverted pavement experimental setup was in collaboration with the National Stone, Sand & Gravel Association. The No. 10 screenings were selected to promote the development of more sustainable road construction practices. While the laboratory tests suggest that No. 10 screenings are a suitable subbase material, the performance of the byproduct needs further in-service evaluation as part of a holistic pavement system. Additional laboratory testing of other No. 10 screening materials is also required to quantify their variability and suitability as a subbase material or as a constituent in treated bases. The lessons learned from this experiment with quarry byproducts should lead to a better understanding of its suitability. Limitations should be evaluated, particularly in the context of the different climatic regions and other local design requirements.

In addition, inverted pavement systems can also be considered a sustainable construction technology due to the thinner pavement surface layer. The inverted pavement lanes at the new PTF used about half the cement percentage (i.e., 4 percent) compared to that of conventional CTB mix design to mitigate the potential of reflective shrinkage cracks; the use of less cement improves the sustainability aspect. Furthermore, batching the CTB with No. 10 screenings offers another potential sustainable aspect to inverted pavements. Like the use of No. 10 screenings, the highly compacted unbound layer sandwiched between the CTB below and the thin asphalt layer above needs to be evaluated for frost susceptibility in colder climates. Inverted pavement technology also has the potential to be combined with full-depth reclamation methods for road reconstruction projects. Regardless, future testing of the inverted pavement system at PTF-3 is an opportunity to conduct a side-by-side comparison between the different pavement structures and perhaps pave the way for more in-service road test sections with this innovative technology.

Other planned work includes measuring the dynamic pavement response under accelerated loading conditions at different degrees of subsurface saturation and assessing different gradations of standard crushed material to better understand the sensitivity of G/S in both drainage quality and stiffness of unbound materials. Additionally, as part of monitoring the health of the pavement field, the subsurface moisture in each pavement pit will be measured throughout the

service life to better quantify pavement deterioration and performance due to aging and fatigue while implementing preservation techniques to extend the life of the pavements.

PTF-3 provides a unique opportunity to advance the geotechnical aspects of pavements and many other multidisciplinary needs through dedicated research, which all started with selecting and characterizing the pavement foundation materials.

ACKNOWLEDGMENTS

The authors wish to acknowledge and thank the following technical contributors to this project: Mohammad Wasif Naqvi for data review and updates; Ashley Carey for literature review and CTB data collection and analysis; Thomas Gebrenegus for laboratory testing and literature review; Scott Parobek for ATPB technical assistance and laboratory testing; Hesham Razzaghi, Catherine Dunn, and Jonathan Long for geotechnical laboratory testing; Michael Elwardany for technical input on ATPB; and the National Stone, Sand & Gravel Association and Vulcan Materials, specifically Kevin Vaughn and Bob Howsman, for technical input and insights on inverted pavements and base selection.

REFERENCES

AASHTO. 1972. *AASHTO Interim Guide for Design of Pavement Structures*. Washington, DC: American Association of State Highway and Transportation Officials.

AASHTO. 1986. *Guide for Design of Pavement Structures*. Washington, DC: American Association of State Highway and Transportation Officials.

AASHTO. 1993. *Guide for Design of Pavement Structures*. Washington, DC: American Association of State Highway and Transportation Officials.

AASHTO. 2010. *Guide for the Local Calibration of the Mechanistic-Empirical Pavement Design Guide*. Washington, DC: American Association of State Highway and Transportation Officials.

AASHTO. 2019. *Standard Method of Test for Moisture-Density Relations of Soil-Cement Mixtures*. AASHTO T 134-19. Washington, DC: American Association of State Highway and Transportation Officials.

AASHTO. 2020a. *Mechanistic-Empirical Pavement Design Guide: A Manual of Practice*. 3rd edition. Washington, DC: American Association of State Highway and Transportation Officials.

AASHTO. 2020b. *AASHTOWare Pavement ME Design* (software). Version 3.

AASHTO. 2020c. *Standard Practice for Reducing Samples of Aggregate to Testing Size*. AASHTO R 76-16 Washington, DC: American Association of State Highway and Transportation Officials.

AASHTO. 2021a. *Standard Method of Test for Determining the Resilient Modulus of Soils and Aggregate Materials*. AASHTO T 307-99. Washington DC: American Association of State Highway and Transportation Officials.

AASHTO. 2021b. *Classification of Soils and Soil-Aggregate Mixtures for Highway Construction Purposes*. AASHTO M 145-91. Washington, DC: American Association of State Highway and Transportation Officials.

AASHTO. 2022a. *Standard Method of Test for Moisture-Density Relations of Soils Using a 4.54-kg (10-lb) Rammer and a 457-mm (18-in.) Drop*. AASHTO T 180-22. Washington, DC: American Association of State Highway and Transportation Officials.

AASHTO. 2022b. *Standard Method of Test for Specific Gravity of Soils*. AASHTO T 100-22. Washington, DC: American Association of State Highway and Transportation Officials.

AASHTO. 2022c. *Standard Method of Test for Particle Size Analysis of Soils*. AASHTO T 88-22. Washington, DC: American Association of State Highway and Transportation Officials.

AASHTO. 2022d. *Standard Method of Test for Determining the Liquid Limit of Soils.* AASHTO T 89-22. Washington, DC: American Association of State Highway and Transportation Officials.

AASHTO. 2022e. *Standard Method of Test for Determining the Plastic Limit and Plasticity Index of Soils*. AASHTO T 90-22. Washington, DC: American Association of State Highway and Transportation Officials.

AASHTO. 2022f. *Standard Method of Test for Flexural Strength of Concrete (Using Simple Beam with Third-Point Loading*. AASHTO T 97 M/T 97-23. Washington, DC: American Association of State Highway and Transportation Officials.

AASHTO. 2022g. *Standard Specification for Sizes of Aggregate for Road and Bridge Construction*. AASHTO M 43-05. Washington, DC: American Association of State Highway and Transportation Officials.

AASHTO. 2022h. *Standard Method of Test for Moisture-Density Relations of Soils Using a 2.5-kg (5.5-lb) Rammer and a 305-mm (12-in.) Drop*. AASHTO T 99-22. Washington DC: American Association of State Highway and Transportation Officials.

AASHTO. 2022i. *Standard Method of Test for Specific Gravity and Absorption of Fine Aggregate*. AASHTO T 84-22. Washington, DC: American Association of State Highway and Transportation Officials.

AASHTO. 2022j. *Standard Method of Test for Specific Gravity and Absorption of Coarse Aggregate*. AASHTO T 85-22. Washington, DC: American Association of State Highway and Transportation Officials.

AASHTO. 2022k. *Standard Method of Test for Preparing and Determining the Density of Asphalt Mixture Specimens by Means of the Superpave Gyratory Compactor*. AASHTO T 312-19. Washington, DC: American Association of State Highway and Transportation Officials.

AASHTO. 2022l. *Determining Aggregate Shape Properties by Means of Digital Image Analysis*. AASHTO T 381-22. Washington, DC: American Association of State Highway and Transportation Officials.

AASHTO. 2022m. *Standard Method of Test for the California Bearing Ratio*. AASHTO T 193-22. Washington, DC: American Association of State Highway and Transportation Officials.

AASHTO. 2022n. *Standard Method of Test for Resistance of Coarse Aggregate to Degradation by Abrasion in the Micro-Deval Apparatus*. AASHTO T 327-22. Washington, DC: American Association of State Highway and Transportation Officials.

AASHTO. 2022o. *Standard Method of Test for Resistance of Compacted Asphalt Mixtures to Moisture-Induced Damage*. AASHTO T 283-22. Washington, DC: American Association of State Highway and Transportation Officials.

AASHTO. 2022p. *Standard Practice for Determining Aggregate Source Shape Values from Digital Image Analysis Shape Properties*. AASHTO R 91-18. Washington, DC: American Association of State Highway and Transportation Officials.

AASHTO. 2023a. *Standard Method of Test for Permeability of Granular Soils (Constant Head)*. AASHTO T 215-23. Washington, DC: American Association of State Highway and Transportation Officials.

AASHTO. 2023b. *Standard Specification for Performance-Graded Asphalt Binder*. AASHTO M 320-23. Washington, DC: American Association of State Highway and Transportation Officials.

AASHTO. 2023c. *Standard Specification for Performance-Graded Asphalt Binder Using Multiple Stress Creep Recovery (MSCR) Test*. AASHTO M 332-23. Washington, DC: American Association of State Highway and Transportation Officials.

AASHTO. 2023d. *Standard Method of Test for Theoretical Maximum Specific Gravity (Gmm) and Density of Asphalt Mixtures*. AASHTO T 209-23. Washington, DC: American Association of State Highway and Transportation Officials.

AASHTO. 2023e. *Standard Method of Test for Bulk Specific Gravity (Gmb) and Density of Compacted Asphalt Mixtures Using Automatic Vacuum Sealing Method*. AASHTO T 331-23. Washington, DC: American Association of State Highway and Transportation Officials.

Abu-Farsakh, M., S. Dhakal, and Q. Chen. 2015. "Laboratory Characterization of Cementitiously Treated/Stabilized Very Weak Subgrade Soil Under Cyclic Loading." *Soils and Foundations* 55, no. 3: 504–516.

Adams, M. T., J. E. Nicks, and R. Carvalho. 2024. *Redesign of the Third Generation FHWA Pavement Test Facility*. Publication No. FHWA-HRT-24-124. Washington, DC: Federal Highway Administration.

Anderson, D. A., P. Sebaaly, N. Tabatabaee, R. Bonaquist, and C. Churilla. 1988. *Pavement Testing Facility—Pavement Performance of the Initial Two Test Sections*. Report No. FHWA-RD-88-060. Washington, DC: Federal Highway Administration.

Ardah, A., M. Abu-Farsakh, and Q. Chen. 2016. "Evaluating the Performance of Cementitious Treated/Stabilized Very Weak and Wet Subgrade Soils for Sustainable Pavement." In *Geo-Chicago 2016: Geotechnics for Sustainable Energy*. A. Farid, A. De, K. R. Reddy, N. Yesiller, and D. Zekkos (eds.), pp. 567–576.

Arinze, E. E., J. C. Agunwamba, and B. O. Mama. 2018. "Performance of Quarry Dust-Cement Stabilized Lateritic Soil as a Highway Construction Material." *Electronic Journal of Geotechnical Engineering* 23, no. 4: 783–796.

ASTM. 2009. *Standard Test Method for Specific Heat of Liquids and Solids*. ASTM D2766. West Conshohocken, PA: ASTM International.

ASTM. 2016. *Standard Test Methods for Determination of the Soil Water Characteristic Curve for Desorption Using Hanging Column, Pressure Extractor, Chilled Mirror Hygrometer, or Centrifuge*. ASTM D6836. West Conshohocken, PA: ASTM International.

ASTM. 2017a. *Standard Test Methods for Liquid Limit, Plastic Limit, and Plasticity Index of Soils*. ASTM D4318-17e1. West Conshohocken, PA: ASTM International.

ASTM. 2017b. *Standard Test Methods for Compressive Strength of Molded Soil-Cement Cylinders*. ASTM D1633. West Conshohocken, PA: ASTM International.

ASTM. 2017c. *Standard Practice for Classification of Soils for Engineering Purposes (Unified Soil Classification System)*. ASTM D2487. West Conshohocken, PA: ASTM International.

ASTM. 2017d. *Standard Test Methods for Compressive Strength of Molded Soil-Cement Cylinders*. ASTM D559/D559M. West Conshohocken, PA: ASTM International.

ASTM. 2019. *Standard Test Method for Sieve Analysis of Fine and Coarse Aggregates*. ASTM C136. West Conshohocken, PA: ASTM International.

ASTM. 2022a. *Standard Test Method for Marshall Stability and Flow of Asphalt Mixtures*. ASTM D6927-22. West Conshohocken, PA: ASTM International.

ASTM. 2022b. *Standard Test Method for Static Modulus of Elasticity and Poisson's Ratio of Concrete in Compression*. ASTM C469/C469M. West Conshohocken, PA: ASTM International.

ASTM. 2023a. *Standard Test Method for Thermal Conductivity and Thermal Diffusivity by Modulated Temperature Differential Scanning Calorimetry*. ASTM E1952. West Conshohocken, PA: ASTM International.

ASTM. 2023b. *Standard Test Method for Materials Finer than 75-μm (No. 200) Sieve in Mineral Aggregates by Washing*. ASTM C117. West Conshohocken, PA: ASTM International.

ASTM. 2023c. *Standard Practice for Use of Unbounded Caps in Determination of Compressive Strength of Hardened Cylindrical Concrete Specimens*. ASTM C1231/C1231M. West Conshohocken, PA: ASTM International.

Aytekin, B., A. Mardani, and Y. S. Ünsever. 2023. "Performance Assessment of Recycled Waste Materials for Use in Unbound Pavement Layers: A Case Study From Turkey." *Construction and Building Materials* 402: 133004.

Bamigboye, G. O., D. E. Bassey, D. O. Olukanni, B. U. Ngene, D. Adegoke, A. O. Odetoyan, M. A. Kareem, D. O. Enabulele, and A. T. Nworgu. 2021. "Waste Materials in Highway Applications: An Overview on Generation and Utilization Implications of Sustainability." *Journal of Cleaner Production* 283: 124581.

Bonaquist, R. F. 1993. *Pavement Testing Facility – Phase 1 Final Report*. Report No. FHWA-RD-92-121. Washington, DC: Federal Highway Administration.

Buchanan, S. 2010. *Inverted Pavement Systems*. Naperville, IL: Vulcan Materials Resource Center. https://www.vulcaninnovations.com/public/pdf/4-Inverted-Pavement-Systems.pdf, last accessed August 19, 2024.

Cakuru, M., R. K. Tenywa, S. Jjuuko, and D. Kalumba. 2021. "Strength Assessment of Quarry Dust Treated Soil – Reclaimed Asphalt Pavement (RAP) Mixture." Presented at *Advances in Transportation Geotechnics*. Virtual conference.

California Department of Transportation. 2019. "Construction Details for Treated Permeable Bases." In *Construction Manual*. Sacramento, CA: California Department of Transportation. Chapter 4, Section 29.

Cardosa, J. 2008. "Inverted Pavements: Georgia Experience." Presented at *National Aggregate Base Conference*. Alexandria, VA: National Stone, Sand & Gravel Association.

Carey A. S., L. A. Cooley, Jr., A. Middleton, W. G. Sullivan, L. E. W. Ayers, and I. L. Howard. 2022. "Statewide Survey of Chemically Stabilized Soil Properties for Mechanistic-Empirical Pavement Design." *ACI Materials Journal* 119, no. 5: 227–238.

Casagrande, A., and W. L. Shannon. 1952. "Base Course Drainage for Airport Pavements." *Transactions of the American Society of Civil Engineers* 117, no. 1: 792–814.

Christopher, B. R., C. Schwartz, and R. Boudreau. 2006. *Geotechnical Aspects of Pavements*. FHWA-NHI-05-037. Washington, DC: Federal Highway Administration.

Department of Transport. 1996. *Technical Recommendations for Highways 4: Structural Design of Flexible Pavements for Interurban and Rural Roads.* Pretoria, South Africa: Department of Transport. TRH4-1996-Flexible-Pavement-Design.pdf, last accessed November 13, 2024.

Etim, R. K., D. U. Ekpo, I. C. Attah, and K. C. Onyelowe. 2021. "Effect of Micro Sized Quarry Dust Particle on the Compaction and Strength Properties of Cement Stabilized Lateritic Soil." *Cleaner Materials* 2:100023.

Federal Aviation Administration. 2008. *Appendix G: Design of Subsurface Pavement Drainage Systems* Washington, DC: Federal Aviation Administration. pp. 9–10. https://www.faa.gov/documentLibrary/media/Advisory_Circular/150_5320_5c_chg1.pdf, last accessed August 19, 2024.

FHWA. 1992. *Drainable Pavement Systems Participant Notebook: Demonstration Project 87*. Report No. FHWA-SA-92-008. Washington, DC: Federal Highway Administration.

FHWA. 2004. "Design Guide Implementation Survey." PowerPoint presentation. https://www.fhwa.dot.gov/pavement/dgit/dgitsurvey.pdf, last accessed August 19, 2024.

FHWA. 2014. *Standard Specifications for Construction of Roads and Bridges on Federal Highway Projects*. Report No. FP-14. Washington, DC: Federal Highway Administration. https://highways.dot.gov/sites/fhwa.dot.gov/files/docs/federal-lands/specs/12851/fp14.pdf, last accessed November 5, 2024.

Federal Republic of Nigeria. 2013. *Highway Manual Part 1: Design; Volume III: Pavements and Materials Design*. Abuja, Nigeria: Federal Republic of Nigeria.

FDOT. 2015. *Florida Method of Test for Measurement of Water Permeability of Compacted Asphalt Paving Mixtures.* Publication No. FDOT FM 5-565. Gainesville, FL: Florida Department of Transportation.

Frost, J. D. 2017. *Long-term Performance of Granular Bases Including the Effect of Wet-Dry Cycles on Inverted Base Pavement Performance*. Report No. FHWA-GA-17-1510. Atlanta, GA: Georgia Department of Transportation.

Garcia, J., and K. Hansen. 2001. *HMA Pavement Mix Type Selection Guide*. Information Series 128. Washington, DC: Federal Highway Administration and National Asphalt Pavement Association.

Geary, G. M. 2018. *User Review of the AASHTO "Guide for the Local Calibration of the Mechanistic-Empirical Pavement Design Guide*." Report No. NCHRP 20-07/Task 422. Washington, DC: Transportation Research Board.

Gebrenegus, T., T. A. Michael, J. E. Nicks, and R. L. Carvalho. 2022. "Optimization of an Aggregate Base Course Considering Permeability and Stiffness." Presented at *Geo-Congress 2022*. Charlotte, NC: American Society of Civil Engineers.

Ghaaowd, I., M. Adams, J. Nicks, and S. Parobeck. 2024. "Laboratory Testing to Design an Asphalt Treated Permeable Base for the Federal Highway Administration's Pavement Test Facility." Presented at the *5th International Conference on Transportation Geotechnics*. Sydney, Australia: Transport Research Centre.

Ghaaowd, I. I., T. A. Michael, J. E. Nicks, and E. A. Cox. 2022. "An Evaluation of a Quarry Byproduct Material for Use in an Inverted Pavement System." Presented at *Geo-Congress 2022.* Charlotte, NC: American Society of Civil Engineers.

Harrigan, E. T. 2002. *Performance of Pavement Subsurface Drainage*. National Cooperative Highway Research Program Research Results Digest No. 268. Washington, DC: Transportation Research Board of the National Academies.

Harvey, J., B. Tsai, F. Long, and D. Hung. 1998. "Asphalt-Treated Permeable Base: Laboratory Testing, Performance, and Predictions." *Transportation Research Record: Journal of the Transportation Research Board* 1629, no. 1: 127–136. https://doi.org/10.3141/1629-15, last accessed August 19, 2024.

Harvey, J. T., B.-W. Tsai, F. Long, and D. Hung. 1999. *CAL/APT Program—Asphalt Treated Permeable Base*. Report No. FHWA/CA/OR-99/09. Sacramento, CA: California Department of Transportation.

Hatipoglu, M., B. Cetin, and A. H. Aydilek. 2020. "Effect of Fines Content on Hydraulic and Mechanical Performance of Unbound Granular Base Aggregates." *Journal of Transportation Engineering, Part B: Pavements* 146, no. 1: 04019036. https://doi.org/10.1061/JPEODX.0000141, last accessed August 19, 2024.

Highway Research Board. 1962. *The AASHO Road Test: Report 2 Materials and Construction*. Special Report 61B. Publication No. 951. Washington, DC: National Academy of Sciences–National Research Council.

Hossain, M. S., and D. S. Lane. 2015. *Development of a Catalog of Resilient Modulus Values for Aggregate Base for Use with the Mechanistic-Empirical Pavement Design Guide (MEPDG)*. Report No. FHWA/VCTIR 15-R13. Charlottesville, VA: Virginia Center for Transportation Innovation and Research.

Indiana DOT. 2013. "Project Categories and Pavement Types." In *2013 Design Manual.* Indianapolis, IN: Indiana Department of Transportation. Chapter 602.

Johnson, C. W. 1961. "Comparative Studies of Combinations of Treated and Untreated Bases and Subbases for Flexible Pavements." *Highway Research Bulletin* 289: 44–61.

Jones, H. A., and R. H. Jones. 1989. *Unbound Aggregates in Roads*. London, UK: Butterworths.

Kipp, W., B. Walters, and W. F. Ahearn. 2013. *Evaluation of Asphalt Treated Permeable Base*. Report No. 2013-09. Montpelier, VT: Vermont Agency of Transportation.

Koerner, R. M., J. R. Koerner, and G. R. Koerner. 2018. *Status of Pavement Design Methods Used by US DOTs and Inclusion of Geosynthetics Therein*. GSI White Paper No. 40. Folsom, PA: Geosynthetic Institute.

Maine DOT. 1999. *Experimental Utilization of Permeable Base*. Experimental Construction Project No. ME 98-08. Augusta, ME: Maine Department of Transportation.

Masad, E., T. Al-Rousan, J. Button, D. Little, and E. Tutumluer. 2007. *Test Methods for Characterizing Aggregate Shape, Texture, and Angularity*. NCHRP Report 555. Washington, DC: National Cooperative Highway Research Program.

Meininger, R. C., and S. J. Stokowski. 2011 "Wherefore Art Thou Aggregate Resources for Highways?" *Public Roads* 75, no. 3. https://highways.dot.gov/public-roads/septemberoctober-2011/wherefore-art-thou-aggregate-resources-highways, last accessed November 28, 2023.

Meyers, M. A. P. 2021. *Engineering Brief No. 102: Asphalt Treated Permeable Base Course*. Washington, DC: Federal Aviation Administration.

Narzary, B. K., and K. U. Ahamad. 2020. “Estimation of Equivalent Modulus of Fine-Grained Subgrade Soil from Numerical Model.” *Journal of Transportation Engineering, Part B: Pavements* 147, no. 1. https://doi.org/10.1061/JPEODX.0000246, last accessed August 19, 2024.

Nazarian, S., M. Mazari, I. Abdallah, A. Puppala, L. Mohammad, and M. Abu-Farsakh. 2014. *Modulus-Based Construction Specification for Compaction of Earthwork and Unbound Aggregate*. Washington, DC: Transportation Research Board. https://onlinepubs.trb.org/onlinepubs/nchrp/docs/NCHRP10-84_FR.pdf, last accessed August 19, 2024.

Nweke, O. M., and C. O. Okogbue. 2017. “The Potential of Cement Stabilized Shale Quarry Dust for Possible Use as a Road Foundation Material.” *International Journal of Geo-Engineering*, 8:29.

Ooi, P. S. K., A. R. Archilla, and K. G. Sandefur. 2004. “Resilient Modulus Models for Compacted Cohesive Soils." *Transportation Research Record* 1874, no. 1: 115–124. https://doi.org/10.3141/1874-13, last accessed August 19, 2024.

Ozer, H., and I. L. Al-Qad. 2021. *Louisiana Experience with Inverted Pavement Systems*. Publication No. FHWA-HIF-19-082. Washington, DC: Federal Highway Administration. https://www.fhwa.dot.gov/pavement/sustainability/case_studies/hif19082.pdf, last accessed August 20, 2024.

Papadopoulos, E., and J. C. Santamarina. 2019. “Inverted Base Pavements: Construction and Performance.” *International Journal of Pavement Engineering* 20, no. 6: 697–703.

Peng, L., D. Ge, S. Lv, Y. Xue, J. Chen, H. Sun, and J. Wang. 2023. “Use of Waste Rubber Particles in Cement-Stabilized Aggregate for the Eco-Friendly Pavement Base Layer Construction: Laboratory Performance and Field Application.” *Construction and Building Materials* 402: 133023.

Puppala, A. J., A. Pedarla, B. Chittoori, V. K. Ganne, and S. Nazarian. 2017. “Long-Term Durability Studies on Chemically Treated Reclaimed Asphalt Pavement Material as a Base Layer for Pavements.” *Transportation Research Record* 2654: 1–9.

Qamhia, I. I. A., and E. Tutumluer. 2021. *Review of Improved Subgrade and Stabilized Subbases to Evaluate Performance of Concrete Pavements*. Report No. FHWA-ICT-21-011. Springfield, IL: Illinois Department of Transportation.

Quang, N. D., and J. C. Chai. 2015. “Permeability of Lime- and Cement-Treated Clayey Soils.” *Canadian Geotechnical Journal* 52, no. 9: 1221–1227. https://doi.org/10.1139/cgj-2014-0134, last accessed August 20, 2024.

SANRA. 1998. *High-Performance Crushed-Stone Bases (G1) Used on South African Highways—A General Overview*. Pretoria, South Africa: South African National Roads Agency.

Sridharan, A., T. G. Soosan, B. T. Jose, and B. M. Abraham. 2006. “Shear Strength Studies on Soil-Quarry Dust Mixtures.” *Geotechnical and Geological Engineering* 24: 1163–1179.

Tanyu, B. F., S. Ullah, and E. Akmaz. 2021. *Optimizing Reclaimed Asphalt Pavement (RAP) Content in Unbound Base Aggregate*. Report No. FHWA/VTRC 22-R9. Richmond, VA: Virginia Department of Transportation.

Timm, D. H., M. M. Robbins, N. Tran, and C. Rodezno. 2014. *Flexible Pavement Design – State of Practice*. NCAT Report 14-04. Auburn, AL: National Center for Asphalt Technology.

Transportation Research Board. 2004. *Guide for Mechanistic-Empirical Design of New and Rehabilitated Pavement Structures*. Report No. NCHRP 1-37A. Washington, DC: Transportation Research Board.

Tutumluer, E., and R. D. Barksdale. 1995. “Inverted Flexible Pavement Response and Performance.” *Transportation Research Record* 1482: 102–110.

Underwood, B. S., M. Guddati, and V. Samu. 2020. *Evaluation of Inverted Pavement for NC Roadways*. Report No. FHWA/NC/2020-017. Raleigh, NC: North Carolina Department of Transportation.

USACE. 1970. *Laboratory Soil Testing*. Publication No. EM 1110-2-1906. Vicksburg, MS: Waterways Experiment Station.

USACE. 1986. *Seepage Analysis and Control for Dams*. Publication No. EM 1110-2-1901. Vicksburg, MS: U.S. Army Corps of Engineers.

Van Til, C. J., B. F. McCullough, B. A. Vallerga, and R. G. Hicks. 1972. *Evaluation of AASHO Interim Guides for Design of Pavement Structures*. NCHRP Report 128. Washington, DC: National Academy of Sciences–National Academy of Engineering.

VDOT. 2016. *2016 Road and Bridges Specifications: Division III—Roadway Construction*. Richmond, VA: Virginia Department of Transportation. https://www.vdot.virginia.gov/media/vdotvirginiagov/doing-business/technical-guidance-and-support/technical-guidance-documents/construction/migrated-acc/VDOT2016_3Specs_acc071522.pdf, last accessed November 5, 2024.

VDOT. 2000. *Virginia Test Method 40 – Determining Cement Content of Freshly Mixed Cement-Aggregate Mixtures*. Richmond, VA: Virginia Department of Transportation.

VDOT. 2020. *Road and Bridge Specifications*. Richmond, VA: Virginia Department of Transportation.

Vizcarra, G. O. C., M. D. T. Casagrande, and L. M. Goretti da Motta. 2018. “Applicability of Municipal Solid Waste Incineration Ash on Base Layers of Pavements.” *Journal of Materials in Civil Engineering* 26, no. 6: 06014005.

Webb, D., G. Sholar, J. Musselman, P. Upshaw, and G. Page. 2007. *An Evaluation of Asphalt Treated Permeable Base*. Report No. FL/DOT/SMO/07-511. Tallahassee, FL: Florida Department of Transportation.

Weingart, R. 2010. "Inverted Pavements: Virginia Experience." Webinar from AFTRE Webinar Presentation. National Stone, Sand, & Gravel Association. June 1, 2010.

WSDOT. 2023. *Local Agency General Special Provisions (GSPs): Asphalt Treated Permeable Base (ATPB). Section 4-SA2*. Olympia, WA: Washington State Department of Transportation.

WSDOT. 2024. "Volumetric Properties of Asphalt Mixtures." In *WSDOT Materials Manual*. Publication No. M 46-01.44. Olympia, WA: Washington State Department of Transportation. https://wsdot.wa.gov/publications/manuals/fulltext/M46-01/TM13.pdf, last accessed April 4, 2024.

Xi, J., B. Huang, T. Hani, and P. Polaczyk. 2022. *Evaluating the Performance of Inverted Pavements in Tennessee*. Report No. RES 220-12. Nashville, TN: Tennessee Department of Transportation.

Xiao, Y., and E. Tutumluer. 2012. *Best Value Granular Material for Road Foundations*. Report No. MN/RC 2012-01. St. Paul, MN: Minnesota Department of Transportation.

Zhou, H., L. Moore, J. Huddleston, and J. Gower. 1992. *Free Draining Base Materials Properties*. Report No. FHWA-OR-RD-92-11. Salem, OR: Oregon Department of Transportation.

Recycled
Recyclable

Recommended citation: Federal Highway Administration,
Selection and Characterization of the Foundation Materials for the Third-Generation FHWA Pavement Test Facility
(Washington, DC: 2024) https://doi.org/10.21949/1521622

HRDI-40/12-24(WEB)E